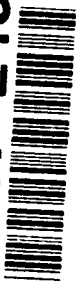


AD-A267 243



NAVAL POSTGRADUATE SCHOOL Monterey, California



DTIC
SELECTE
JUL 28 1993
S E D

THESIS

THERMAL STRESSES OF A TRIMATERIAL MEDIUM
IN A NONUNIFORM TEMPERATURE FIELD

by

Michael Joseph Neibert

March 1993

Thesis Advisor:
Co-Advisor:

David Salinas
Young Kwon

Approved for public release; distribution is unlimited

98

98 6

93-16926



REPORT DOCUMENTATION PAGE			Form Approved OMB No. 0704-0188	
Public reporting burden for this collection of information is estimated to average 1 hour per response, including the time for reviewing instructions, searching existing data sources, gathering and maintaining the data needed, and completing and reviewing the collection of information. Send comments regarding this burden estimate or any other aspect of this collection of information, including suggestions for reducing this burden, to Washington Headquarters Services, Directorate for Information Operations and Reports, 1215 Jefferson Davis Highway, Suite 1204, Arlington, VA 22202-4302, and to the Office of Management and Budget, Paperwork Reduction Project (0704-0188), Washington, DC 20503.				
1. AGENCY USE ONLY (Leave blank)		2. REPORT DATE March 1993		3. REPORT TYPE AND DATES COVERED Master's Thesis March 1993
4. TITLE AND SUBTITLE Thermal Stresses of a Trimaterial Medium in a Nonuniform Temperature Field			5. FUNDING NUMBERS	
6. AUTHOR(S) Michael Joseph Neibert				
7. PERFORMING ORGANIZATION NAME(S) AND ADDRESS(ES) Naval Postgraduate School Monterey, CA 93943-5000			8. PERFORMING ORGANIZATION REPORT NUMBER	
9. SPONSORING / MONITORING AGENCY NAME(S) AND ADDRESS(ES) Naval Postgraduate School Monterey, CA 93943-5000			10. SPONSORING / MONITORING AGENCY REPORT NUMBER	
11. SUPPLEMENTARY NOTES The views expressed are those of the author and do not reflect the official policy or position of the Department of Defense or the U.S. Government				
12a. DISTRIBUTION / AVAILABILITY STATEMENT Approved for public release; distribution is unlimited			12b. DISTRIBUTION CODE	
13. ABSTRACT (Maximum 200 words) The objective of this investigation was to conduct a parametric study of the effect of a nonuniform temperature field on the system behavior of a trilayered medium. In particular, the resulting shear and normal stresses along the media interfaces are analyzed. A finite element model utilizing a recently developed element which provides for both axial and lateral displacement continuity is employed. First, the effect of the material properties, that is, Young's Modulus and coefficient of thermal expansion, is examined. Then, the effect of the geometric properties, that is, length and thickness dimensions of the midlayer, is analyzed. Finally, a study of the effect of a nonuniform temperature field on the trimaterial medium is conducted.				
14. SUBJECT TERMS Thermoelastic Stresses, Multilayered Media, Nonuniform Temperature Fields			15. NUMBER OF PAGES 108	
			16. PRICE CODE	
17. SECURITY CLASSIFICATION OF REPORT unclassified	18. SECURITY CLASSIFICATION OF THIS PAGE unclassified	19. SECURITY CLASSIFICATION OF ABSTRACT unclassified	20. LIMITATION OF ABSTRACT SAR	

Approved for public release: Distribution is unlimited.

Thermal Stresses of a Trimaterial Medium in a Nonuniform
Temperature Field

by

Michael Joseph Neibert
Lieutenant, United States Navy
B.S., Colorado State University, 1981

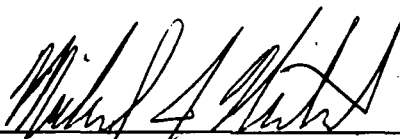
Submitted in partial fulfillment of the
requirements for the degree of

MASTER OF SCIENCE IN MECHANICAL ENGINEERING

from the

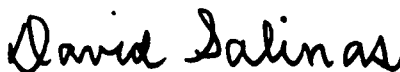
NAVAL POSTGRADUATE SCHOOL
March 1993

Author:

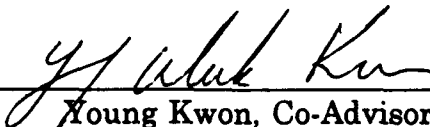


Michael Joseph Neibert

Approved by:



David Salinas, Thesis Advisor



Young Kwon, Co-Advisor



Matthew D. Kelleher, Chairman
Department of Mechanical Engineering

ABSTRACT

The objective of this investigation was to conduct a parametric study of the effect of a nonuniform temperature field on the system behavior of a trilayered medium. In particular, the resulting shear and normal stresses along the media interfaces are analyzed. A finite element model utilizing a recently developed element which provides for both axial and lateral displacement continuity is employed. First, the effect of the material properties, that is, Young's Modulus and coefficient of thermal expansion, is examined. Then, the effect of the geometric properties, that is, length and thickness dimensions of the midlayer, is analyzed. Finally, a study of the effect of a nonuniform temperature field on the trimaterial medium is conducted.

DTIC QUALITY INSPECTED 5

Accession For	
NTIS GRA&I	<input checked="checked" type="checkbox"/>
DTIC TAB	<input type="checkbox"/>
Unannounced	<input type="checkbox"/>
Justification	
By _____	
Distribution/	
Availability Codes	
Dist	Avail and/or Special
A-1	

TABLE OF CONTENTS

I.	INTRODUCTION	1
II.	FEM MODEL FORMULATION	5
	A. PROGRAM DEVELOPMENT	5
	B. PROGRAM INPUT	12
	C. PROGRAM OUTPUT	13
III.	EFFECT OF MATERIAL PROPERTIES	14
	A. CASES 1 AND 2	16
	B. CASES 3, 4, AND 5	20
	C. CASES 3, 6, 7, AND 8	24
	D. CASES 7, 9, 10, AND 11	29
	E. SUMMARY	29
IV.	EFFECT OF MIDLAYER THICKNESS	36
	A. NORMAL STRESS DISTRIBUTION	36
	B. SHEAR STRESS DISTRIBUTION	39
	C. SUMMARY	45
V.	EFFECT OF MIDLAYER LENGTH	49
	A. NORMAL STRESS DISTRIBUTION	49
	B. SHEAR STRESS DISTRIBUTION	52
	C. SUMMARY	56

VI. EFFECT OF NONUNIFORM TEMPERATURE DISTRIBUTION . .	57
A. NORMAL STRESS DISTRIBUTION	58
B. SHEAR STRESS DISTRIBUTION	60
C. SUMMARY	64
VII. SUMMARY AND CONCLUSIONS	66
A. EFFECT OF MATERIAL PROPERTIES	66
B. EFFECT OF MIDLAYER THICKNESS	67
C. EFFECT OF MIDLAYER LENGTH	67
D. EFFECT OF NONUNIFORM TEMPERATURE DISTRIBUTION	68
E. RECOMMENDATIONS FOR FURTHER RESEARCH	68
APPENDIX A: FEM PROGRAM	69
APPENDIX B: PROGRAM EXEC	76
APPENDIX C: INPUT FILE	77
APPENDIX D: OUTPUT FILE	81
LIST OF REFERENCES	98
INITIAL DISTRIBUTION LIST	99

LIST OF FIGURES

Figure 1.1	Electronic Package	2
Figure 1.2	Tri-Material Configuration	4
Figure 2.1	A Typical Element With Six Degrees of Freedom	5
Figure 2.2	Finite Element Analysis Mesh for Tri-Material Configuration	13
Figure 3.1	Tri-Material Configuration	14
Figure 3.2	Normal Stress at Interfaces for Cases 1 and 2	17
Figure 3.3	Shear Stress at Interfaces for Cases 1 and 2	18
Figure 3.4	Shear and Normal Stresses on the Midlayer for Cases 1 and 2	19
Figure 3.5	Normal Stress at Interfaces for Cases 3, 4, and 5	21
Figure 3.6	Shear Stress at Interfaces for Cases 3, 4, and 5	22
Figure 3.7	Shear and Normal Stresses on the Midlayer for Cases 3, 4, and 5	23
Figure 3.8	Normal Stress at Interfaces for Cases 3, 6, 7, and 8	25
Figure 3.9	Shear Stress at Interfaces for Cases 3, 6, 7, and 8	26
Figure 3.10	Shear and Normal Stresses on the Midlayer for Cases 3 and 8	27
Figure 3.11	Shear and Normal Stresses on the Midlayer for Cases 6 and 7	28
Figure 3.12	Normal Stress at interfaces for Cases 7, 9, 10, and 11	30
Figure 3.13	Shear Stress at interfaces for Cases 7, 9, 10, and 11	31

Figure 3.14	Shear and Normal Stresses on the Midlayer for Cases 7 and 9	32
Figure 3.15	Shear and Normal Stresses on the Midlayer for Cases 10 and 11	33
Figure 4.1	Tri-Material Configuration for Cases 5, 12, 13, 14, and 15 .	37
Figure 4.2	Normal Stresses at the Interfaces for Case 5, 12, 13, 14, and 15	38
Figure 4.3	2-D and 3-D Plots of Normal Stress/Maximum Normal Stress at the Upper Interface for Cases 5, 12, 13, 14, and 15	40
Figure 4.4	2-D and 3-D Plots of Normal Stress/Maximum Normal Stress at the Lower Interface for Cases 5, 12, 13, 14, and 15	41
Figure 4.5	Shear and Normal Stresses on the Midlayer for Cases 5, 12, and 13	42
Figure 4.6	Shear and Normal Stresses on the Midlayer for Cases 14 and 15	43
Figure 4.7	Shear Stresses at the Interfaces for Cases 5, 12, 13, 14, and 15	44
Figure 4.8	2-D and 3-D Plots of Shear Stress/Maximum Shear Stress at the Upper Interface for Cases 5, 12, 13, 14, and 15	46
Figure 4.9	2-D and 3-D Plots of Shear Stress/Maximum Shear Stress at the Lower Interface for Cases 5, 12, 13, 14, and 15	47
Figure 5.1	Tri-Material Configurations for Cases 12, 16, 17, 18, 19, and 20	50
Figure 5.2	Normal Stresses at Interfaces as a Function of Non-dimensional Location for Cases 12, 16, 17, 18, 19, and 20	51
Figure 5.3	Shear and Normal Stresses on the Midlayer for Cases 12, 16, and 17	53

Figure 5.4	Shear and Normal Stresses on the Midlayer for Cases 18, 19, and 20	54
Figure 5.5	Shear Stresses at Interfaces as a function of Non-dimensional Location for Cases 12, 16, 17, 18, 19, and 20	55
Figure 6.1	Tri-Material Configuration for Cases 21, 22, 23, and 24	57
Figure 6.2	Material A Linear Temperature Distribution for Case 24 ...	58
Figure 6.3	Normal Stresses at the Interfaces for Cases 21, 22, 23, and 24	59
Figure 6.4	Shear and Normal Stresses on the Midlayer for Cases 21 and 22	61
Figure 6.5	Shear and Normal Stresses on the Midlayer for Cases 23 and 24	62
Figure 6.6	Shear Stresses at the Interfaces for Cases 21, 22, 23, and 24	63

I. INTRODUCTION

The history of thermoelastic stresses on layered materials begins with Timoshenko. In a 1925 paper [Ref. 1], he first discussed the case of a directly bonded bi-material configuration. He studied bi-material thermostats modeled in the form of high aspect ratio beams subjected to uniform heating or cooling. Bearing stresses in closed form expressions were presented and it was noted that there was not an elementary way of determining the shear stress distribution along the bearing surface. The curvature of the beams at a given temperature was shown to be related to the beam geometry, the elastic constants of the materials, and their coefficients of thermal expansion.

Goland and Reissner [Ref. 2] and Christensen [Ref. 3] studied the shear and peeling stresses along the interface of single lap adhesive joints subjected to axial loads. Goland and Reissner derived closed form analytical solutions which showed that the peak peeling and shear stresses occurred at the joint edges. Additionally, it was shown that all stresses depended on the joint dimensions and the stiffness properties of the plates. Christensen performed his analysis using the finite element method. He determined that a large stress gradient existed across the thickness of the adhesive as well as along the lap, especially near the ends of the lap. Neither study investigated the effect of temperature on system behavior. Burgreen [Ref. 4] analytically

computed interfacial shear stresses in layered beams and examined the behavior of a bi-metallic beam subjected to a transverse temperature variation. Lau [Ref. 5] derived closed form stress analysis solutions for a chip in a semi-infinite substrate and a chip on substrate with finite thickness subjected to temperature rises.

A typical electronic package consists of a semi-conductor (chip) attached to a substrate material by an adhesive as depicted in Figure 1.1. Placing more power in an ever decreasing space is the trend in electronic component packaging. Power densities of 12.5 MW/m^3 have been reached by today's integrated circuit technology [Ref. 6] and future integrated circuits are expected to have at least twice this power density leading to higher operating temperatures. The resulting high operating temperatures give rise to thermal cycling causing thermal fatigue at the different material interfaces and can lead to premature failure of the circuit. To prevent failure, a maximum temperature of between 100°C and 110°C at a semiconductor junction has been set by the military [Ref. 7].

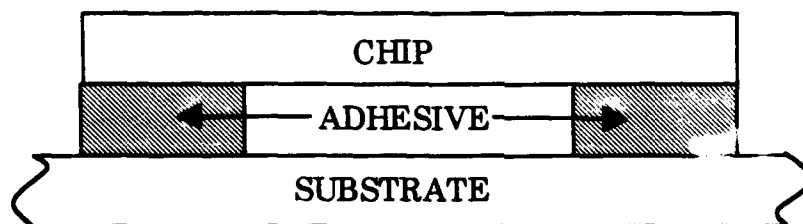


Figure 1.1 Electronic Package

While conducting a literature search, numerous studies concerning the topic of thermal response of electronic packages was uncovered. In perhaps one of the most extensive studies, Suhir [Ref. 8] reviewed work conducted on bi-material and tri-material electronic packages that were either subjected to a uniform temperature or an applied axial load. For the bi-material configuration, it was determined that the maximum peeling and shear stresses along the interface occurred at the outer edges of the assembly. Additionally, it was shown that the stresses depended upon the axial and interfacial compliances of the component layers.

Royce [Ref. 9], Riches [Ref. 10], and Chung [Ref. 11] all state that the primary cause of mechanical stresses that are induced in electronic packages are a result of the difference in coefficients of thermal expansion of the different materials in the assembly. Royce commented that thermal cycling during normal operation could give rise to thermal fatigue at the various material interfaces and could lead to premature failure of the structure. Rich reported that the types of stresses that arose from thermal mismatch consisted of stresses normal to the chip and interfacial stresses. He predicted that normal stresses in the chip were at a maximum in the chip center and decreased to zero at the chip edge. However, the interfacial stresses were zero at the center and rose to a maximum at the edge. Rich concluded that compliance and thickness of the chip attachment materials were critical to controlling the stresses imposed. Two ways to reduce or avoid thermally

induced stresses in electronic packages was proposed by Chung. The first was stress reduction by coefficient of thermal expansion matching and the second was stress reduction by the use of extremely flexible adhesives.

The purpose of this investigation was to gain further insight and understanding into the effects that the various system parameters have on thermally induced behavior of an electronic package as shown on Figure 1.1.

To achieve this, the electronic package was generalized into a tri-material configuration as displayed in Figure 1.2 and a parametric study was conducted using finite element analysis. First, the effect of the material properties, Young's Modulus and coefficient of thermal expansion, was examined. Next, the length of the midlayer was varied. Then, the effect of midlayer thickness on system behavior was studied. Finally, nonuniform temperature fields were imposed on the tri-material configuration.

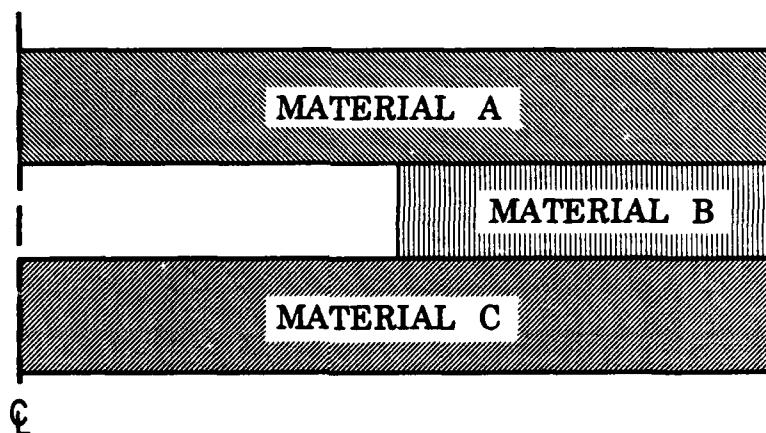


Figure 1.2 Tri-Material Configuration

II. FEM MODEL FORMULATION

The purpose of this investigation was to determine the stresses resulting from a nonuniform temperature field on a tri-material configuration. To accomplish this, a finite element method (FEM) program was constructed. This program is presented in Appendix A and the program exec is in Appendix B.

A. PROGRAM DEVELOPMENT

A recently developed element which provides for both axial and lateral displacement continuity was utilized in the stress formulation. As shown in Figure 2.1, each element has six degrees of freedom; axial displacements at the four corner points; and lateral displacements at the two ends.

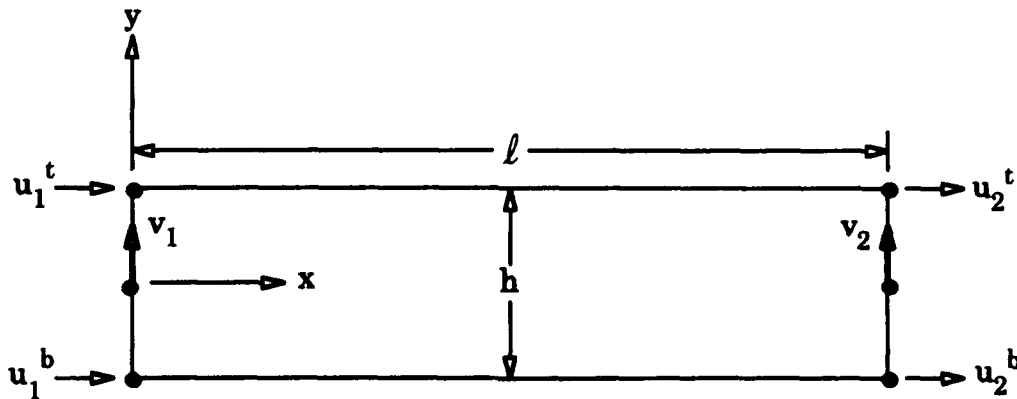


Figure 2.1 A Typical Element With Six Degrees Of Freedom

The lateral displacement field is determined by linear interpolation

$$\bar{v}^e = N_1 v_1^e + N_2 v_2^e \quad (2.1)$$

where v_1 and v_2 are the lateral displacements at the ends and where the linear shape functions N_1 and N_2 are given by

$$N_1 = \frac{1}{l}(l-x) \quad N_2 = \frac{x}{l} \quad (2.2)$$

resulting in

$$v(x) = \sum_{i=1}^2 N_i(x) v_i \quad (2.3)$$

The axial displacement field is assumed to be linear in both the axial and transverse direction. That is,

$$\tilde{u}_1^e = H_1^b u_1^b + H_1^t u_1^t \quad (2.4)$$

$$\tilde{u}_2^e = H_2^b u_2^b + H_2^t u_2^t \quad (2.5)$$

where superscripts b and t refer to the bottom and top respectively. The linear shape functions H_1 and H_2 are given by

$$H_1^b = H_2^b = \frac{1}{h}(h-y) \quad H_1^t = H_2^t = \frac{y}{h} \quad (2.6)$$

resulting in

$$u(x,y) = \sum_{i=1}^2 N_i(x) [H_1(y) u_i^b + H_2(y) u_i^t] \quad (2.7)$$

From strain-displacement relations

$$\epsilon_x = \frac{\partial u}{\partial x} = \frac{\partial}{\partial x} \left(\sum_{i=1}^2 N_i(x) H_1(y) u_i^b + \sum_{i=1}^2 N_i(x) H_2(y) u_i^t \right) \quad (2.8)$$

or

$$e_x = \sum_{i=1}^2 \frac{\partial N_i}{\partial x} (H_1 u_i^b + H_2 u_i^t) \quad (2.9)$$

and

$$\gamma_{xy} = \frac{\partial u}{\partial y} + \frac{\partial v}{\partial x} \quad (2.10)$$

$$\gamma_{xy} = \frac{\partial}{\partial y} \left\{ \sum_{i=1}^2 N_i (H_1 u_i^b + H_2 u_i^t) \right\} + \frac{\partial}{\partial x} \left\{ \sum_{i=1}^2 N_i v_i \right\} \quad (2.11)$$

or

$$\gamma_{xy} = \sum_{i=1}^2 N_i \left\{ \frac{\partial H_1}{\partial y} u_i^b + \frac{\partial H_2}{\partial y} u_i^t \right\} + \sum_{i=1}^2 \frac{\partial N_i}{\partial x} v_i \quad (2.12)$$

The derivatives of the linear shape functions are

$$\frac{\partial N_1}{\partial x} = -\frac{1}{l} \quad \frac{\partial N_2}{\partial x} = \frac{1}{l} \quad \frac{\partial H_1}{\partial y} = -\frac{1}{h} \quad \frac{\partial H_2}{\partial y} = \frac{1}{h} \quad (2.13)$$

This results in

$$e_x = \frac{H_1(y)}{l} (u_2^b - u_1^b) + \frac{H_2(y)}{l} (u_2^t - u_1^t) \quad (2.14)$$

and

$$\gamma_{xy} = \frac{N_1(x)}{h} (u_1^t - u_1^b) + \frac{N_2(x)}{h} (u_2^t - u_2^b) + \frac{v_2 - v_1}{l} \quad (2.15)$$

Defining the axial displacement vector as

$$\{\delta_B\}^T = \langle u_1^b \quad u_1^t \quad u_2^b \quad u_2^t \rangle \quad (2.16)$$

and the stiffness matrix as

$$[K_B] = \int_0^l \int_0^h \{B\} E \{B\}^T dy dx \quad (2.17)$$

where the B vector is

$$\{B\}^T = \langle \frac{\partial N_1}{\partial x} H_1 \quad \frac{\partial N_1}{\partial x} H_2 \quad \frac{\partial N_2}{\partial x} H_1 \quad \frac{\partial N_2}{\partial x} H_2 \rangle \quad (2.18)$$

and the force vector due to temperature as

$$\{F_B\} = \frac{Eh}{6I} \int_0^l \int_0^h \{B\} E \alpha \Delta T dy dx \quad (2.19)$$

gives the bending matrix equation as

$$[K_B] \{\delta_B\} = \{F_B\} \quad (2.20)$$

Equation 2.20 defines the bending behavior. Additionally, the stiffness matrix can be shown as

$$[K_B] = \frac{Eh}{6I} \begin{bmatrix} 2 & 1 & -2 & -1 \\ 1 & 2 & -1 & -2 \\ -2 & -1 & 2 & 1 \\ 1 & -2 & 1 & 2 \end{bmatrix} \quad (2.21)$$

Behavior due to shear is obtained as follows. Define the row vector of displacement degrees of freedom as

$$\{\delta_s\}^T = \langle u_1^b \quad u_1^t \quad v_1 \quad u_2^b \quad u_2^t \quad v_2 \rangle \quad (2.22)$$

The shear stiffness matrix is given by

$$[K_s] = \int_0^l \int_0^h \{B\}^T G \{B\} dy dx \quad (2.23)$$

where

$$\{B\}^T = \left(N_1 \frac{\partial H_1}{\partial y} \quad N_2 \frac{\partial H_2}{\partial y} \quad \frac{\partial N_1}{\partial x} \quad N_2 \frac{\partial H_1}{\partial y} \quad N_2 \frac{\partial H_2}{\partial y} \quad \frac{\partial N_2}{\partial x} \right) \quad (2.24)$$

which gives the equations for shear behavior

$$[K_s] \{\delta_s\} = \{0\} \quad (2.25)$$

Additionally, the stiffness matrix can be shown as

$$[K_s] = G \begin{bmatrix} \frac{l}{4h} & \frac{-l}{4h} & \frac{1}{2} & \frac{l}{4h} & \frac{-l}{4h} & \frac{-1}{2} \\ \frac{-l}{4h} & \frac{l}{4h} & \frac{-1}{2} & \frac{-l}{4h} & \frac{l}{4h} & \frac{1}{2} \\ \frac{1}{2} & \frac{-1}{2} & \frac{h}{l} & \frac{1}{2} & \frac{-1}{2} & \frac{-h}{l} \\ \frac{l}{4h} & \frac{-l}{4h} & \frac{1}{2} & \frac{l}{4h} & \frac{-l}{4h} & \frac{-1}{2} \\ \frac{-l}{4h} & \frac{l}{4h} & \frac{-1}{2} & \frac{-l}{4h} & \frac{l}{4h} & \frac{1}{2} \\ \frac{-1}{2} & \frac{1}{2} & \frac{-h}{l} & \frac{-1}{2} & \frac{1}{2} & \frac{h}{l} \end{bmatrix} \quad (2.26)$$

The system matrix for bending and shear is

$$[K] = [K_b] + [K_s] \quad (2.27)$$

Let

$$a = \frac{Gl}{4h} \quad b = \frac{Gh}{l} \quad c = \frac{Eh}{6l} \quad d = \frac{G}{2} \quad (2.28)$$

then

$$[K] = \begin{bmatrix} a+2c & -a+c & d & a-2c & -a-c & -d \\ -a+c & a+2c & -d & -a-c & a-2c & d \\ d & -d & b & d & -d & -b \\ a-2c & -a-c & d & a+2c & -a+c & -d \\ -a-c & a-2c & -d & -a+c & a+2c & d \\ -d & d & -b & -d & d & b \end{bmatrix} \quad (2.29)$$

The force vector due to a temperature field is

$$\{F^e\} = \Omega^e \int_0^l \int_0^h \{B\} dy dx \quad (2.30)$$

where

$$\Omega^e = (E\alpha \Delta T)^e \quad (2.31)$$

or

$$\{F^e\} = \Omega^e \int_0^l \int_0^h \left\{ \begin{array}{c} \frac{\partial N_1}{\partial x} H_1 \\ \frac{\partial N_2}{\partial x} H_2 \\ 0 \\ \frac{\partial N_2}{\partial x} H_1 \\ \frac{\partial N_1}{\partial x} H_2 \\ 0 \end{array} \right\} dy dx \quad (2.32)$$

Let

$$\Lambda^e = \Omega^e \frac{h}{2} \quad (2.33)$$

then

$$\{F^e\} = \Lambda^e \begin{Bmatrix} -1 \\ -1 \\ 0 \\ 1 \\ 1 \\ 0 \end{Bmatrix} \quad (2.34)$$

After solving

$$[K]\{\delta\} = \{F\} \quad (2.35)$$

for $\{\delta\}$, the stresses can be calculated. For the e^{th} element, the bending stress is

$$\sigma_x = E \epsilon_x \quad (2.36)$$

or

$$\sigma_x^{b_e} = \frac{1}{l} (u_2^b - u_1^b) = \frac{\delta_4 - \delta_1}{l} \quad (2.37)$$

$$\sigma_x^{t_e} = \frac{1}{l} (u_2^t - u_1^t) = \frac{\delta_5 - \delta_2}{l} \quad (2.38)$$

where $\sigma_x^{b_e}$ and $\sigma_x^{t_e}$ are the bending stresses acting on the e^{th} element at the

bottom and top respectfully. The shear stress is

$$\tau_{xy} = G\gamma_{xy} \quad (2.39)$$

or

$$\tau_{xy}^{b_e} = G \left\{ \frac{u_1^t - u_1^b}{h} + \frac{v_2 - v_1}{l} \right\} = G \left\{ \frac{\delta_2 - \delta_1}{h} + \frac{\delta_6 - \delta_3}{l} \right\} \quad (2.40)$$

$$\tau_{xy}^{t_e} = G \left\{ \frac{u_2^t - u_2^b}{h} + \frac{v_2 - v_1}{l} \right\} = G \left\{ \frac{\delta_5 - \delta_4}{h} + \frac{\delta_6 - \delta_3}{l} \right\} \quad (2.41)$$

where $\tau_{xy}^{b_e}$ and $\tau_{xy}^{t_e}$ are the shear stresses acting on the e^{th} element at the bottom and top respectfully. Finally

$$\tau_{AVE}^e = \frac{G}{2} \left\{ \frac{(\delta_2 + \delta_5) - (\delta_1 + \delta_4)}{h} + \frac{2(\delta_6 - \delta_3)}{l} \right\} \quad (2.42)$$

B. PROGRAM INPUT

The input file for the finite element program is displayed in Appendix C. A mesh grid with 200 elements as shown in Figure 2.2 is generated. The input file allows for variation in both the element layer thicknesses and the element row widths. Values for Young's Modulus, Poisson's Ratio, and the coefficient of thermal expansion can be inputted row by row. Additionally, the temperature for each level of the mesh can be inputted. Appendix C is annotated, showing the placement of the different inputs. All dimensions are in millimeters.

C. PROGRAM OUTPUT

The output file from the finite element program is shown in Appendix D. The force and displacement vectors for each node are outputted. The top and bottom bending stresses and shear stress for each element are also displayed. Additionally, the normal stresses along the material A and material B interface and the material B and material C interface are outputted.

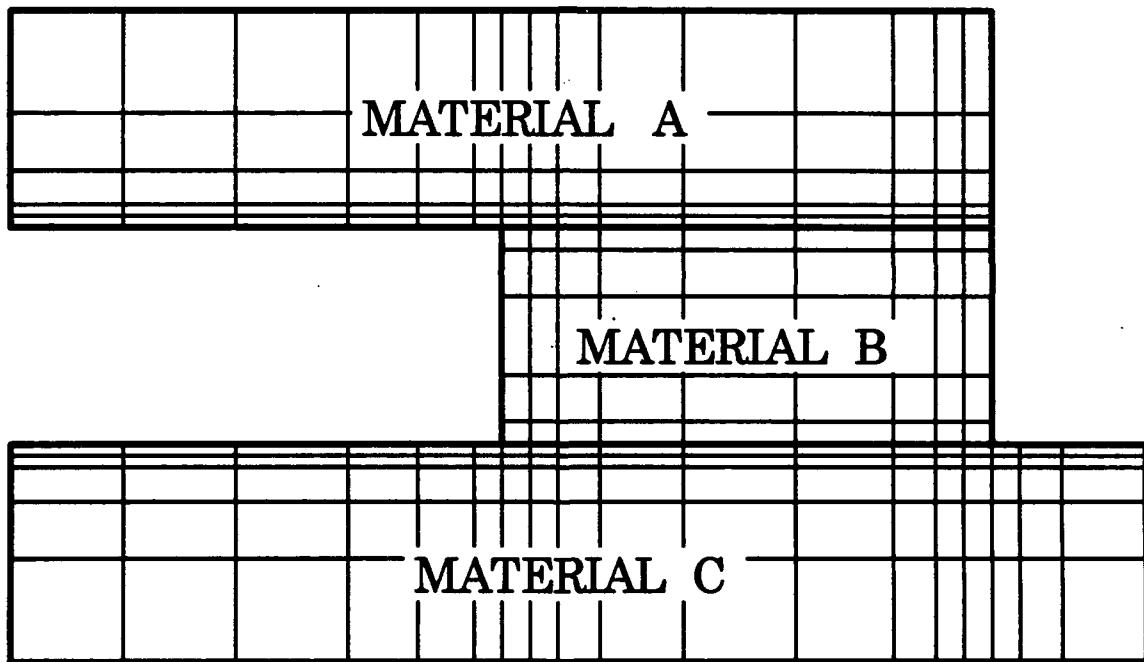


Figure 2.2 Finite Element Analysis Mesh For Tri-material Configuration

III. EFFECT OF MATERIAL PROPERTIES

This chapter studies the effect of Young's Modulus and the coefficient of thermal expansion on the tri-material configuration of Figure 3.1. Several computer runs were made assigning different Young's Modulus values to the three materials while maintaining a constant coefficient of thermal expansion value. No stresses resulted. As a consequence, the remainder of this chapter is concerned with variations in the coefficient of thermal expansion (α_i). Table 3.1 shows the parameters used for the 11 cases that were evaluated. For all cases, Young's Modulus was given a constant value of 100 GPa for the three materials and a change in temperature of 100°C was imposed.

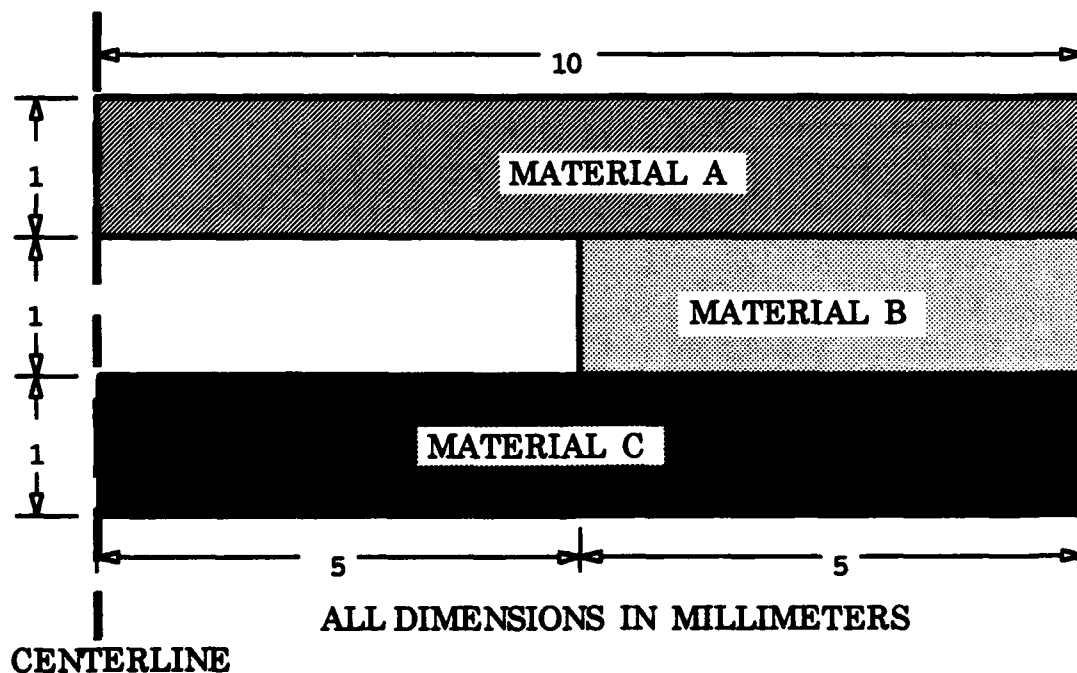


Figure 3.1 Tri-material Configuration

TABLE 3.1 COEFFICIENT OF THERMAL EXPANSION STUDY

CASE	α_A (10^{-6})	α_B (10^{-6})	α_C (10^{-6})
1	100	50	100
2	100	200	100
3	300	100	10
4	300	10	100
5	100	300	10
6	150	100	10
7	200	100	10
8	400	100	10
9	200	100	1
10	200	100	50
11	200	100	75

The eleven cases were grouped into four combinations to allow comparisons to be made. The combinations were:

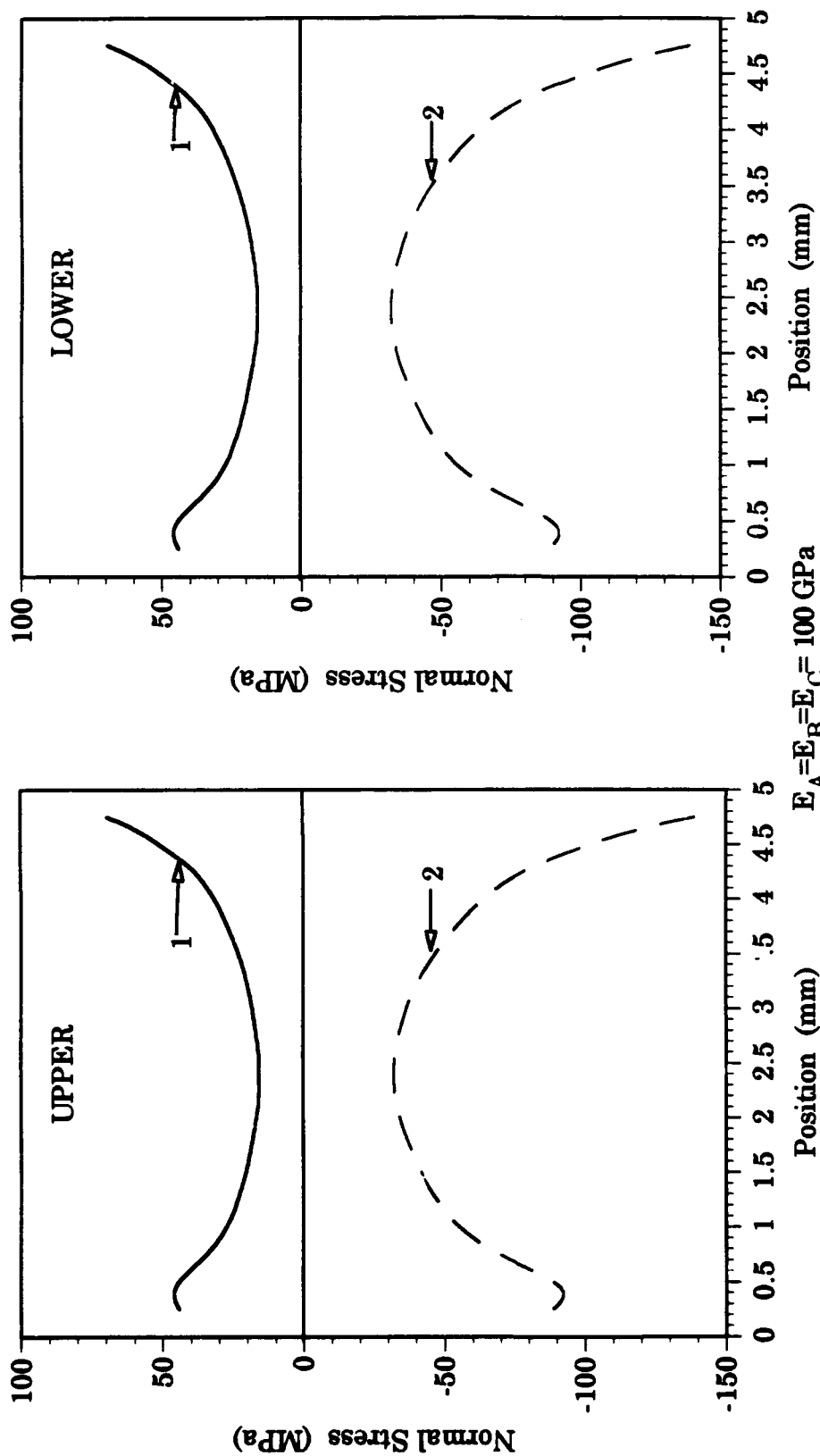
- Cases 1 and 2. α_A and α_C were set equal and α_B was allowed to range from one-half α_A , α_C to twice α_A , α_C .
- Cases 3, 4, and 5. α_A , α_B , and α_C were given different values in different combinations.
- Cases 3, 6, 7, and 8. α_B and α_C were held constant but at different values while α_A was allowed to range at values greater than α_B and α_C .
- Cases 7, 9, 10, and 11. α_A and α_B were held constant but at different values while α_C was allowed to range at values less than α_A and α_B .

A. CASES 1 AND 2

Cases 1 and 2 investigated how the tri-material configuration responded when the top and bottom layers (materials A and C) held the same value of the coefficient of thermal expansion while the middle layer was given values lower (case 1) and higher (case 2).

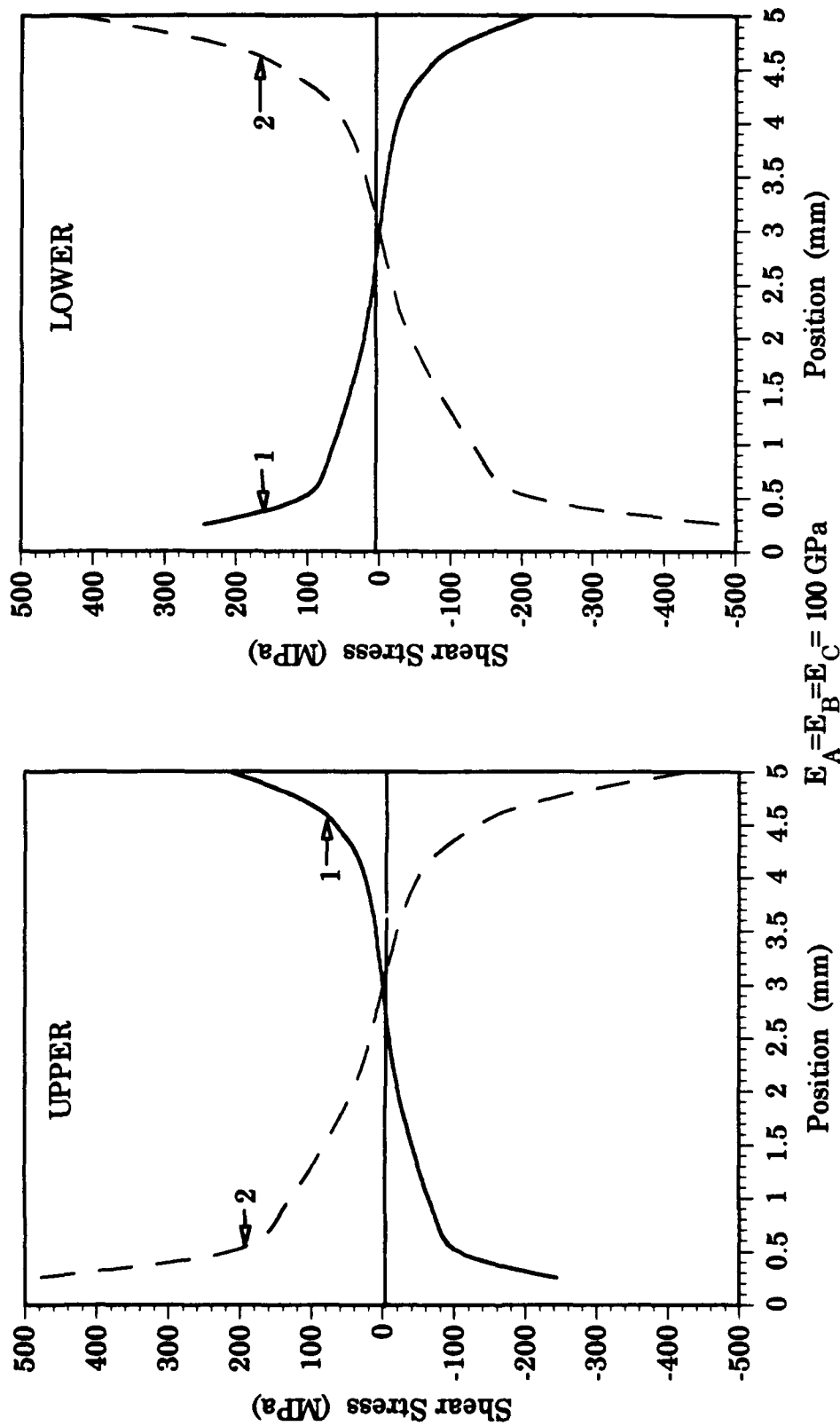
Figure 3.2 is a plot of the normal stress along the upper interface (between materials A and B) and lower interface (between materials B and C) as a function of position. For case 1, both the upper and lower interfaces are in tension, showing that the top and bottom layers with their larger amount of expansion, wanting to peel away from the middle layer. In case 2, the normal stresses at the upper and lower interfaces are all compressive, that is, have bearing stresses. The middle layer wants to expand more than the top and bottom layers and pushes against them. For both cases, the maximum stresses occur at the ends of the configuration.

Figure 3.3 is a graph of the shear stresses acting on the upper and lower interfaces. The shear stresses for case 1 tend to axially extend the midlayer while the shear stresses for case 2 tend to axially compress the midlayer. Figure 3.4 shows the shear and normal stresses acting on the midlayer for cases 1 and 2.



Case	$\alpha_A (\times 10^{-6}/^{\circ}\text{C})$	$\alpha_B (\times 10^{-6}/^{\circ}\text{C})$	$\alpha_C (\times 10^{-6}/^{\circ}\text{C})$
Case 1	100	50	100
Case 2	100	200	100

Figure 3.2 Normal Stress At Interfaces For Cases 1 And 2



Case	$\alpha_A (\times 10^{-6} / ^\circ\text{C})$	$\alpha_B (\times 10^{-6} / ^\circ\text{C})$	$\alpha_C (\times 10^{-6} / ^\circ\text{C})$
1	100	50	100
2	100	200	100

Figure 3.3 Shear Stress At Interfaces For Cases 1 And 2

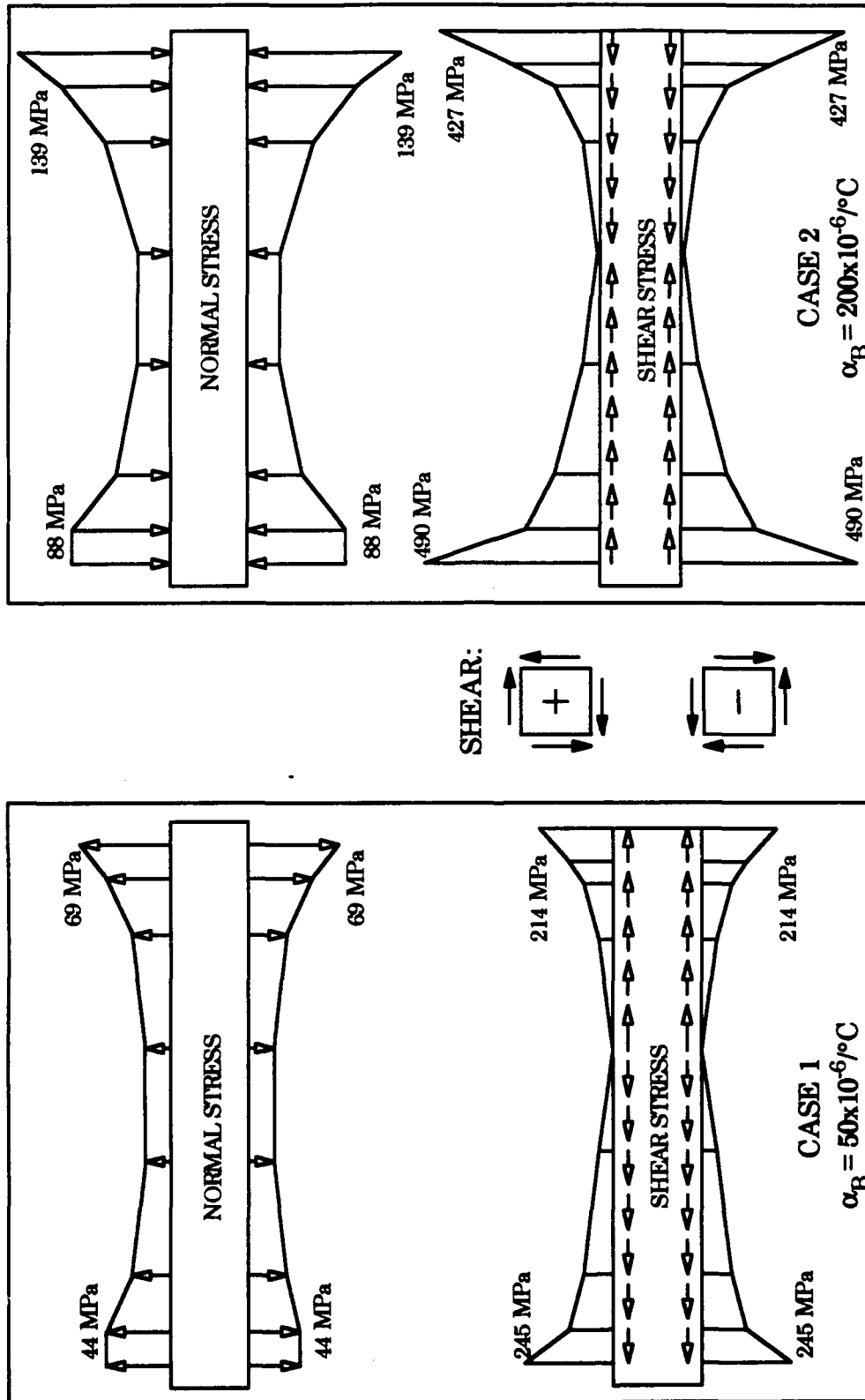


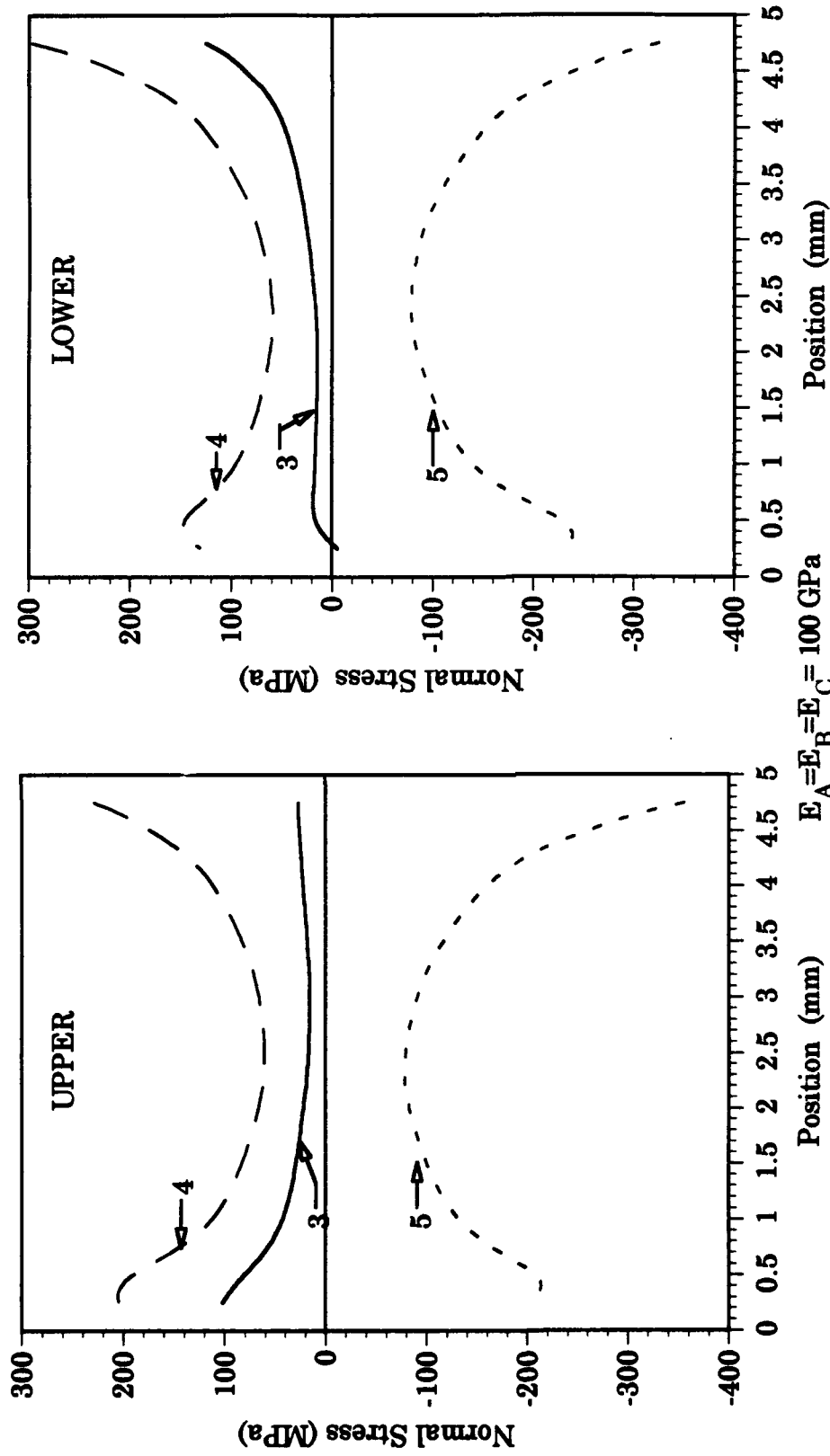
Figure 3.4 Shear And Normal Stresses On The Midlayer For Cases 1 And 2

B. CASES 3, 4, AND 5

Cases 3, 4, and 5 investigated the response of the tri-material configuration when all three layers had different values for the coefficients of thermal expansion. Case 3 was arranged with magnitudes as: $\alpha_A > \alpha_B > \alpha_C$, case 4 as: $\alpha_A > \alpha_C > \alpha_B$, and case 5 as: $\alpha_B > \alpha_A > \alpha_C$.

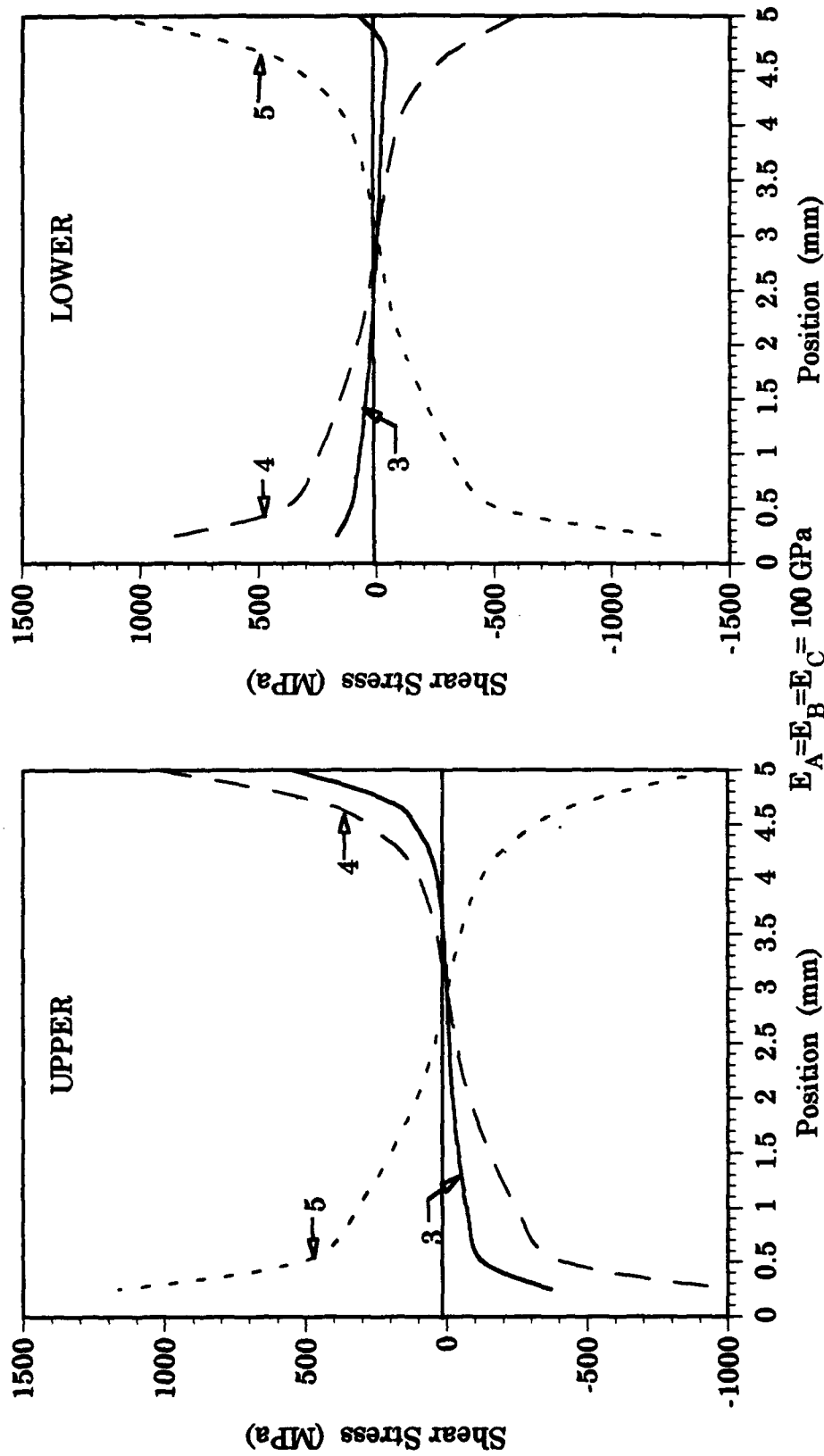
Figure 3.5 is a plot of the normal stresses as a function of position along the upper and lower interfaces. Case 3, with the coefficients of thermal expansion in decreasing order from top to bottom, displayed minimal peeling stresses along the interfaces. Case 4, with the coefficient of thermal expansion lowest in the midlayer, exhibited characteristics similar to case 1. The normal stresses were peeling on both interfaces. Case 5, with the coefficient of thermal expansion in the middle layer the largest, behaved like case 2. The normal stresses along the upper and lower interfaces were bearing throughout.

The plots for the shear stresses along the upper and lower interfaces are shown in Figure 3.6. In case 3 the shearing stresses were the lowest, with material B wanting to elongate axially along the upper interface. The midlayer wanted to axially elongate for case 4 and to axially compress for case 5. This was the same behavior that was observed for cases 1 and 2, respectfully. Figure 3.7 displays the shear and normal stresses acting along the midlayer interface.



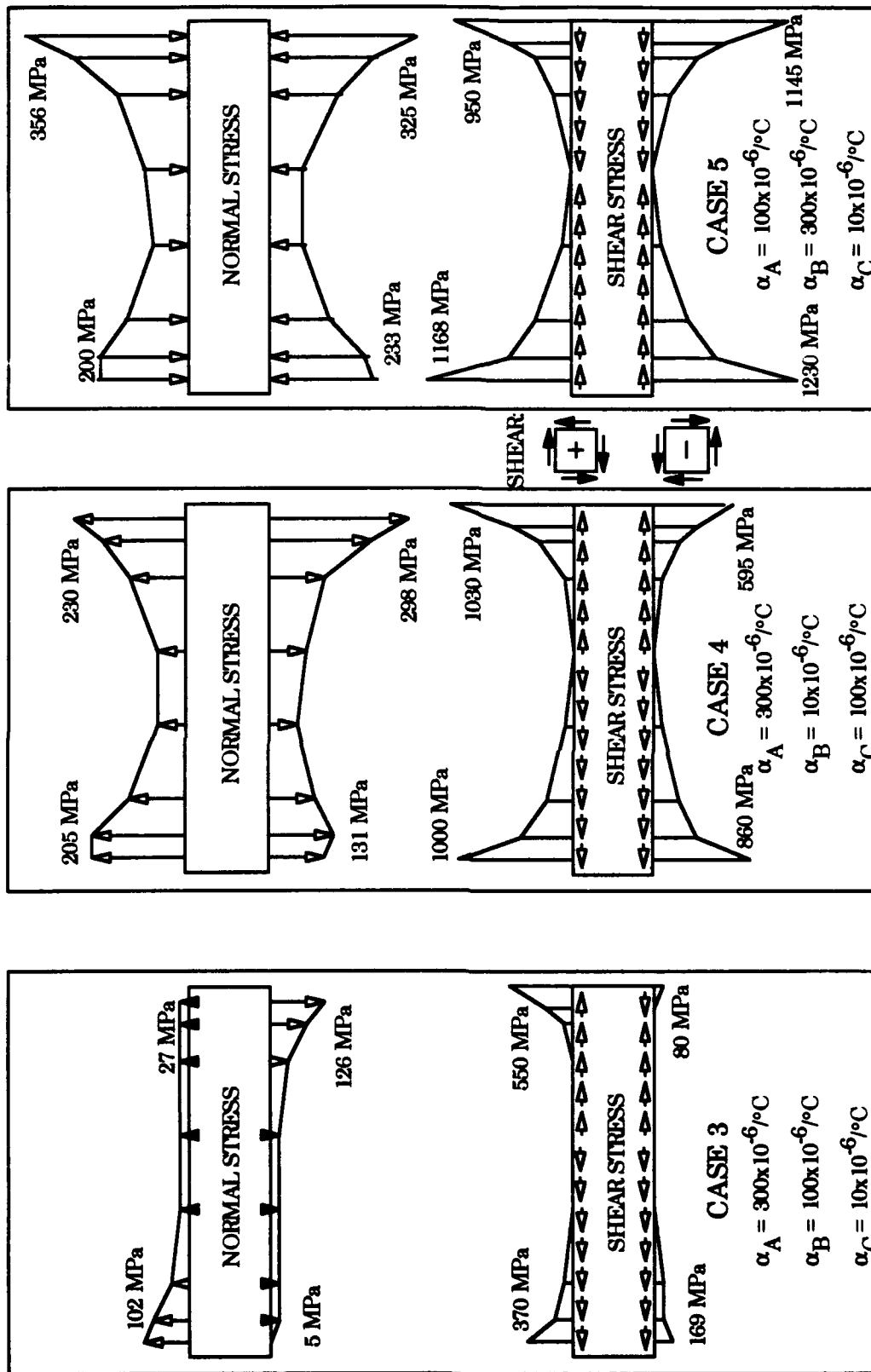
Case	$\alpha_A (\times 10^{-6} / ^\circ\text{C})$	$\alpha_B (\times 10^{-6} / ^\circ\text{C})$	$\alpha_C (\times 10^{-6} / ^\circ\text{C})$
3	300	100	10
4	300	10	100
5	100	300	10

Figure 3.5 Normal Stress At Interfaces For Cases 3, 4, And 5



Case	$\alpha_A (\times 10^{-6} / ^\circ\text{C})$	$\alpha_B (\times 10^{-6} / ^\circ\text{C})$	$\alpha_C (\times 10^{-6} / ^\circ\text{C})$
3	300	100	10
4	300	10	100
5	100	300	10

Figure 3.6 Shear Stress At Interfaces For Cases 3, 4, And 5



$$E_A = E_B = E_C = 100 \text{ GPa}$$

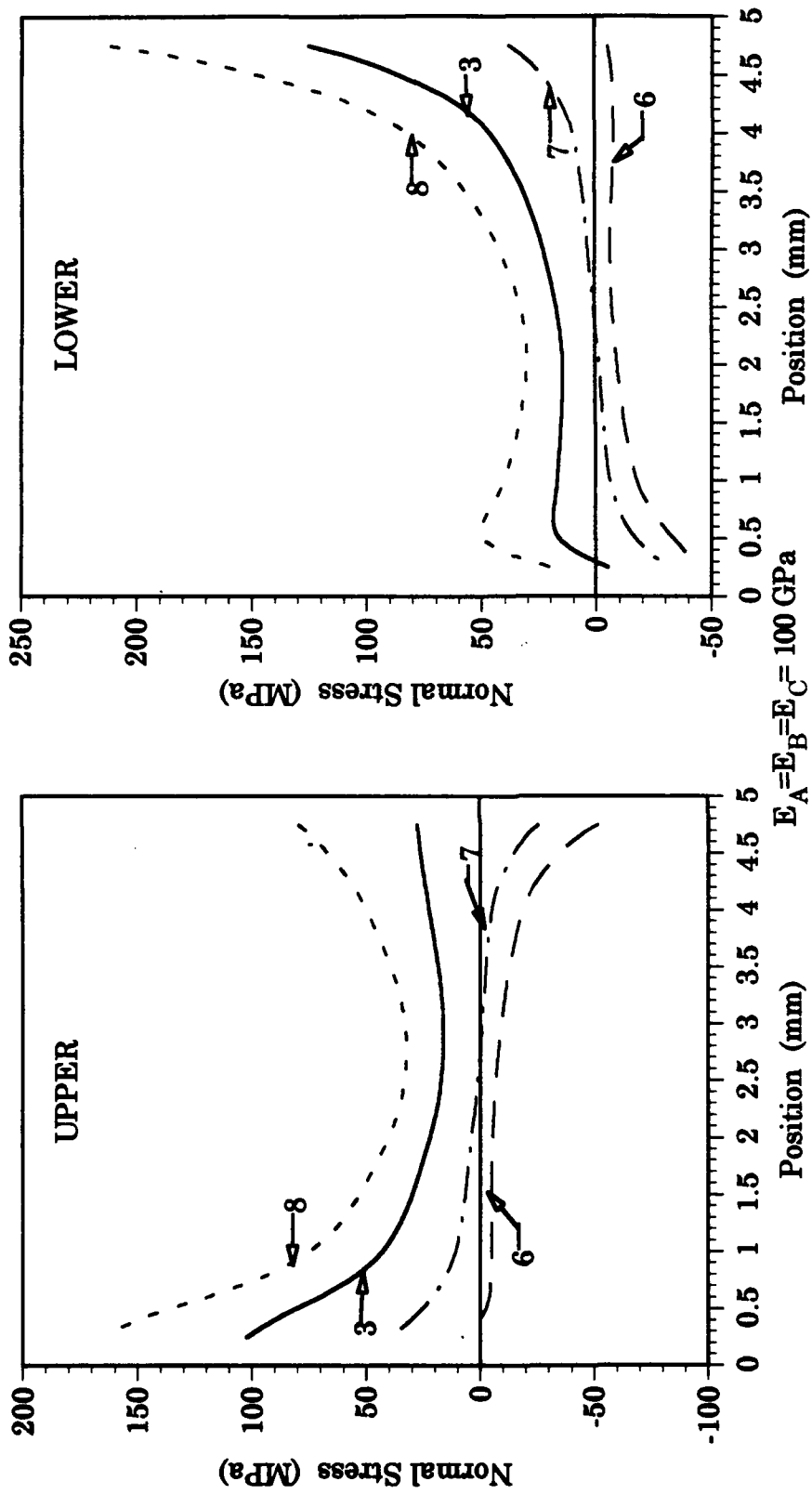
Figure 3.7 Shear And Normal Stresses On The Midlayer For Cases 3, 4, And 5

C. CASES 3, 6, 7, AND 8

This study compared the responses of the tri-material configuration when α_B and α_C were held constant at values lower than α_A (with $\alpha_B > \alpha_C$), and α_A was then allowed to increase as follows: α_A (case 6) $<$ α_A (case 7) $<$ α_A (case 3) $<$ α_A (case 8).

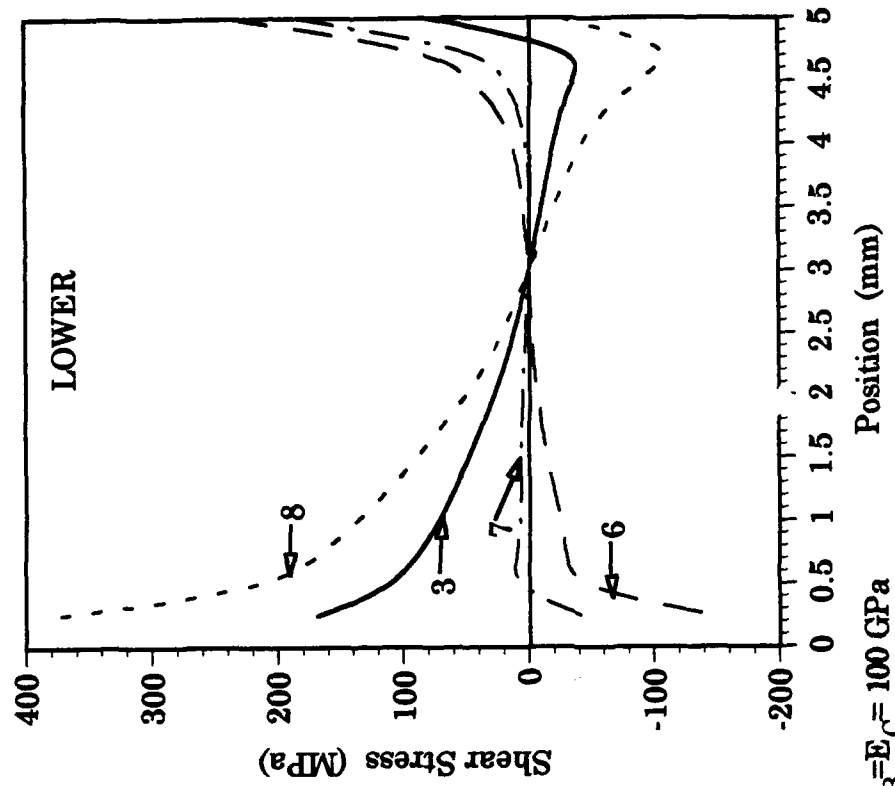
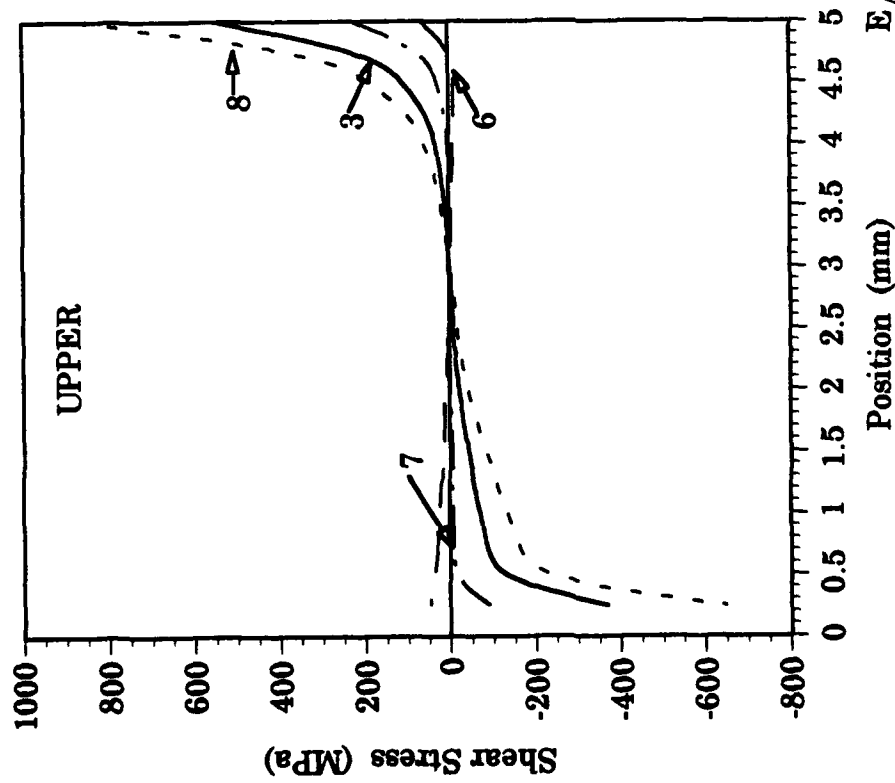
Figure 3.8 is a graph of the normal stresses along the upper and lower interfaces for the midlayer. When the value of the coefficient of thermal expansion for the upper layer was kept reasonably close to the coefficient of thermal expansion of the midlayer (within a factor of two) as shown by cases 6 and 7, the normal stresses tended to be minimal and were mainly bearing. However, when α_A was further increased as in cases 3 and 8, the magnitudes of the normal stresses increased and became peeling throughout the upper and lower midlayer interfaces.

The shear stress plot for the upper and lower interfaces is given in Figure 3.9. Cases 6 and 7 resulted in shearing stresses at both ends of the upper and lower interfaces with minimal shear stresses along the majority of the interface lengths. In cases 3 and 8, the shearing stresses on both interfaces tended to axially stretch the midlayer with case 8 having a larger magnitude of stress. Figures 3.10 and 3.11 display the shear and normal stresses acting on the midlayer for cases 3, 6, 7, and 8.



Case	$\alpha_A (\times 10^{-6} / ^\circ\text{C})$	$\alpha_B (\times 10^{-6} / ^\circ\text{C})$	$\alpha_C (\times 10^{-6} / ^\circ\text{C})$
3	300	100	10
6	150	100	10
7	200	100	10
8	400	100	10

Figure 3.8 Normal Stress At Interfaces For Cases 3, 6, 7, And 8



$E_A = E_B = E_C = 100 \text{ GPa}$

Case	$\alpha_A (\times 10^{-6} / ^\circ\text{C})$	$\alpha_B (\times 10^{-6} / ^\circ\text{C})$	$\alpha_C (\times 10^{-6} / ^\circ\text{C})$
3	300	100	10
6	150	100	10
7	200	100	10
8	400	100	10

Figure 3.9 Shear Stress At Interfaces For Cases 3, 6, 7, And 8

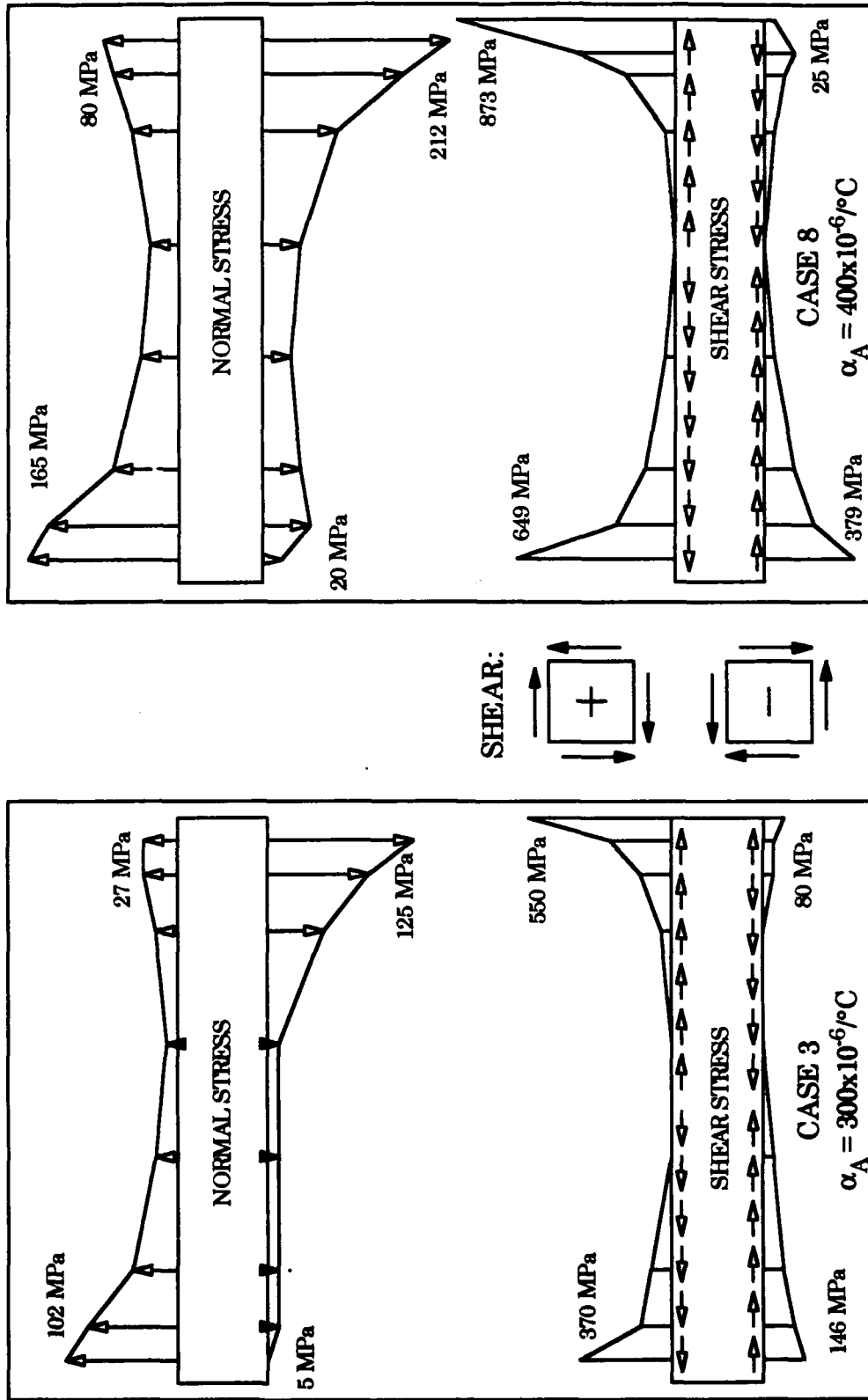


Figure 3.10 Shear And Normal Stresses On The Midlayer For Cases 3 And 8

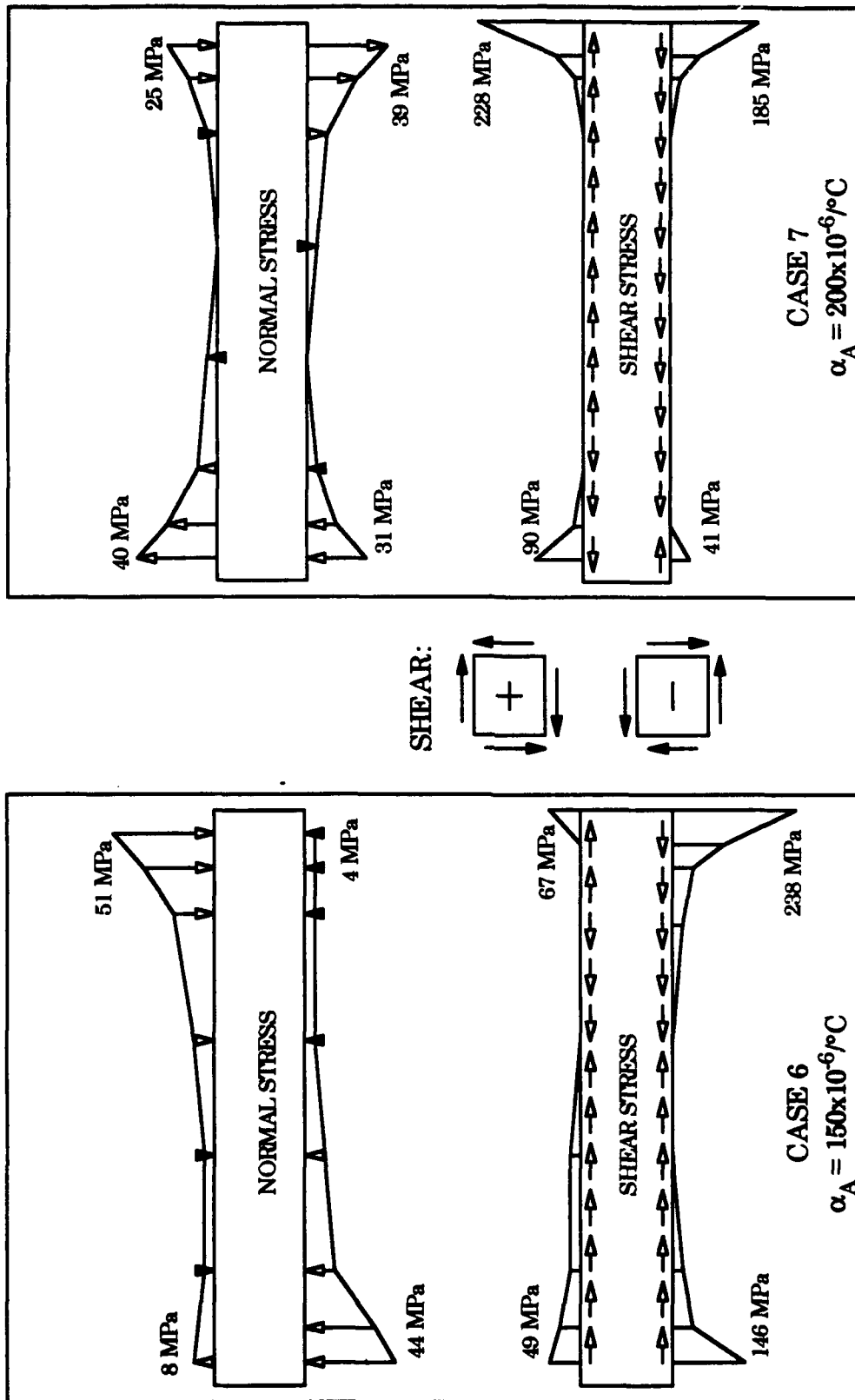


Figure 3.11 Shear And Normal Stresses On The Midlayer For Cases 6 And 7

D. CASES 7, 9, 10, AND 11

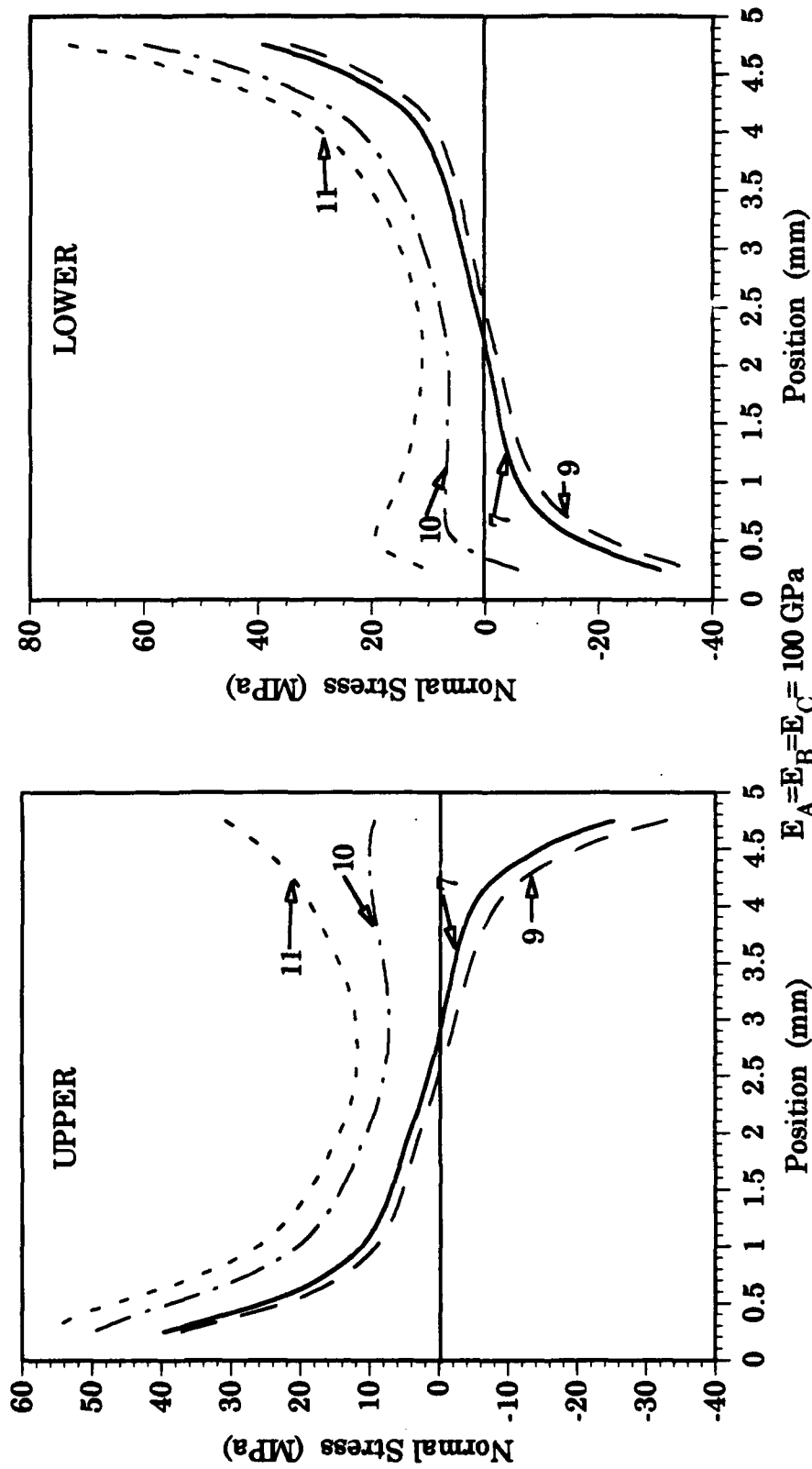
In this grouping, the coefficients of thermal expansion for materials A and B were held constant at values greater than material C (with $\alpha_A > \alpha_B$), and α_C was allowed to increase as follows: α_C (case 9) $<$ α_C (case 7) $<$ α_C (case 10) $<$ α_C (case 11).

Figure 3.12 is a plot of the upper and lower interface normal stresses for the four cases. Similar characteristics were displayed by cases 7 and 9. Along the upper interface the normal stress was initially peeling, decreased to zero, and then became bearing. At the lower interface the normal stresses were initially bearing, went to zero, and then became peeling. For cases 10 and 11 the normal stresses were peeling on both the upper and lower interfaces.

A plot of the shear stresses acting on the midlayer is shown in Figure 3.13. As can be seen, along the upper interface all four cases displayed similar shear stress characteristics with the surface being pulled in axial tension. However, at the lower interface, cases 7 and 9 showed axial compression while cases 10 and 11 displayed axial tension. The shear and normal stresses acting on the midlayer for these four cases are shown in Figure 3.14 and 3.15.

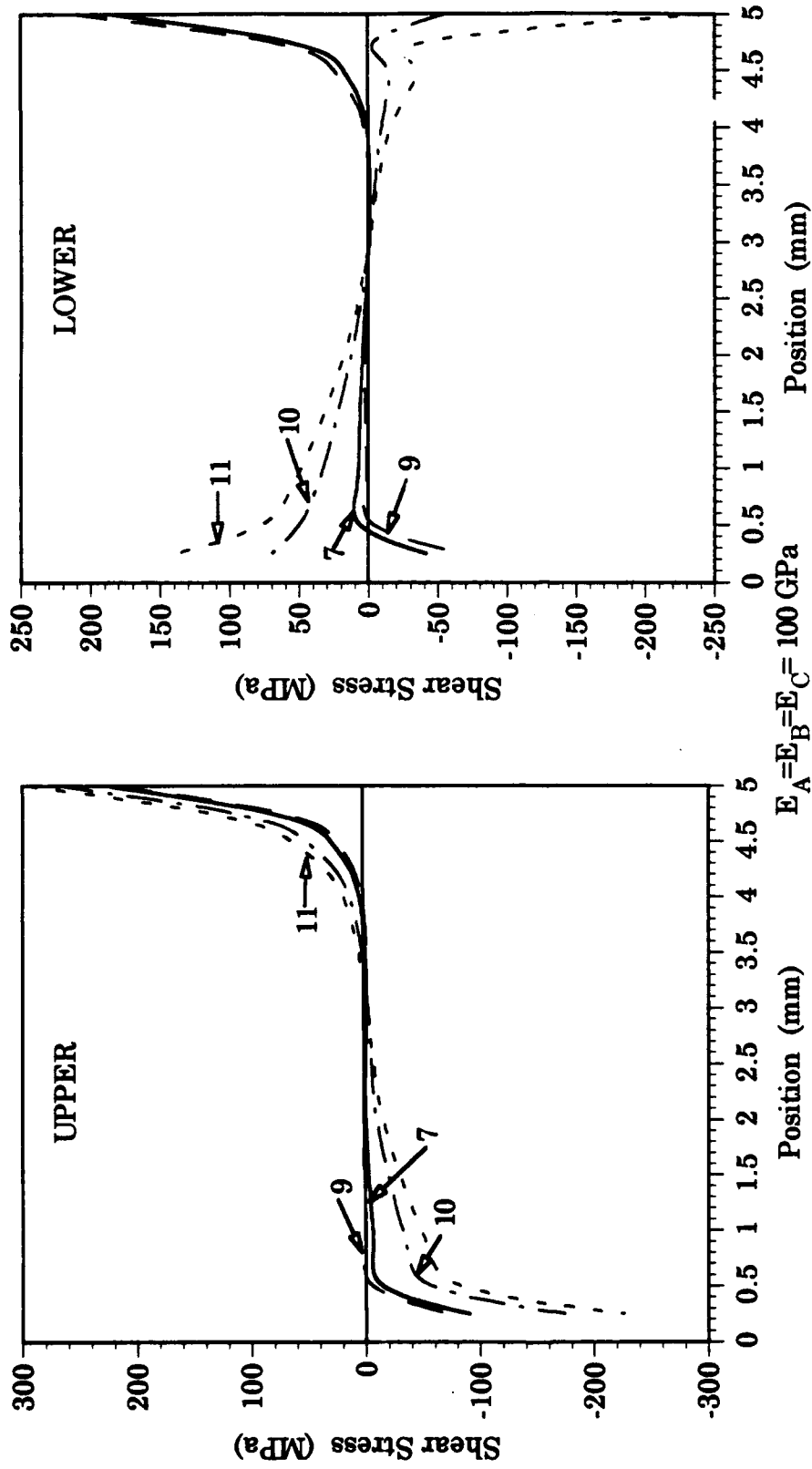
E. SUMMARY

A review of the peeling and shear stresses acting along the upper and lower interfaces reveals force equilibrium in both the lateral and axial directions. However, moment equilibrium is not satisfied exactly. This



Case	$\alpha_A (\times 10^{-6} / ^\circ\text{C})$	$\alpha_B (\times 10^{-6} / ^\circ\text{C})$	$\alpha_C (\times 10^{-6} / ^\circ\text{C})$
7	200	100	10
9	200	100	1
10	200	100	50
11	200	100	75

Figure 3.12 Normal Stresses At Interfaces For Cases 7, 9, 10, And 11



Case	$\alpha_A (\times 10^{-6} / ^\circ\text{C})$	$\alpha_B (\times 10^{-6} / ^\circ\text{C})$	$\alpha_C (\times 10^{-6} / ^\circ\text{C})$
7	200	100	10
9	200	100	1
10	200	100	50
11	200	100	75

Figure 3.13 Shear Stress At Interfaces For Cases 7, 9, 10, And 11

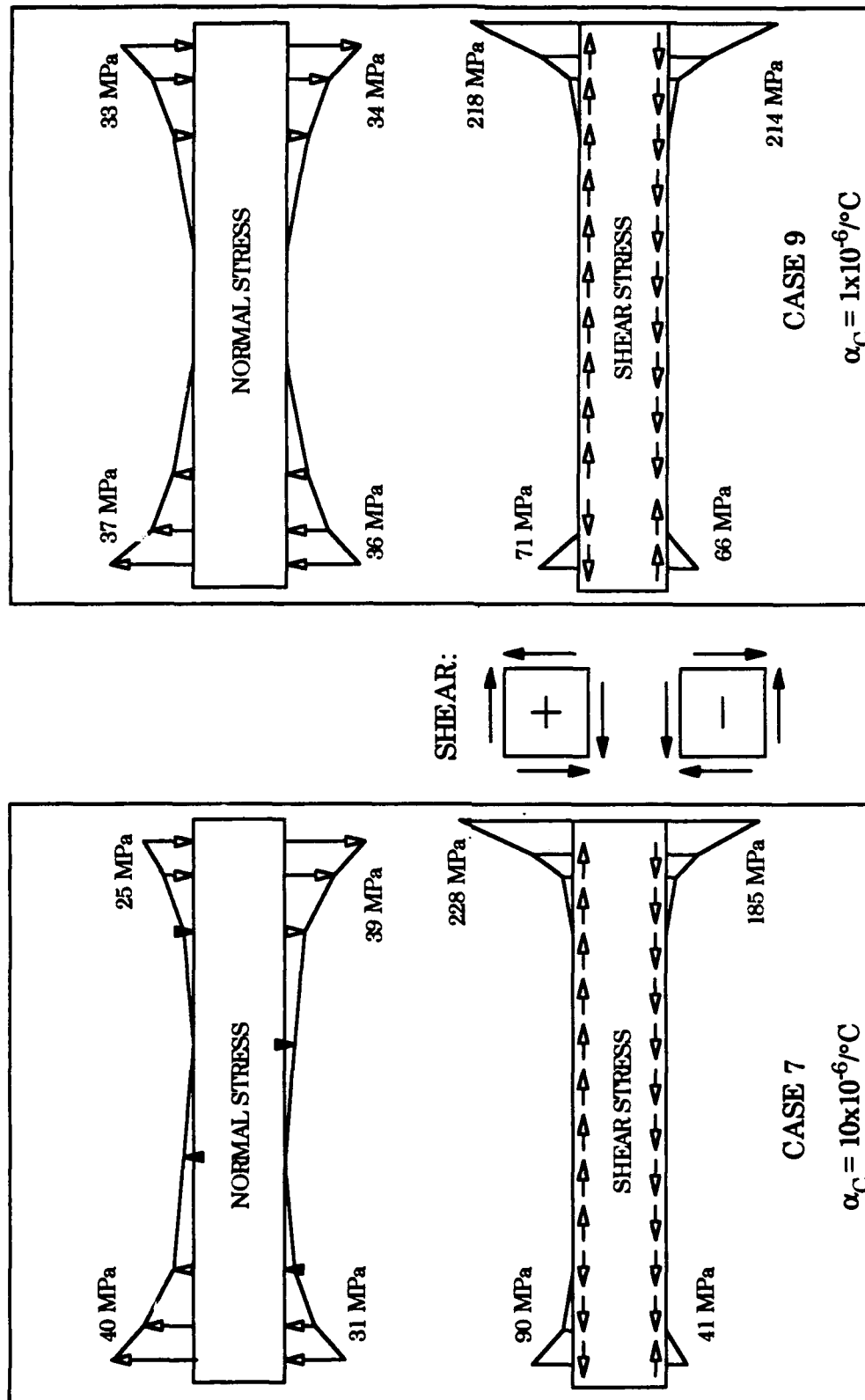
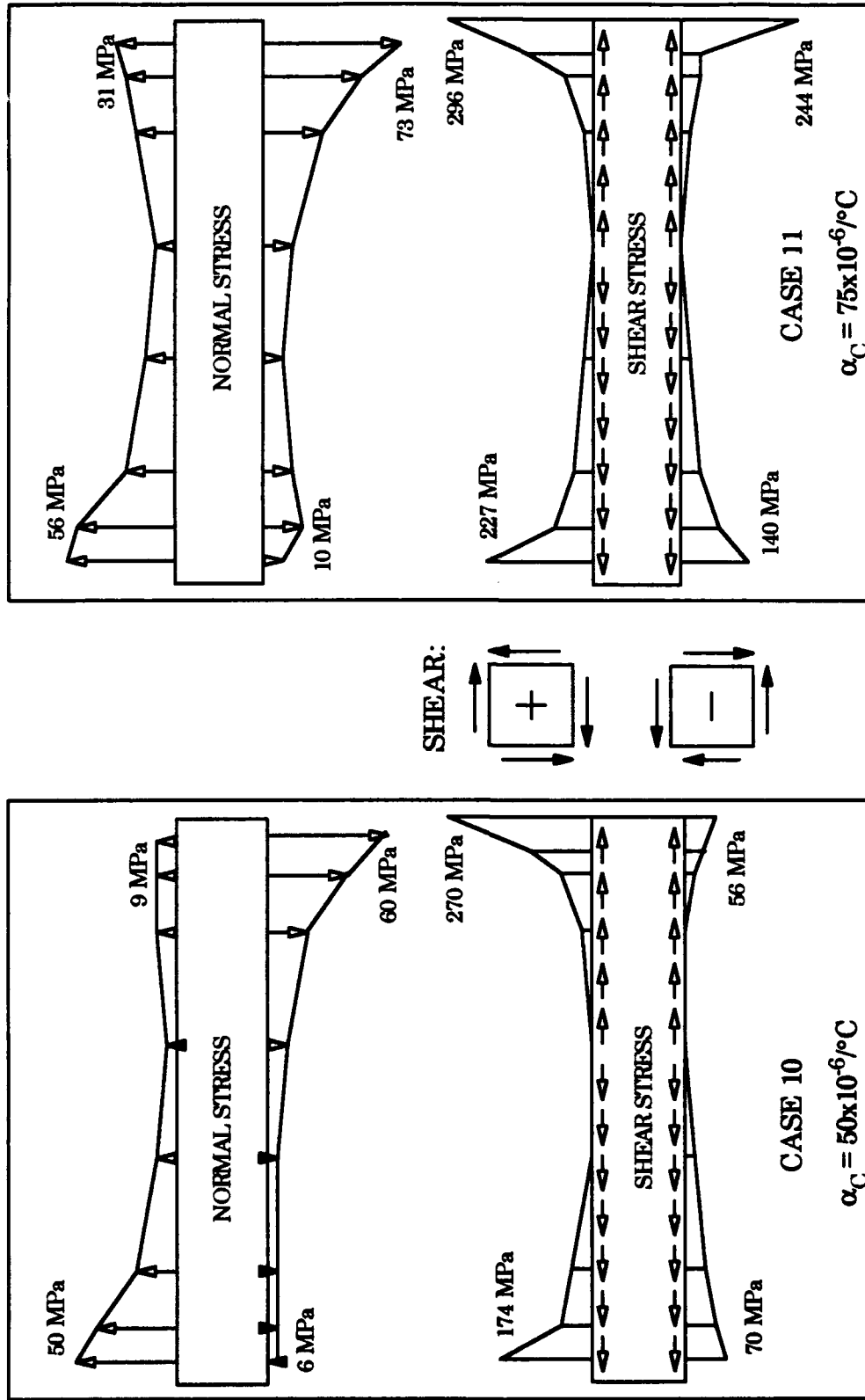


Figure 3.14 Shear And Normal Stresses On The Midlayer For Cases 7 And 9



$$\alpha_A = 200 \times 10^{-6} / ^\circ\text{C} \quad \alpha_B = 100 \times 10^{-6} / ^\circ\text{C}$$

$$E_A = E_B = E_C = 100 \text{ GPa}$$

Figure 3.15 Shear And Normal Stresses On The Midlayer For Cases 10 And 11

deviation is most probably a result of the type of finite element that was chosen.

As expected, when materials A and C were given the same properties, symmetrical stress conditions resulted. This was clearly shown in cases 1 and 2. When the coefficient of thermal expansion in the midlayer was smaller, the upper and lower layers wanted to separate from the middle layer. When the coefficient of thermal expansion for the midlayer was greater, the top and bottom layers tended to compress it.

Maximum peeling stresses occurred when the coefficient of thermal expansion for the top or bottom layer was much greater than the middle layer as shown in case 4. Similarly, the maximum bearing stresses arose when the midlayer coefficient of thermal expansion was greater than the upper and lower layers as evidenced by case 5.

The relative difference in the coefficient of thermal expansion between the layers played a similar role for the shear stresses. The maximum tendency to axially elongate the midlayer occurred when the coefficient of thermal expansion for the middle layer was much less than the upper or lower layers. Additionally, the maximum tendency to axially compress the midlayer happened when the coefficient of thermal expansion for the midlayer was much greater than the top or bottom layers.

Minimal normal stresses resulted when the values of the coefficients of thermal expansion for the upper, middle, and lower approached each other. The conditions for minimum shearing stresses were the same.

The study of cases 7, 9, 10, and 11 produced an interesting result. As can be seen, cases 7 and 9 exhibited very similar stress states even though the coefficients of thermal expansion for the bottom layer differed by a factor of ten. More computer runs were conducted, further reducing the coefficient of expansion by several factors of ten. The changes in the state of stress was minimal.

Finally, when the coefficient of thermal expansion for the tri-material configuration was kept constant and uniform, changing of the Young's Modulus values did not produce any resulting thermally induced stresses.

IV. EFFECT OF MIDLAYER THICKNESS

This chapter investigates the effect of changing the thickness of the midlayer (material B) on the tri-material configuration. Five different midlayer thickness cases were studied and compared. As displayed in Figure 4.1, the following thicknesses for material B were used: 1.00mm (case 5), 0.50mm (case 12), 0.25mm (case 13), 0.10mm (case 14), and 0.05mm (case 15). For all cases, the dimensions of materials A and C were kept constant (10mm length and 1.0mm thickness). Additionally, the length of the midlayer was held at 5mm and the tri-material configuration was given a temperature increase of 100°C. The material properties for the five cases were given the following constant values: $E_A = E_B = E_C = 100 \text{ GPa}$, $\alpha_A = 100 \times 10^{-6}/^\circ\text{C}$, $\alpha_B = 300 \times 10^{-6}/^\circ\text{C}$, and $\alpha_C = 10 \times 10^{-6}/^\circ\text{C}$.

A. NORMAL STRESS DISTRIBUTION

Plots of the normal stresses along the upper and lower interfaces of the midlayer for the five cases are displayed in Figure 4.2. Both the upper and lower normal stress distributions exhibited similar characteristics. The stresses were always bearing along the interfaces for all five cases with the maximum stresses occurring at the left and right ends of the midlayer. For every case, the minimum bearing stress was developed midspan of the interface. As the thickness of material B was decreased, the bearing stresses

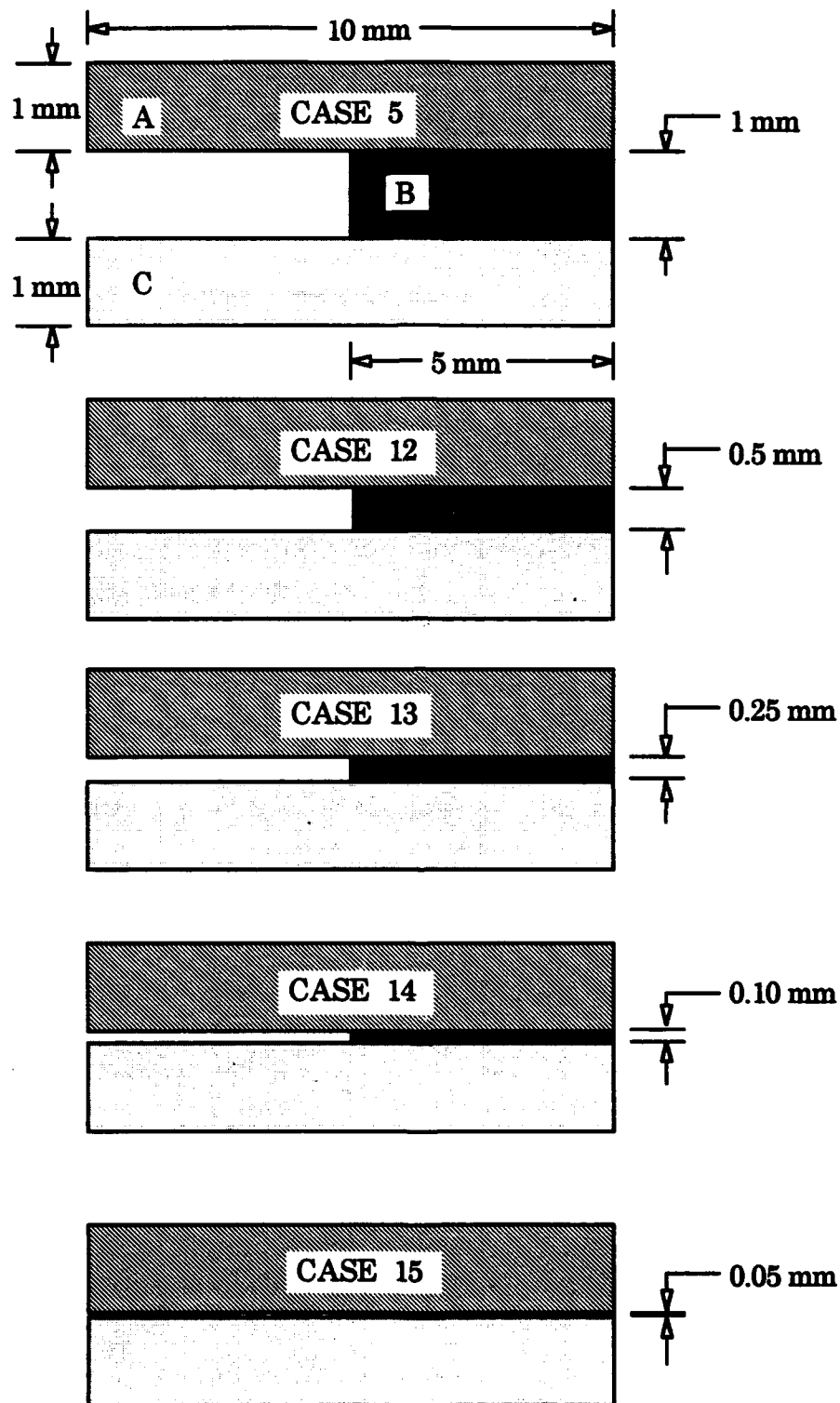
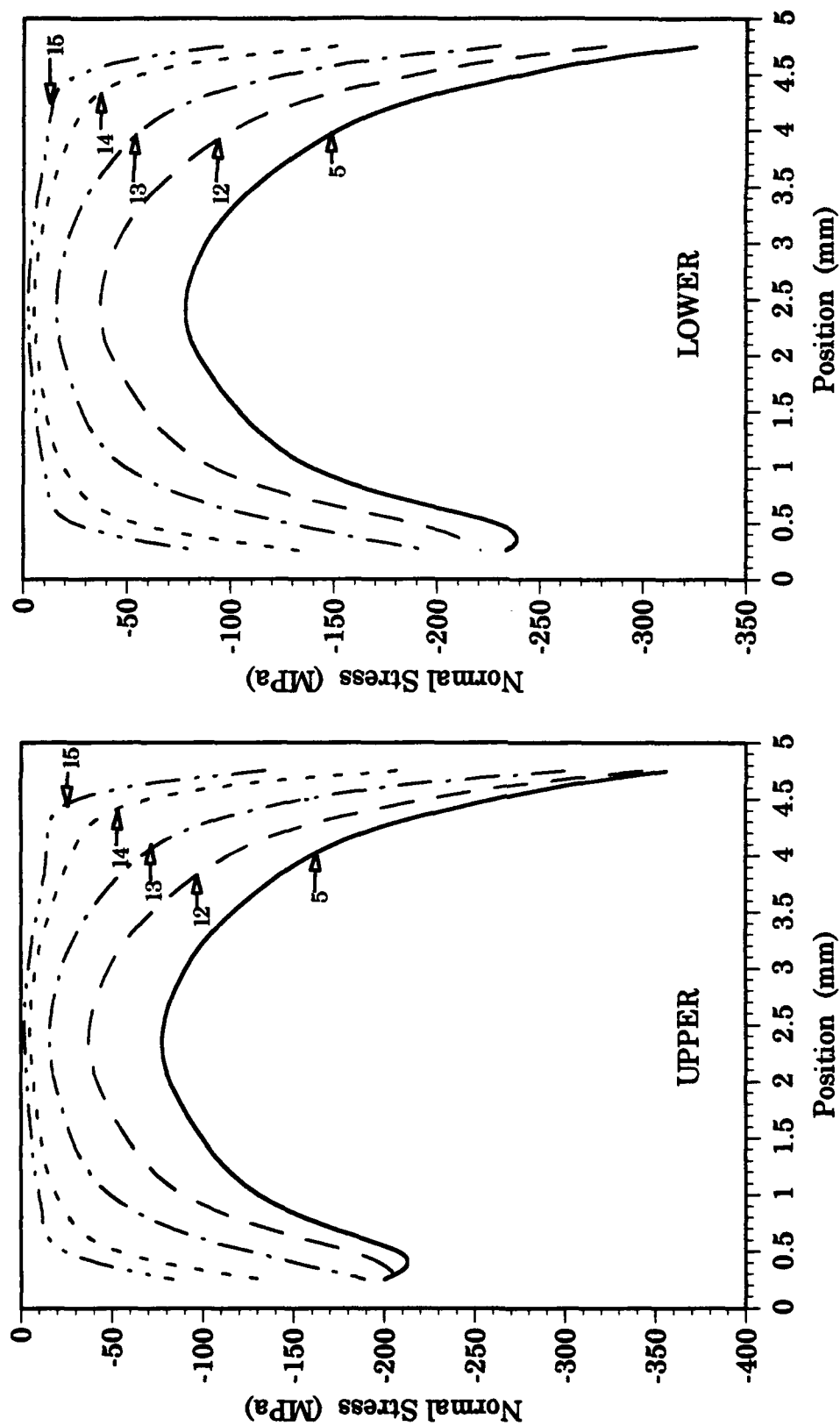


Figure 4.1 Tri-Material Configuration For Cases 5, 12, 13, 14, And 15



Material B Height (mm)	Case 5	Case 12	Case 13	Case 14	Case 15
1	0.5	0.25	0.1	0.05	

$\alpha_A = 100 \times 10^{-6}/^{\circ}\text{C}$ $\alpha_B = 300 \times 10^{-6}/^{\circ}\text{C}$ $\alpha_C = 10 \times 10^{-6}/^{\circ}\text{C}$ $E_A = E_B = E_C = 100 \text{ GPa}$
 Figure 4.2 Normal Stresses At The Interfaces For Cases 5, 12, 13, 14, And 15

similarly decreased. However, the shape of the normal stress distribution curves remained comparable.

Comparisons were made between the maximum of the normal stresses of all five cases on the upper and lower interfaces and the remainder of the normal stresses. Figures 4.3 and 4.4 are two-dimensional and three-dimensional plots of the normal stress/maximum normal stress for the five cases across the upper and lower interfaces, respectfully. For both interfaces, the maximum normal stress occurred in case 5 at the right hand side of the midlayer. Similar characteristics were displayed by all cases for both the upper and lower. As the thickness of the midlayer decreased, the ratio of the normal stress to the maximum normal stress decreased. Of interest was that the thinner material B became, the extent of the midspan that was at a minimum grew. Figures 4.5 and 4.6 show the bearing stresses acting along the upper and lower interfaces of material B.

B. SHEAR STRESS DISTRIBUTION

Figure 4.7 contains plots of the shear stresses across the upper and lower interfaces of material B for cases 5, 12, 13, 14, and 15. Cases 5 and 12 (with their greater thicknesses of material B) displayed similar attributes. The shear stresses, upper and lower, tended to axially compress the midlayer. Cases 13, 14, and 15 (with midlayer thicknesses of 0.25mm, 0.10mm, and 0.05mm) showed peak shear stresses at the left and right ends of the interfaces, but along the majority of the length of span the shear stresses

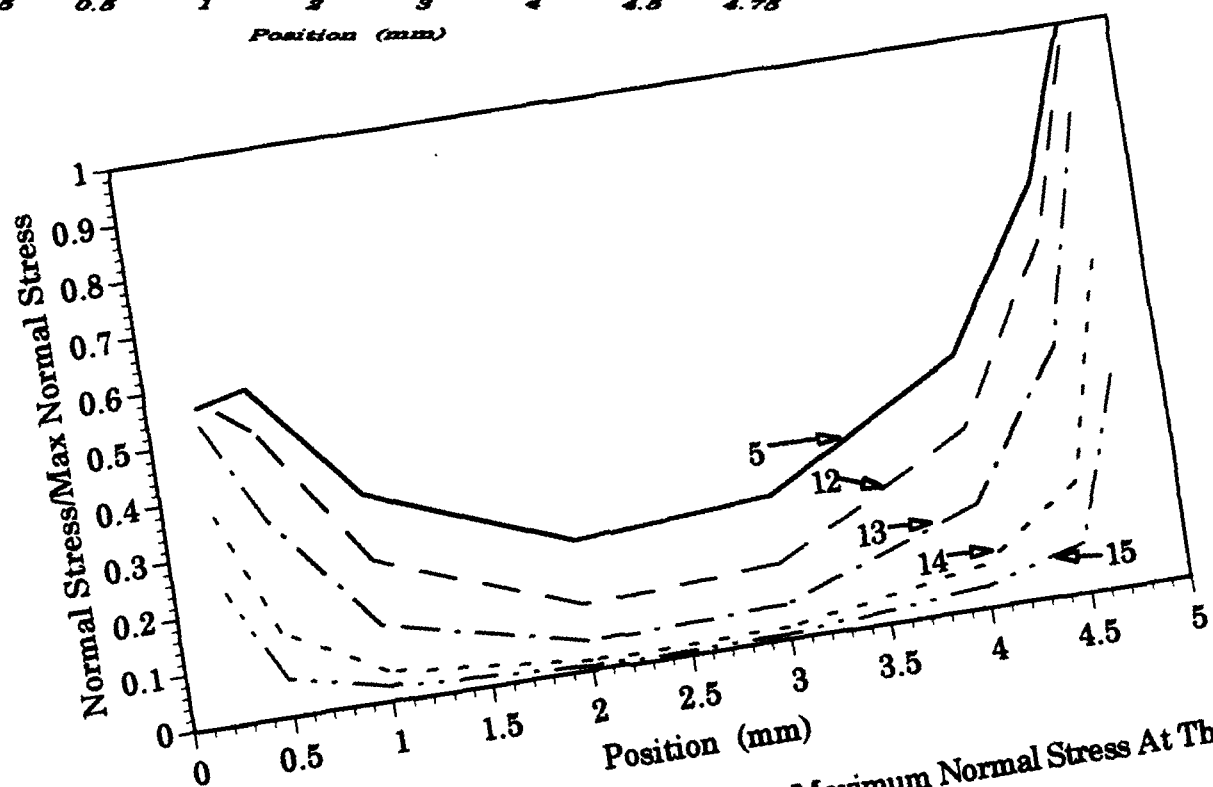
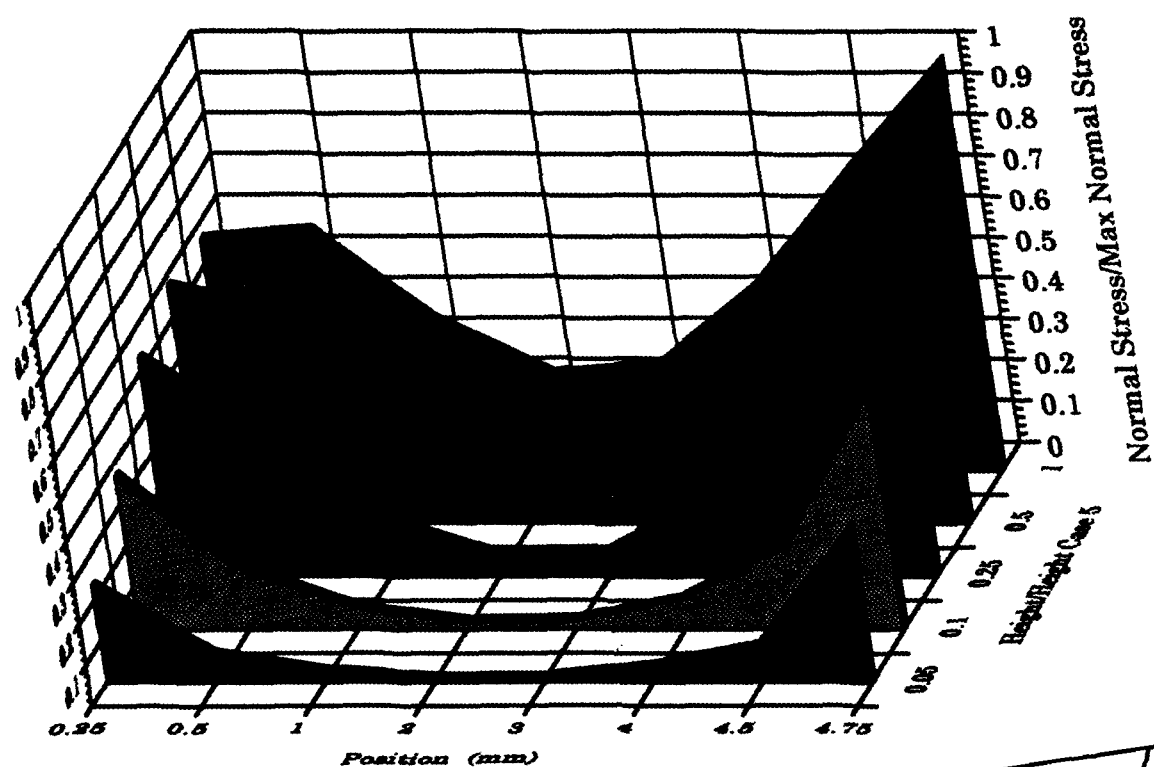


Figure 4.3 2-D And 3-D Plots Of Normal Stress/Maximum Normal Stress At The Upper Interface For Cases 5, 12, 13, 14, And 15

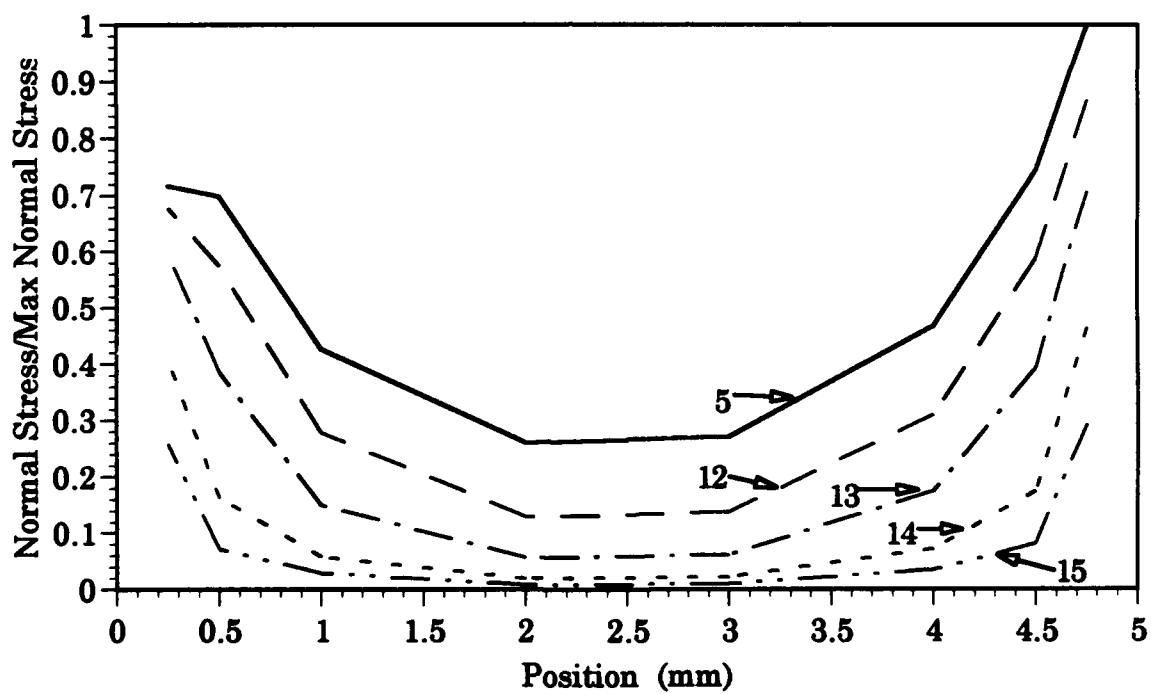
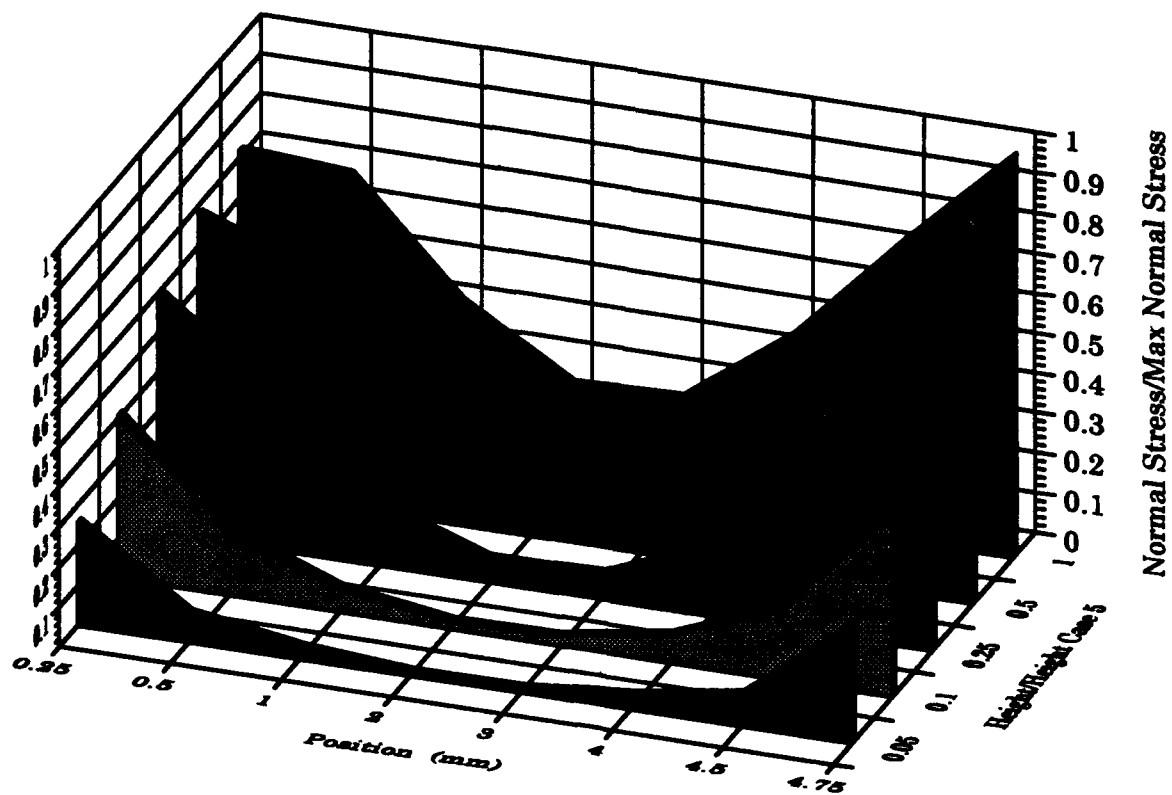
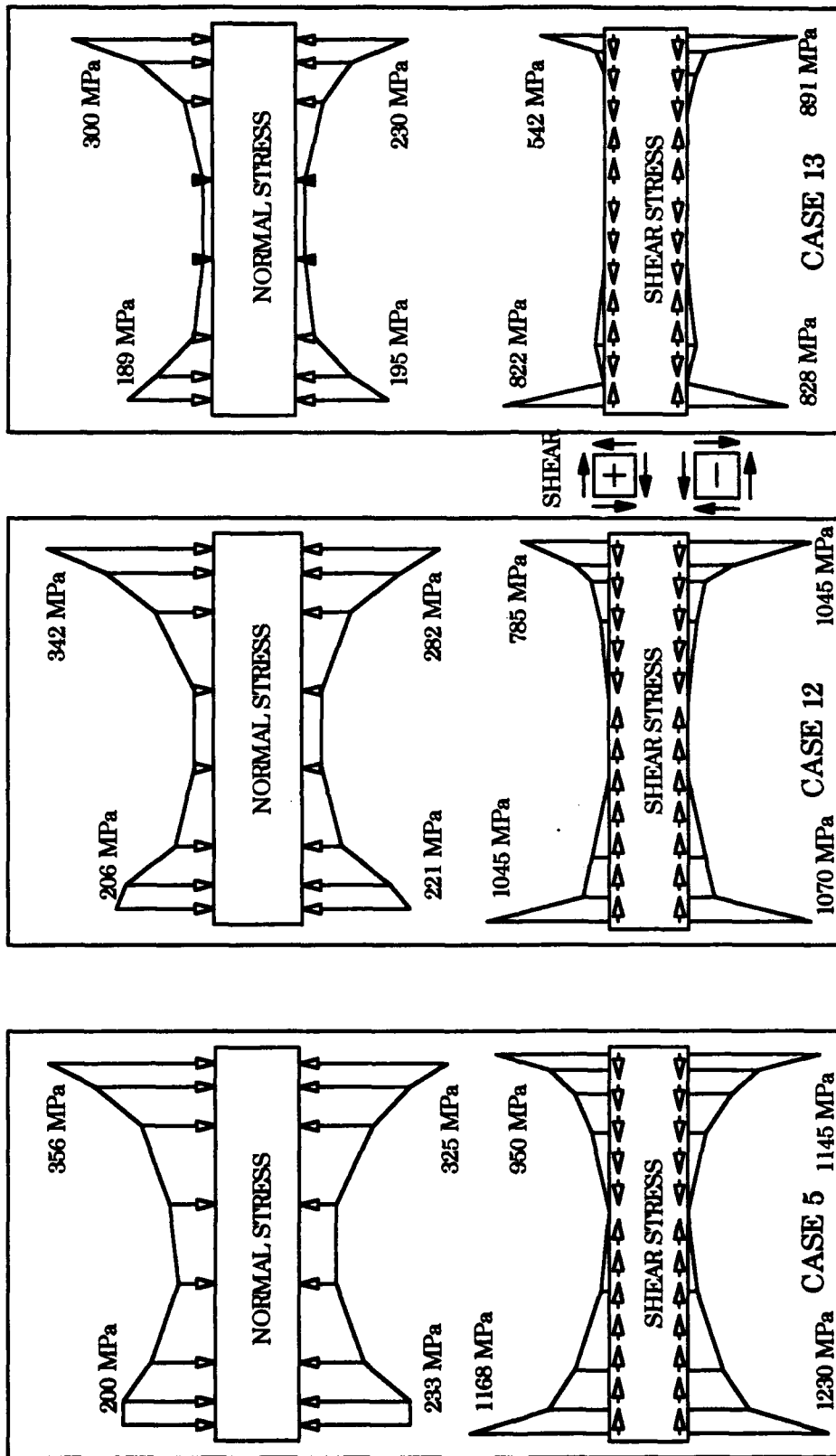


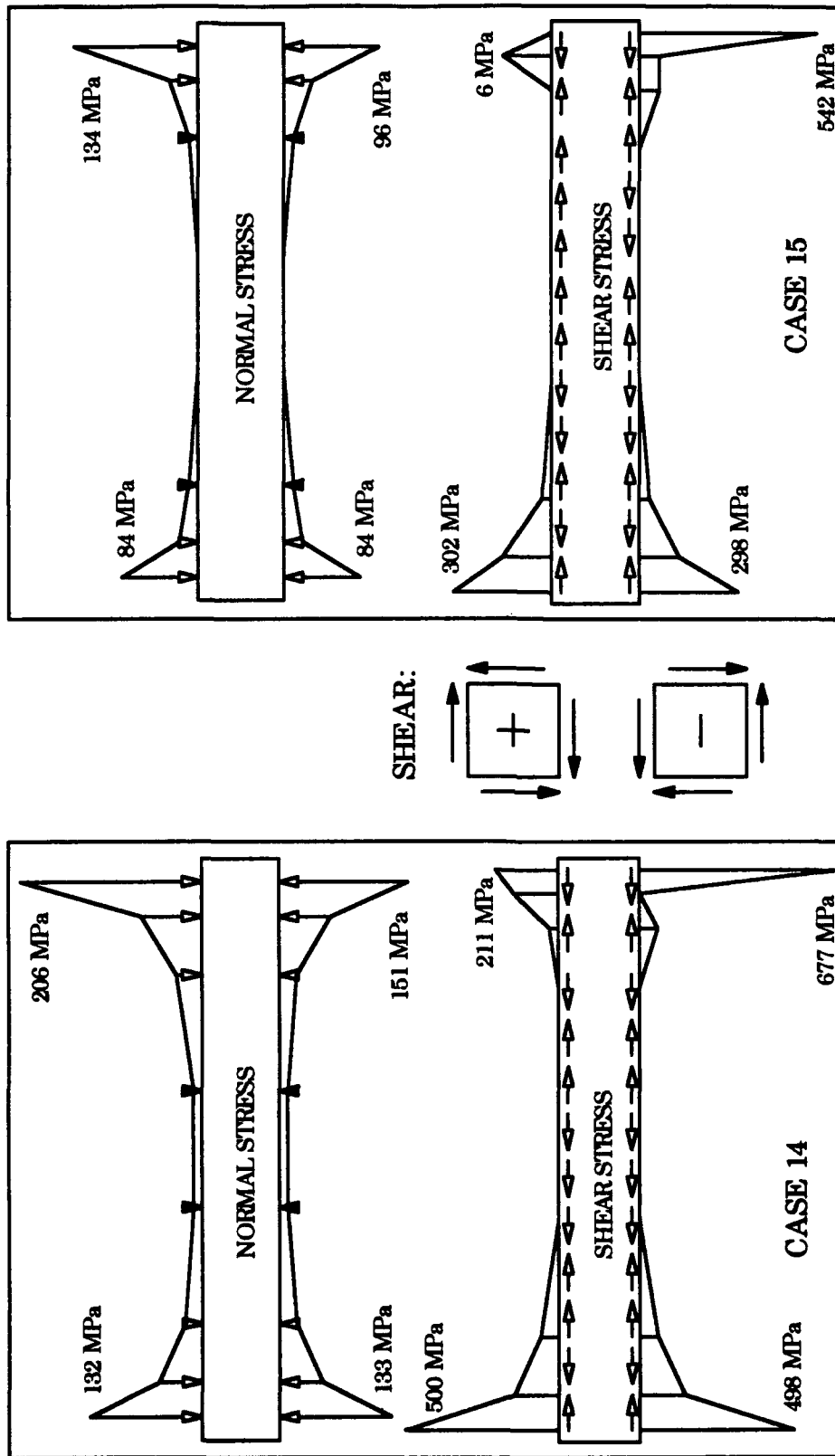
Figure 4.4 2-D And 3-D Plots Of Normal Stress/Maximum Normal Stress At The Lower Interface For Cases 5, 12, 13, 14, And 15



Material B Height (mm)	Case 5	Case 12	Case 13	Case 14	Case 15
	1	0.5	0.25	0.1	0.05

$\alpha_A = 100 \times 10^{-6}/^{\circ}\text{C}$ $\alpha_B = 300 \times 10^{-6}/^{\circ}\text{C}$ $\alpha_C = 10 \times 10^{-6}/^{\circ}\text{C}$ $E_A = E_B = E_C = 100 \text{ GPa}$

Figure 4.5 Shear And Normal Stresses On The Midlayer For Cases 5, 12, And 13

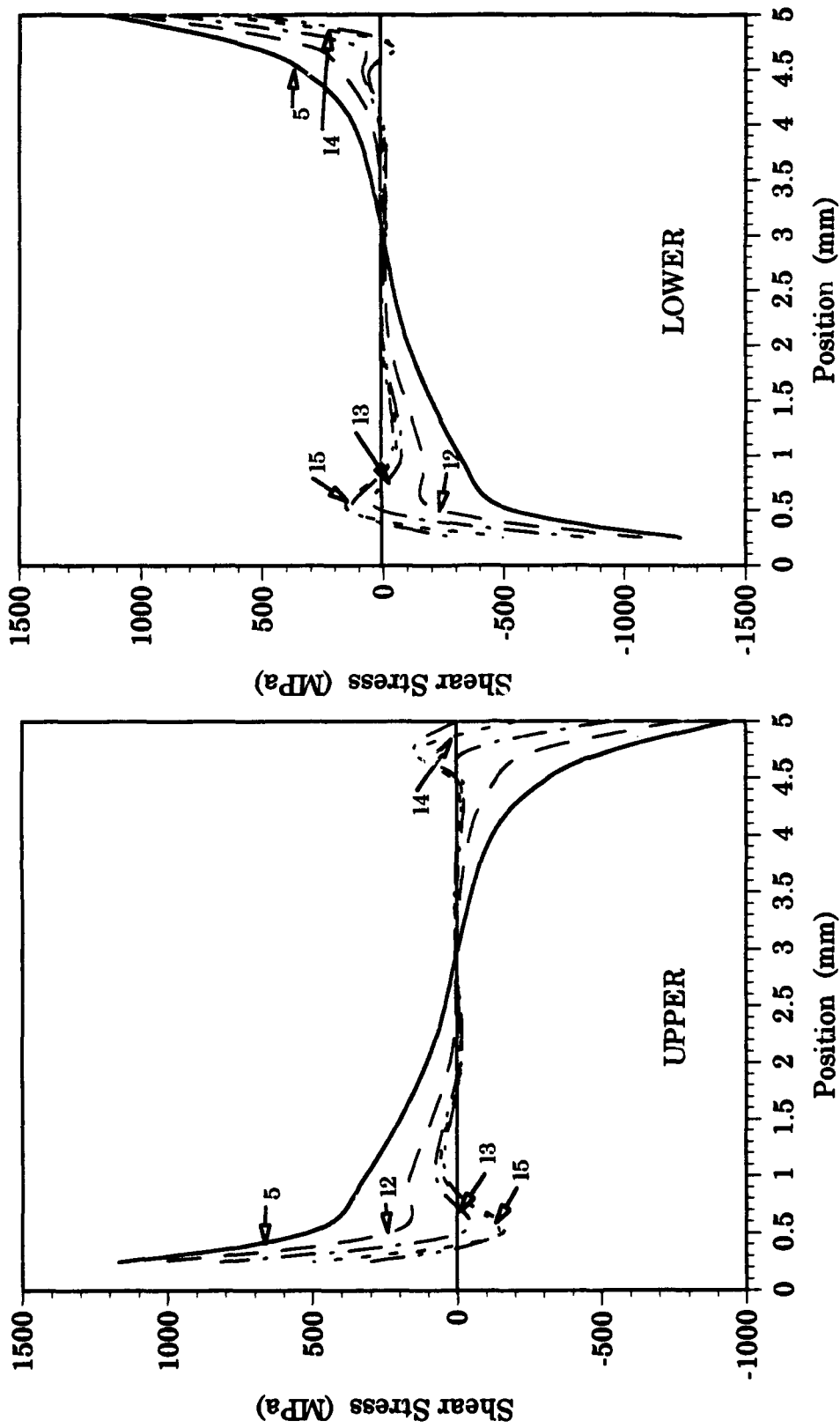


Case 5	Case 12	Case 13	Case 14	Case 15
1	0.5	0.25	0.1	0.05

Material B Height (mm)	1	0.5	0.25	0.1	0.05
------------------------	---	-----	------	-----	------

$\alpha_A = 100 \times 10^{-6} / ^\circ\text{C}$ $\alpha_B = 300 \times 10^{-6} / ^\circ\text{C}$ $\alpha_C = 10 \times 10^{-6} / ^\circ\text{C}$ $E_A = E_B = E_C = 100 \text{ GPa}$

Figure 4.6 Shear And Normal Stresses On The Midlayer For Cases 14 And 15



Material B Height (mm)	Case 5	Case 12	Case 13	Case 14	Case 15
	1	0.5	0.25	0.1	0.05

$\alpha_A = 100 \times 10^{-6}/^{\circ}\text{C}$ $\alpha_B = 300 \times 10^{-6}/^{\circ}\text{C}$ $\alpha_C = 10 \times 10^{-6}/^{\circ}\text{C}$ $E_A = E_B = E_C = 100 \text{ GPa}$

Figure 4.7 Shear Stresses At The Interfaces For Cases 5, 12, 13, 14, and 15

fluctuated around zero. This fluctuation of positive and negative values of the shear stresses from point to point may have been due to a breakdown in the finite element program in dealing with the very small numerical values present.

Comparisons of the ratio of the shear stress at a point to the maximum shear stress found in the group were conducted. Figures 4.8 and 4.9 are two-dimensional and three-dimensional plots of the shear stress/maximum shear stress for the five cases along the upper and lower interfaces, respectively. For both the upper and lower, the maximum shear stress was located at the left end of material B. The two figures were similar, with the shear stress ratios being maximum at the extreme ends of the midlayer and then decreasing to a minimum towards midspan. Of interest, like the normal stress, was that as the thickness decreased, the range of the midspan that was at a minimum increased. Figures 4.5 and 4.6 display the shear stresses acting along the upper and lower interfaces for the midlayer.

C. SUMMARY

The effect of decreasing midlayer thickness on the tri-material configuration was displayed in a number of ways. The normal stresses remained bearing throughout as the midlayer became thinner. The maximum normal and shear stresses decreased with decreasing thickness. Minimal normal and shear stresses extended out further along the span and the stress distributions became more local in nature with the thinning of material B. A conclusion

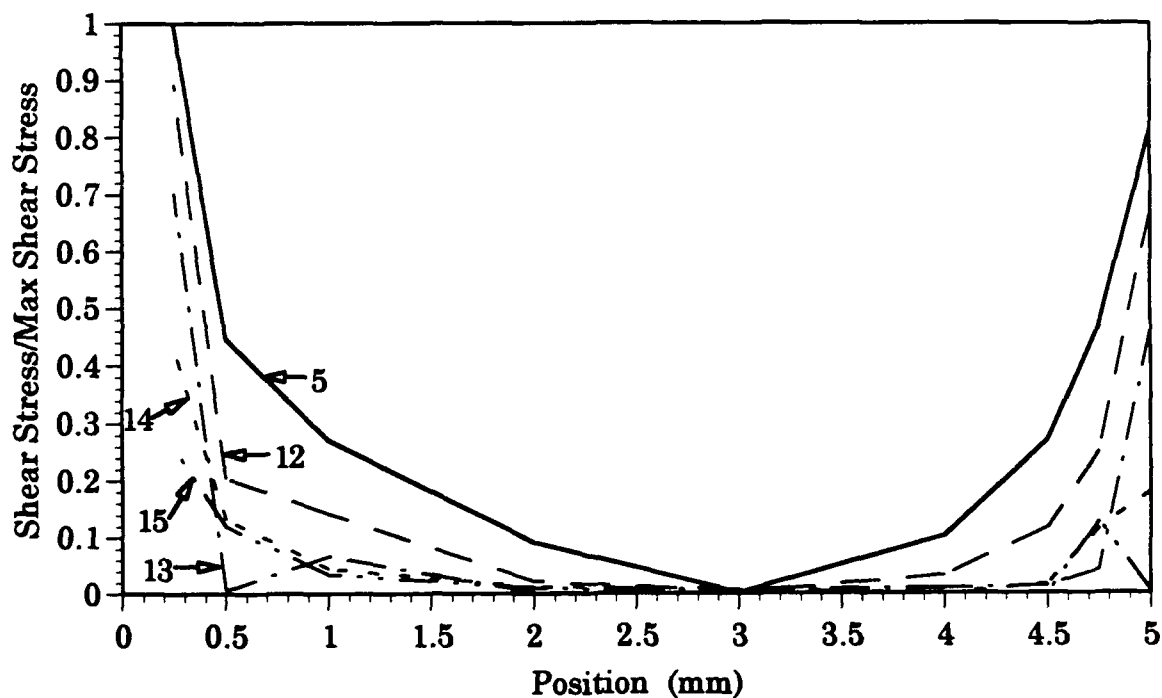
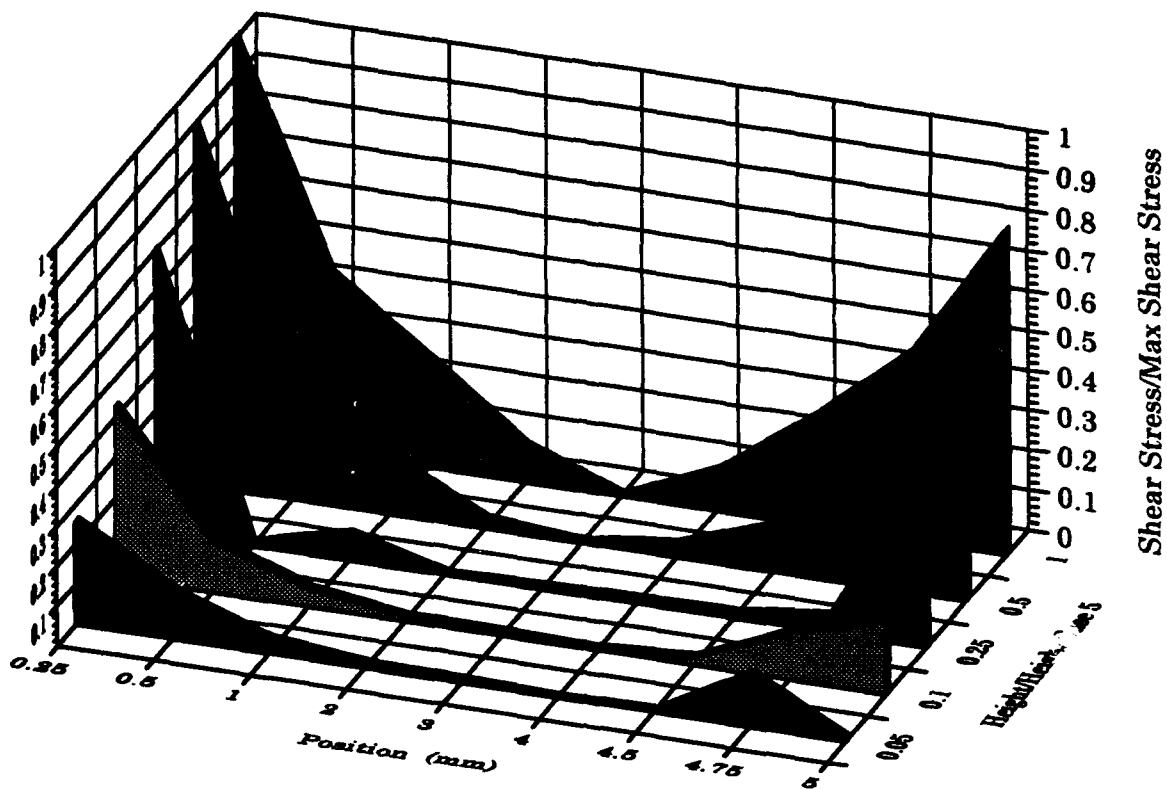


Figure 4.8 2-D And 3-D Plots Of Shear Stress/Maximum Shear Stress At The Upper Interface For Cases 5, 12, 13, 14, And 15

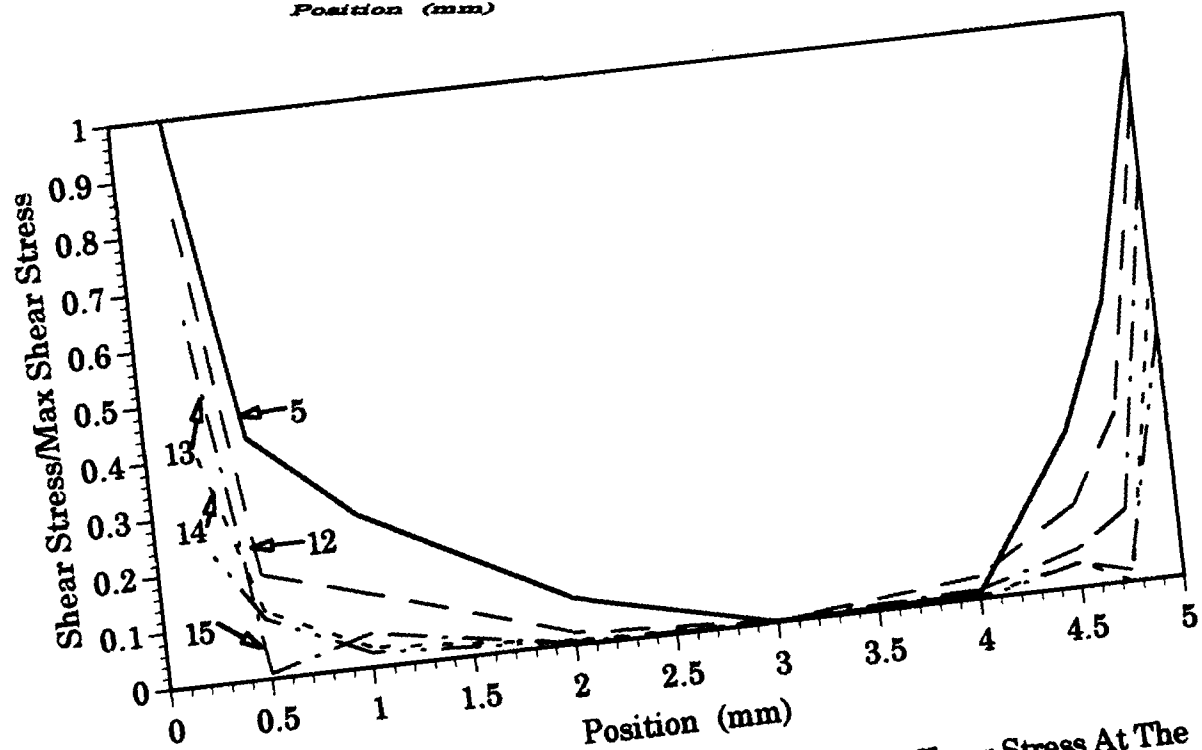
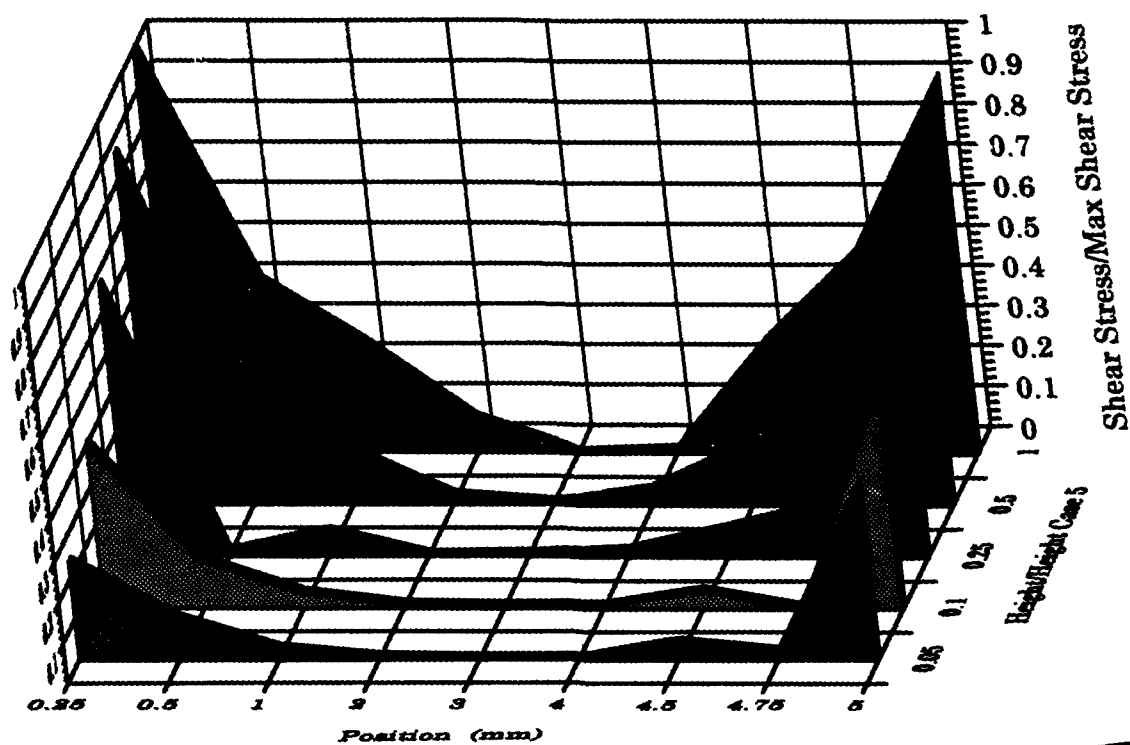


Figure 4.9 2-D And 3-D Plots Of Shear Stress/Maximum Shear Stress At The Lower Interface For Cases 5, 12, 13, 14, And 15

that could be drawn would be that as the thickness of the midlayer continues to decrease, that the only stresses of any consequence along the span exist at the extreme left and right ends of the interfaces. The normal stresses were only one-third to one-half the shear stresses. For both the upper and lower interfaces the maximum normal stresses remained at the far left edge in all cases. The maximum shear stresses along the lower interface moved from the left edge to the right edge as the midlayer thickness was decreased. Finally, the maximum shear stresses along the upper interface remained at the left edge for all cases.

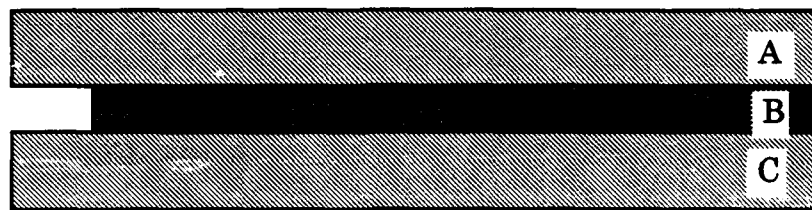
V. EFFECT OF MIDLAYER LENGTH

In this chapter, the effect of the length of the midlayer (material B) on the tri-material configuration was investigated. Six different midlayer lengths were compared and studied. As shown in Figure 5.1, the following lengths for material B were used: 9mm (case 16), 7.5mm (case 17), 5mm (case 12), 2.5mm (case 18), 1mm (case 19), and 0.5mm (case 20). For all cases, the dimensions of materials A and C were kept constant (10mm length and 1mm thickness). Additionally, the thickness of the midlayer was held at 0.5mm and the tri-material configuration was given a temperature increase of 100°C. The material properties for the six cases were as follows: $E_A=E_B=E_C= 100 \text{ GPa}$, $\alpha_A=100 \times 10^{-6}/^\circ\text{C}$, $\alpha_B= 300 \times 10^{-6}/^\circ\text{C}$, and $\alpha_C= 10 \times 10^{-6}/^\circ\text{C}$.

A. NORMAL STRESS DISTRIBUTION

Figure 5.2 contains plots of the normal stresses across the upper and lower interfaces of material B for the six cases. To allow comparison of the different cases the abscissa was constructed to be a non-dimensional location, with the distance along the interface being divided by the total midlayer length for that case.

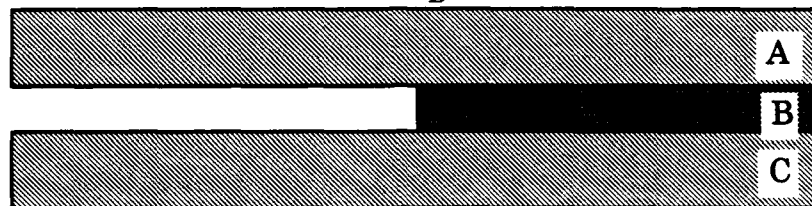
In all six cases, the normal stresses remained bearing across the entire span for both the upper and lower interfaces. Cases 12, 16, 17, and 18 (with midlayer lengths of 5mm, 9mm, 7.5mm, and 2.5mm, respectfully) displayed



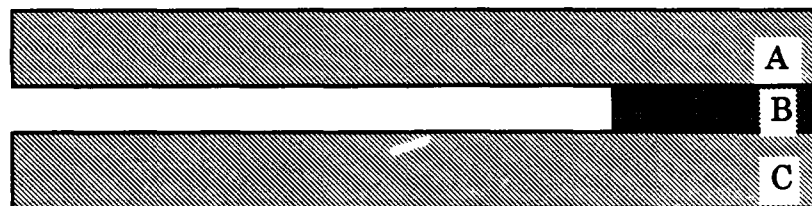
Case 16 $L_B = 9\text{mm}$



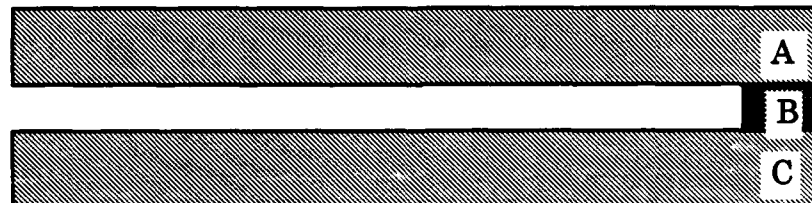
Case 17 $L_B = 7.5\text{mm}$



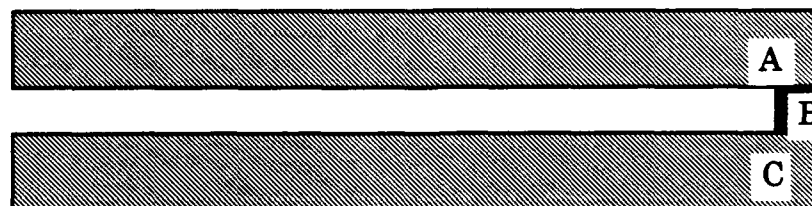
Case 12 $L_B = 5\text{mm}$



Case 18 $L_B = 2.5\text{mm}$



Case 19 $L_B = 1\text{mm}$



Case 20 $L_B = 0.5\text{mm}$

Figure 5.1 Tri-material Configurations For Cases 12, 16, 17, 18, 19, And 20

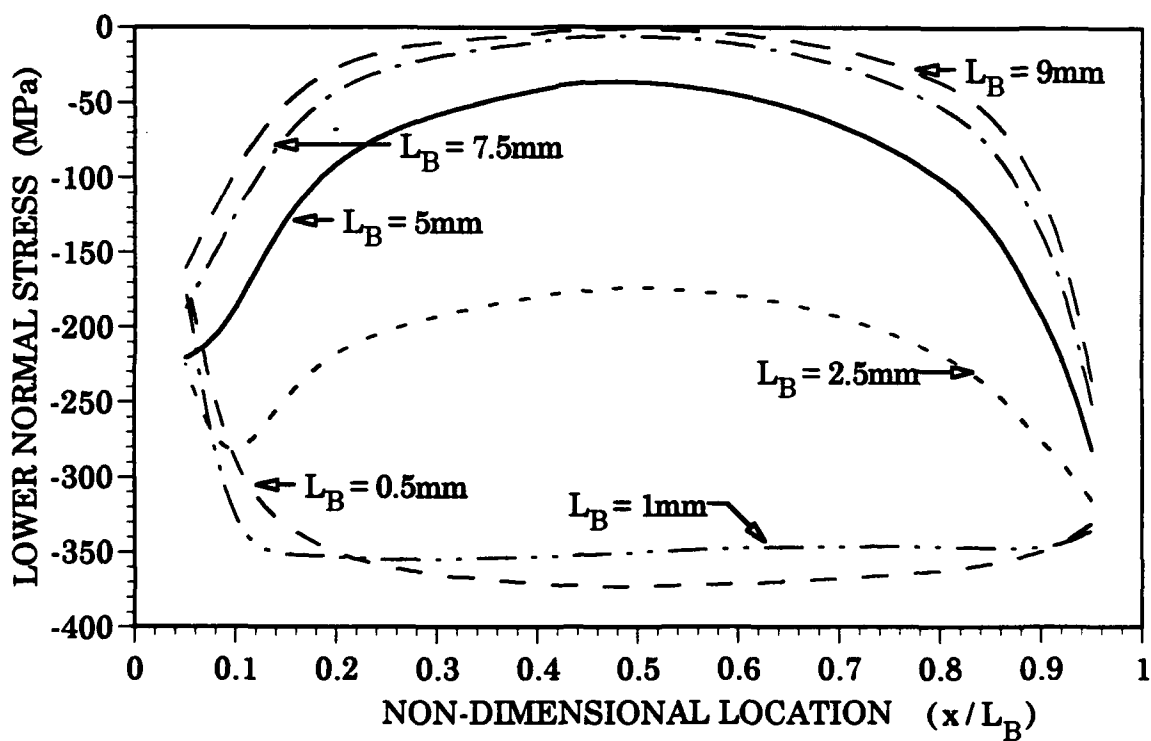
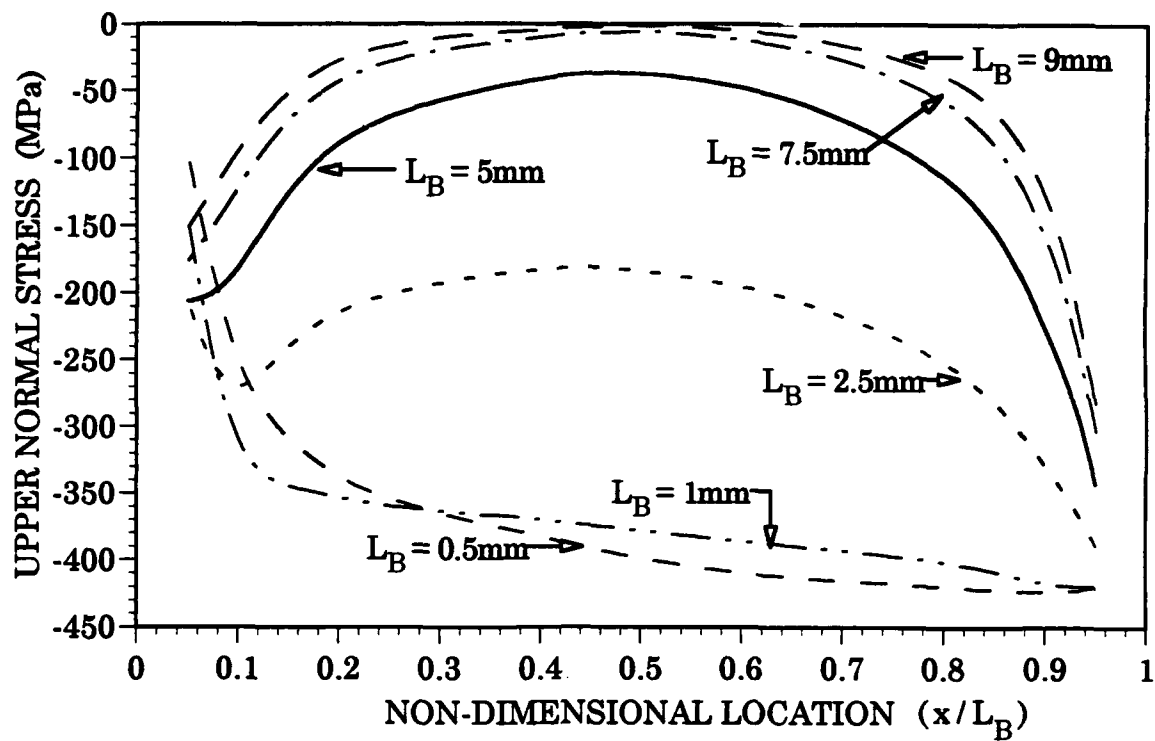


Figure 5.2 Normal Stress At Interfaces As A Function Of Non-dimensional Location For Cases 12, 16, 17, 18, 19, And 20

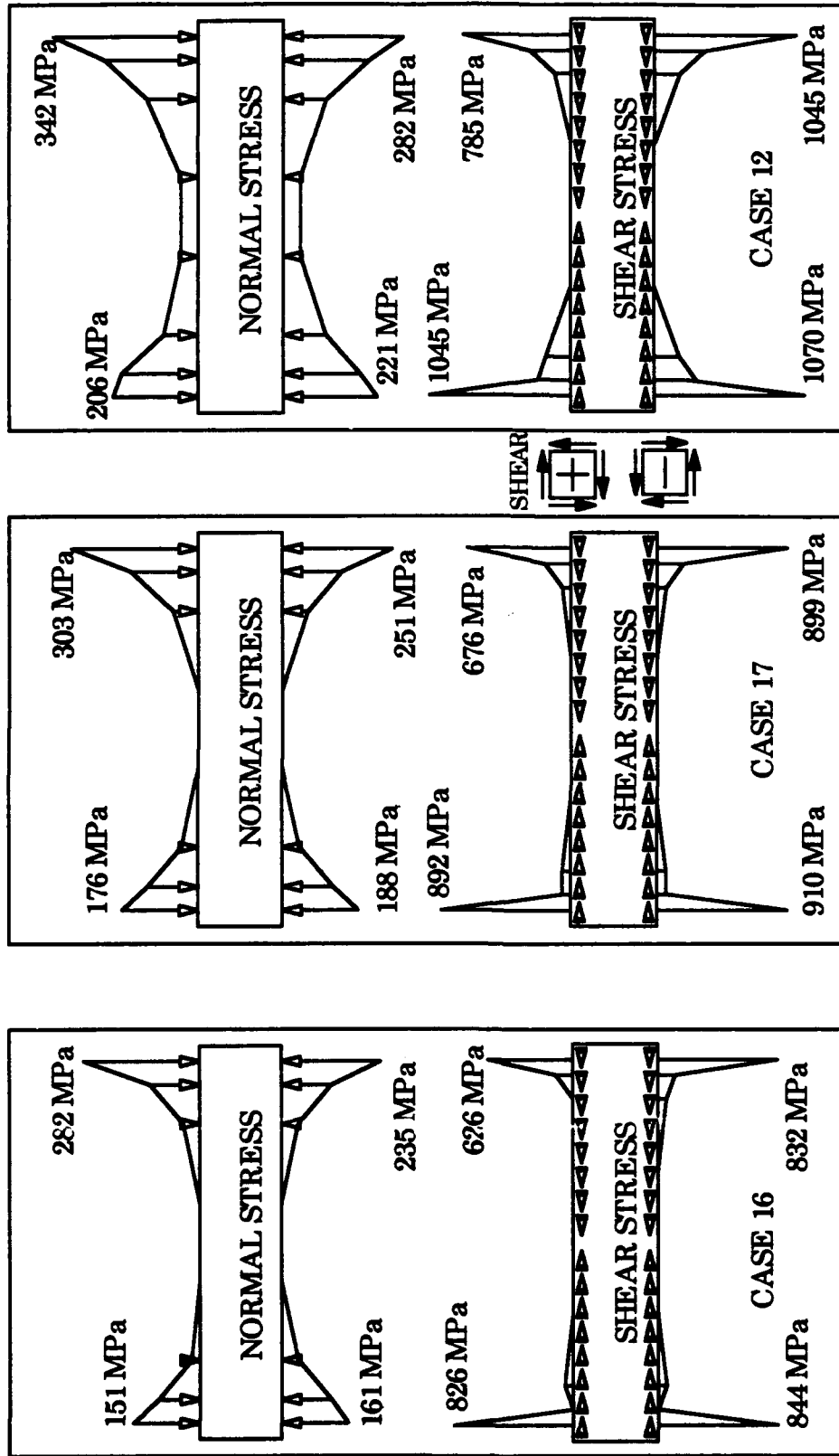
similar characteristics. The maximum bearing stresses occurred at the left and right ends of the midlayer with the minimum being developed at midspan. For midlayer lengths of 9mm and 7.5mm, the stress along the midspan was negligible. As the length was further decreased to 5mm and 2.5mm, the midspan normal stresses increased. The stresses at the left and right ends similarly increased but to a much lesser extent as the length of the above mentioned four cases decreased.

Cases 19 and 20, with the short midlayer lengths of 1mm and 0.5mm, displayed distinctly different normal stress distributions than the four other cases. The left ends of the interfaces had relatively low bearing stresses. Across the remaining 90% of the span, the stress distribution was quite uniform. Figures 5.3 and 5.4 display the normal stresses acting along the upper and lower interfaces of the midlayer.

B. SHEAR STRESS DISTRIBUTION

Plots of the shear stresses along the upper and lower interfaces of the midlayer for cases 12, 16, 17, 18, 19, and 20 are displayed in Figure 5.5. Like the normal stress distribution plots, the abscissa was constructed to be a non-dimensional location, with the distance along the interface being divided by the total midlayer length for that case.

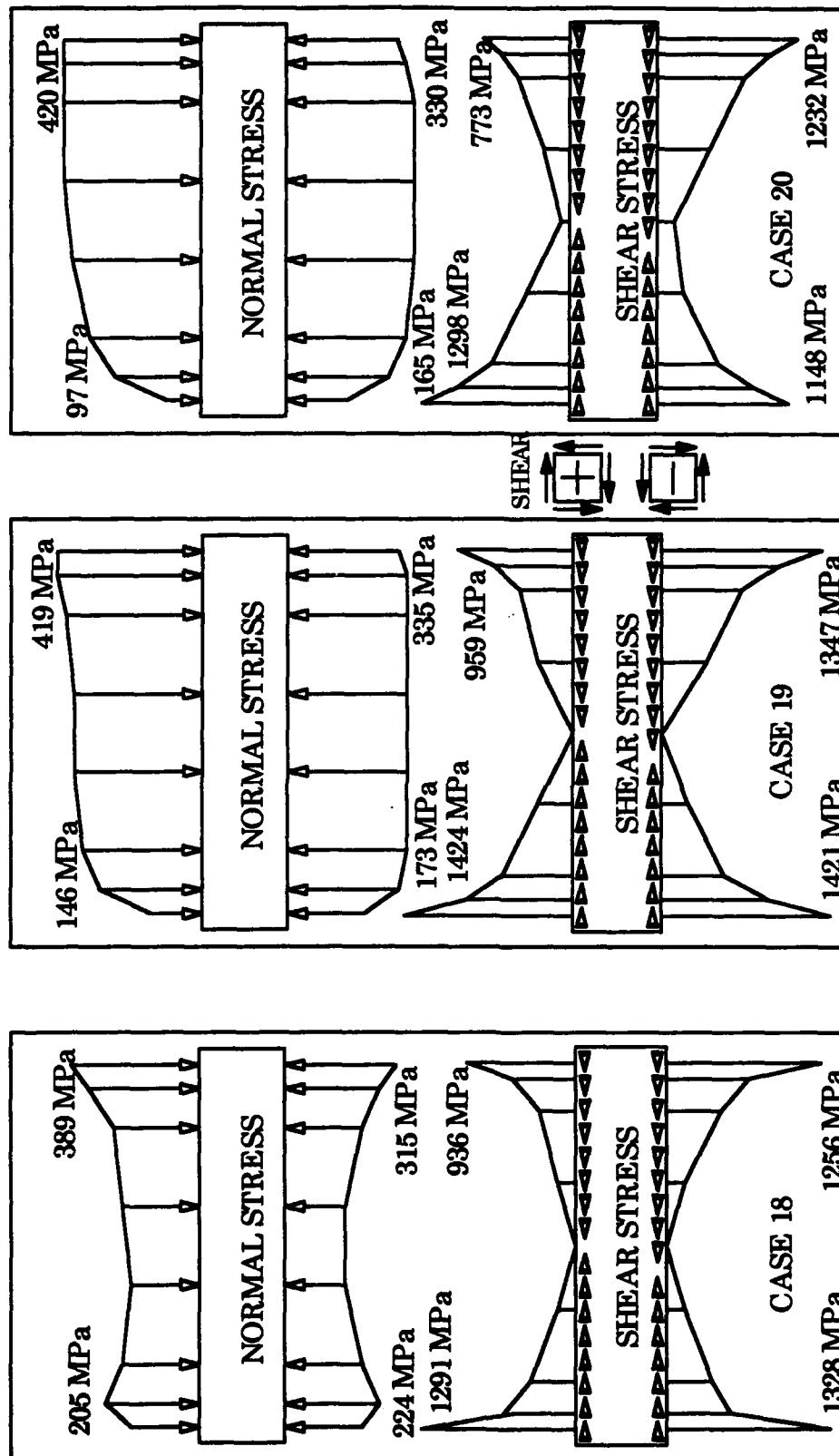
All six cases showed similar attributes with both the upper and lower shear stresses tending to axially compress the midlayer. Additionally, the peak stresses occurred at the extreme left and right ends of the interfaces. For



Material B Length (mm)	Case 12	Case 16	Case 17	Case 18	Case 19	Case 20
	5	9	7.5	2.5	1	0.5

$$\alpha_A = 100 \times 10^{-6} / ^\circ\text{C} \quad \alpha_B = 300 \times 10^{-6} / ^\circ\text{C} \quad \alpha_C = 10 \times 10^{-6} / ^\circ\text{C} \quad E_A = E_B = E_C = 100 \text{ GPa}$$

Figure 5.3 Shear And Normal Stresses On The Midlayer For Cases 12, 16, And 17



Material B Length (mm)	Case 12	Case 16	Case 17	Case 18	Case 19	Case 20
	5	9	7.5	2.5	1	0.5

$$\alpha_A = 100 \times 10^{-6} / ^\circ\text{C} \quad \alpha_B = 300 \times 10^{-6} / ^\circ\text{C} \quad \alpha_C = 10 \times 10^{-6} / ^\circ\text{C} \quad E_A = E_B = E_C = 100 \text{ GPa}$$

Figure 5.4 Shear And Normal Stresses On The Midlayer For Cases 18, 19, And 20

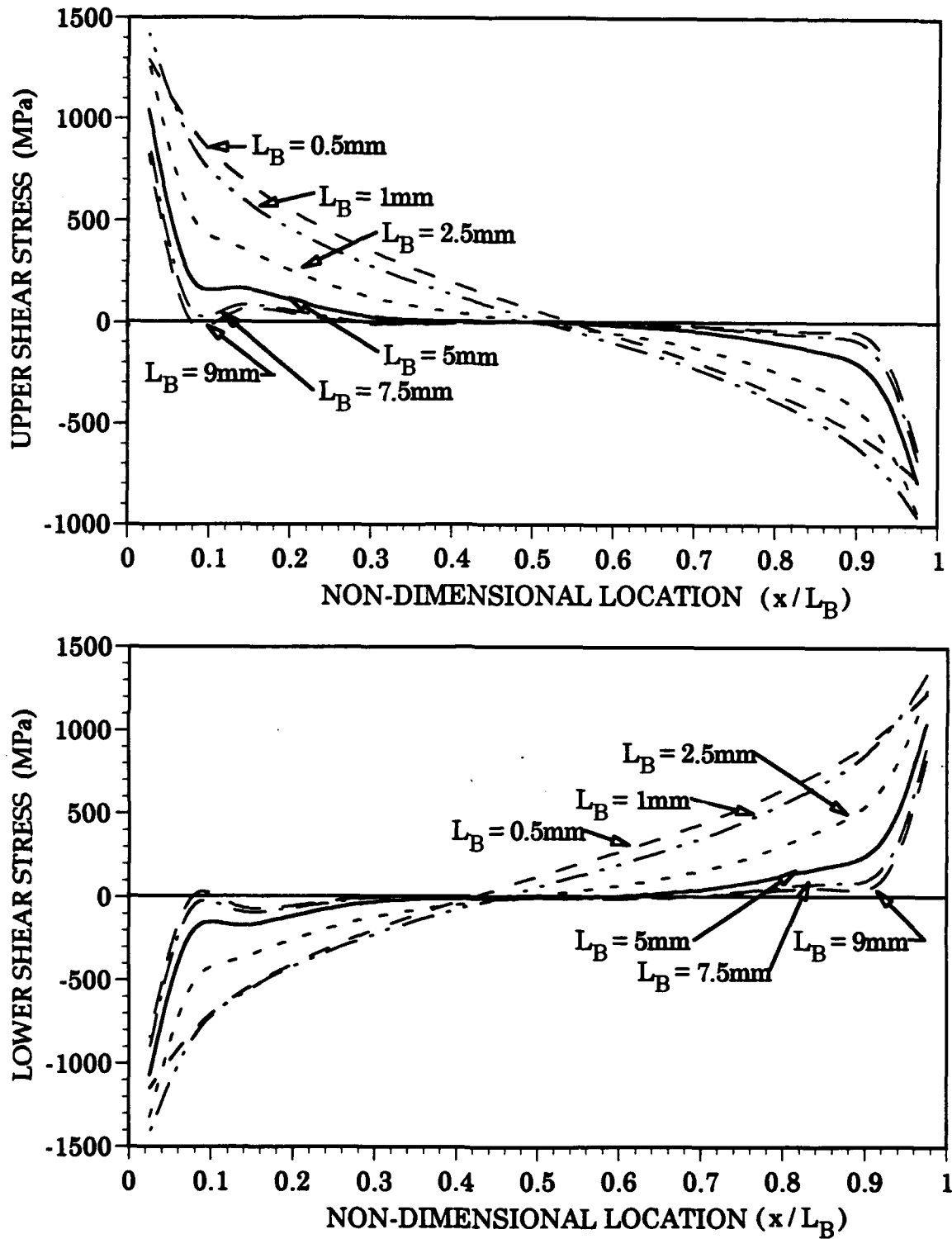


Figure 5.5 Shear Stress At Interfaces As A Function Of Non-dimensional Location For Cases 12, 16, 17, 18, 19, And 20

the greatest length of material B, case 16 with $L_B = 9\text{mm}$, the only non-negligible shear stresses appeared at the ends of the interfaces. As the midlayer length decreased, the extent of the span that experienced appreciable shear stress increased. This is clearly displayed in Figures 5.3 and 5.4.

C. SUMMARY

The effect of changing the midlayer length on the tri-material configuration was shown in numerous ways. As the material B length is shortened, the normal stresses tend to increase and become uniformly distributed across the span. The shear stress became distributed across a greater extent of the interface as the length of the midlayer lessened. The nature of the normal stresses was always bearing and were much less than the shear stresses generated. As the length of the midlayer was decreased to 1mm, shear and normal stresses increased. However, further reduction in length resulted in a slight decrease of both stresses. Except for the shortest length where it was at the right hand edge, the maximum shear stresses occurred at the left hand edge for the upper and lower interfaces. The maximum normal stresses on both interfaces stayed at the right edge. Finally, the maximum upper normal stresses were 10 to 30 percent greater than the maximum lower normal stresses.

VI. EFFECT OF NONUNIFORM TEMPERATURE DISTRIBUTION

Chapters III, IV, and V considered the tri-material configuration as having a uniform temperature increase of 100°C ($\Delta T = 100^{\circ}\text{C}$). In this chapter the temperature increases of the three materials were allowed to vary, and the results were studied and compared. The physical dimensions of the tri-material configuration used in this chapter are shown in Figure 6.1. Materials A and C were both given a length of 10mm and a height of 1mm. Material B was given a length of 2.5mm and a height of 0.1mm. The material properties supplied for all cases studied were as follows: $E_A = E_B = E_C = 100 \text{ GPa}$, $\alpha_A = 100 \times 10^{-6}/^{\circ}\text{C}$, $\alpha_B = 300 \times 10^{-6}/^{\circ}\text{C}$, and $\alpha_C = 10 \times 10^{-6}/^{\circ}\text{C}$.

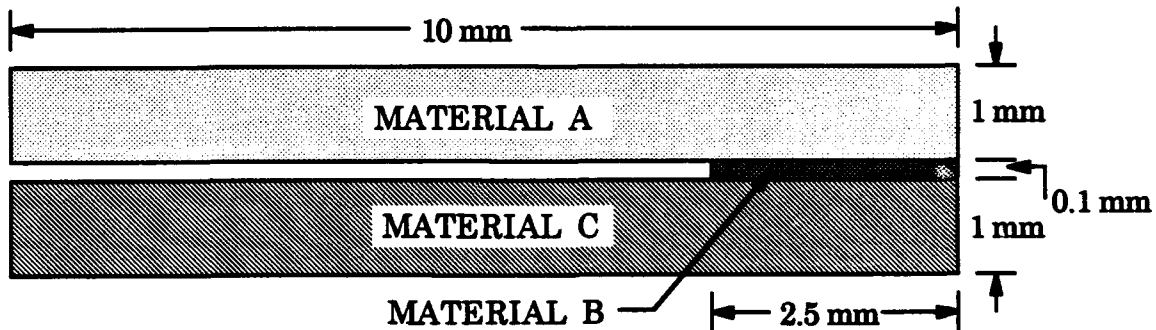


Figure 6.1 Tri-material Configuration For Cases 21, 22, 23, And 24

Four different cases were examined. In case 21, all three materials were allowed a temperature rise of 100°C ($\Delta T_A = \Delta T_B = \Delta T_C = 100^{\circ}\text{C}$). A temperature increase of 200°C for materials A, B, and C ($\Delta T_A = \Delta T_B = \Delta T_C = 200^{\circ}\text{C}$) was studied in case 22. For case 23, material A was assigned a temperature

rise of 200°C while materials B and C were permitted 100°C temperature increases ($\Delta T_A = 200^\circ\text{C}$, $\Delta T_B = \Delta T_C = 100^\circ\text{C}$). Finally, for case 24, material A was allowed to have a linearly decreasing temperature profile. The top layer of material A was set at a temperature increase of 200°C and the temperature rise was then lessened until at the interface of materials A and B the temperature increase was 100°C. This profile is shown in Figure 6.2. Materials B and C were allowed 100°C rises in temperature ($\Delta T_A = \text{linear}$, $\Delta T_B = \Delta T_C = 100^\circ\text{C}$).

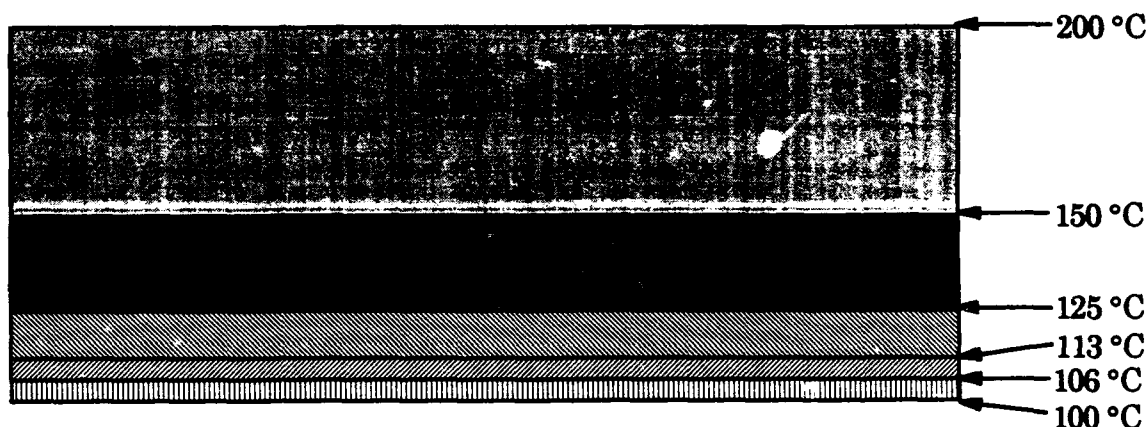
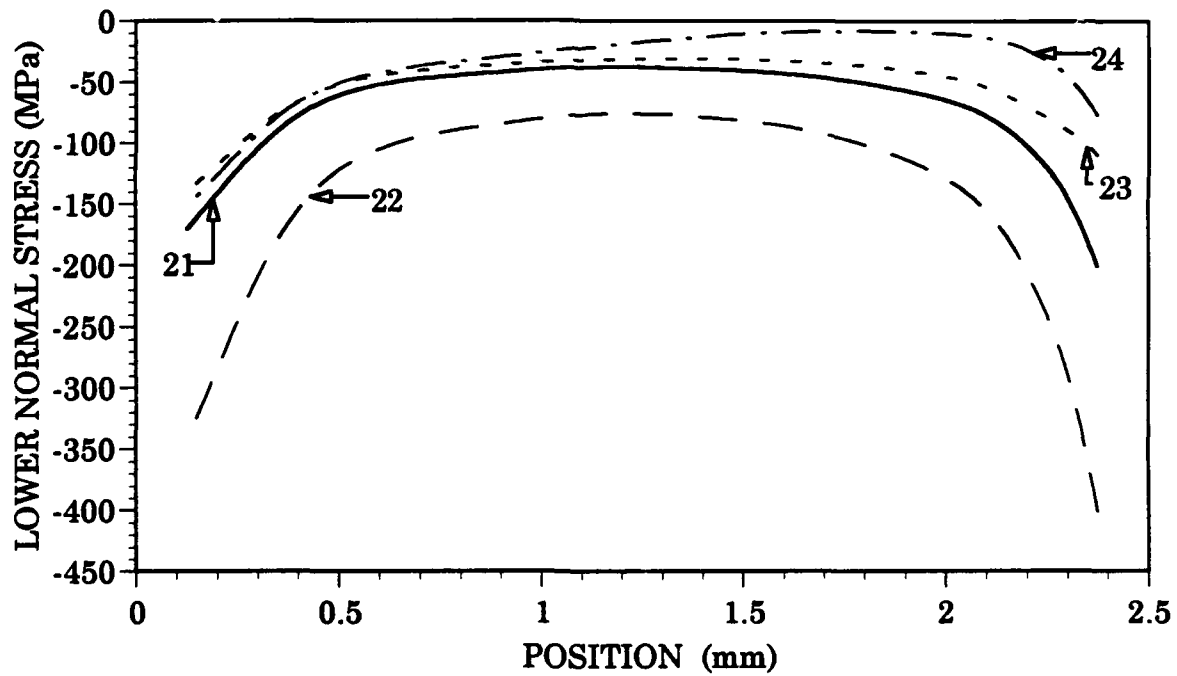
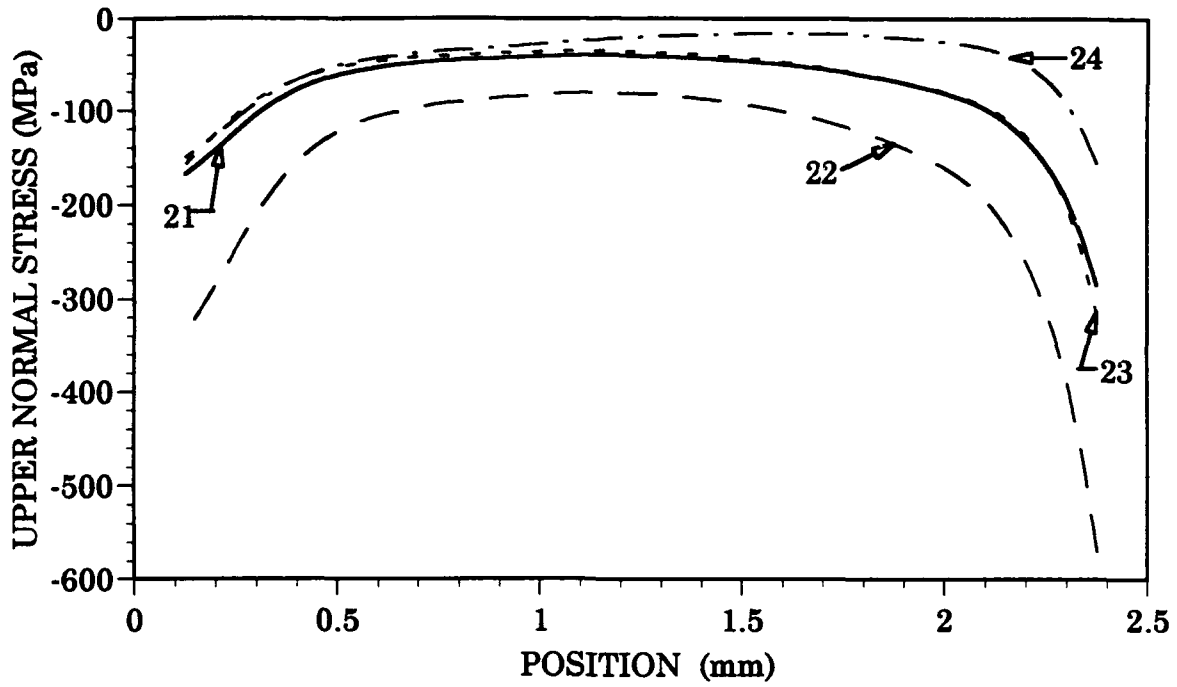


Figure 6.2 Material A Linear Temperature Distribution For Case 24

A. NORMAL STRESS DISTRIBUTION

The normal stresses acting along the upper and lower interfaces of the midlayer for the four cases are shown in Figure 6.3. Similar characteristics were displayed for both the upper and lower normal stress distributions. The maximum stresses occurred at the far left and right ends of the interfaces and were always bearing. For the majority of the midspan the normal stresses were minimal.



	CASE 21	CASE 22	CASE 23	CASE 24
ΔT_A ($^{\circ}\text{C}$)	100	200	200	Linear
ΔT_B ($^{\circ}\text{C}$)	100	200	100	100
ΔT_C ($^{\circ}\text{C}$)	100	200	100	100

Figure 6.3 Normal Stresses At The Interfaces For Cases 21, 22, 23, And 24

A comparison between case 21 and case 22 revealed an interesting point. Case 22, with a tri-material configuration temperature rise of 200°C, resulted in normal stresses which were twice the value of the normal stresses of case 21 ($\Delta T_A = \Delta T_B = \Delta T_C = 100^\circ\text{C}$). This showed the direct relationship between system temperature increase and the resulting increase in normal stresses.

When only material A was given a larger temperature rise, as in case 23 ($\Delta T_A = 200^\circ\text{C}$, $\Delta T_B = \Delta T_C = 100^\circ\text{C}$), the change in system behavior for normal stresses when compared to a uniform temperature field (case 21) was minimal. Along the upper interface the response was nearly identical, with the only difference being the marginally larger bearing stress at the extreme right end for case 23. Across the lower interface, case 23 normal stress values were continuously slightly less than those of case 21.

When the temperature rise in material A was allowed to linearly decrease through its thickness, as in case 24, the resulting normal stress distributions were the lowest of the four cases studied. The maximum stresses developed were approximately one-half of the maximum for the uniform temperature field case.

Figures 6.4 and 6.5 display the normal stress distributions acting on the upper and lower interfaces of the midlayer for the four cases.

B. SHEAR STRESS DISTRIBUTION

Figure 6.6 contains the plots of the shear stress distributions across the upper and lower interfaces for cases 21, 22, 23, and 24. The resulting curves

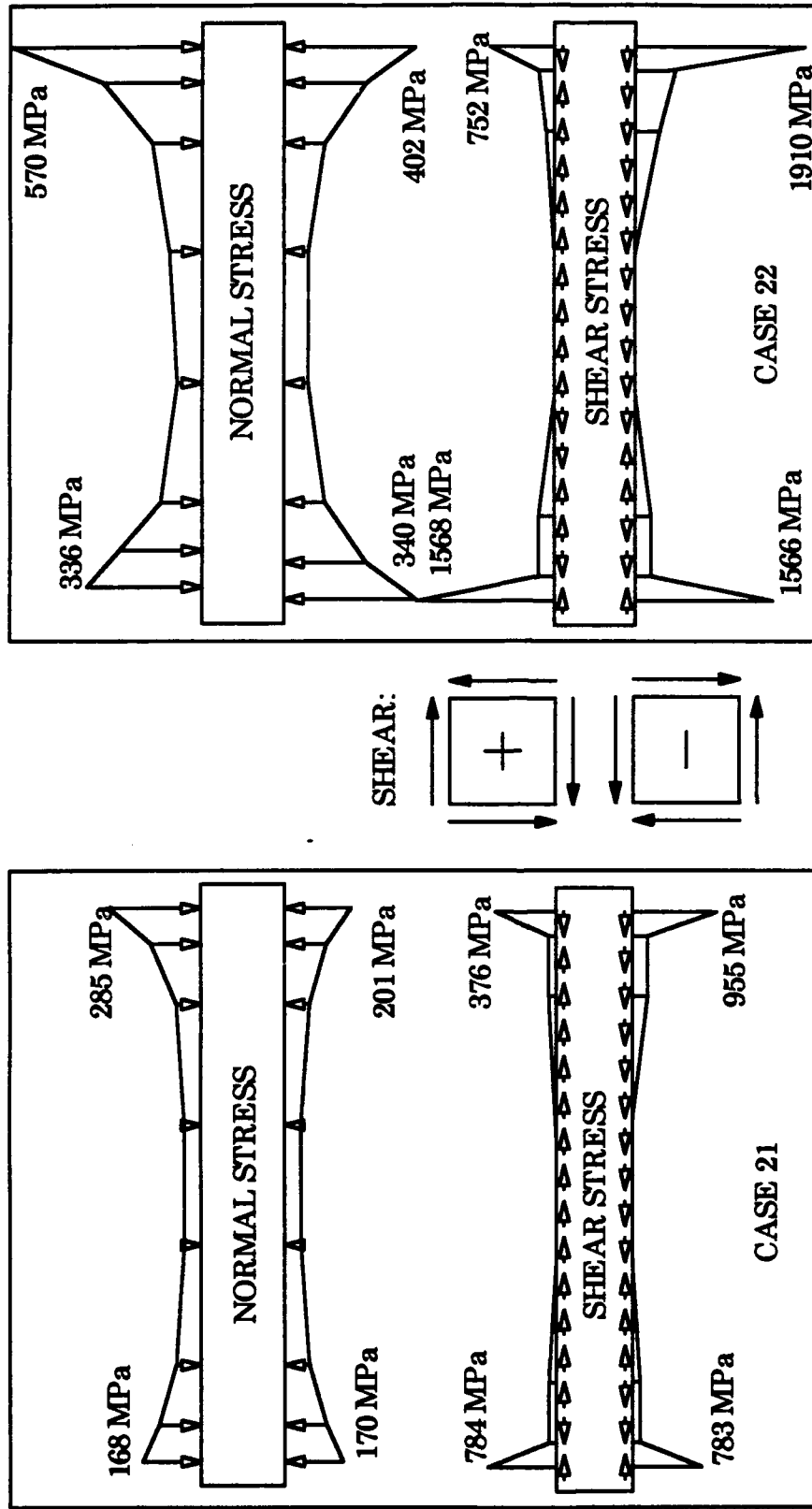
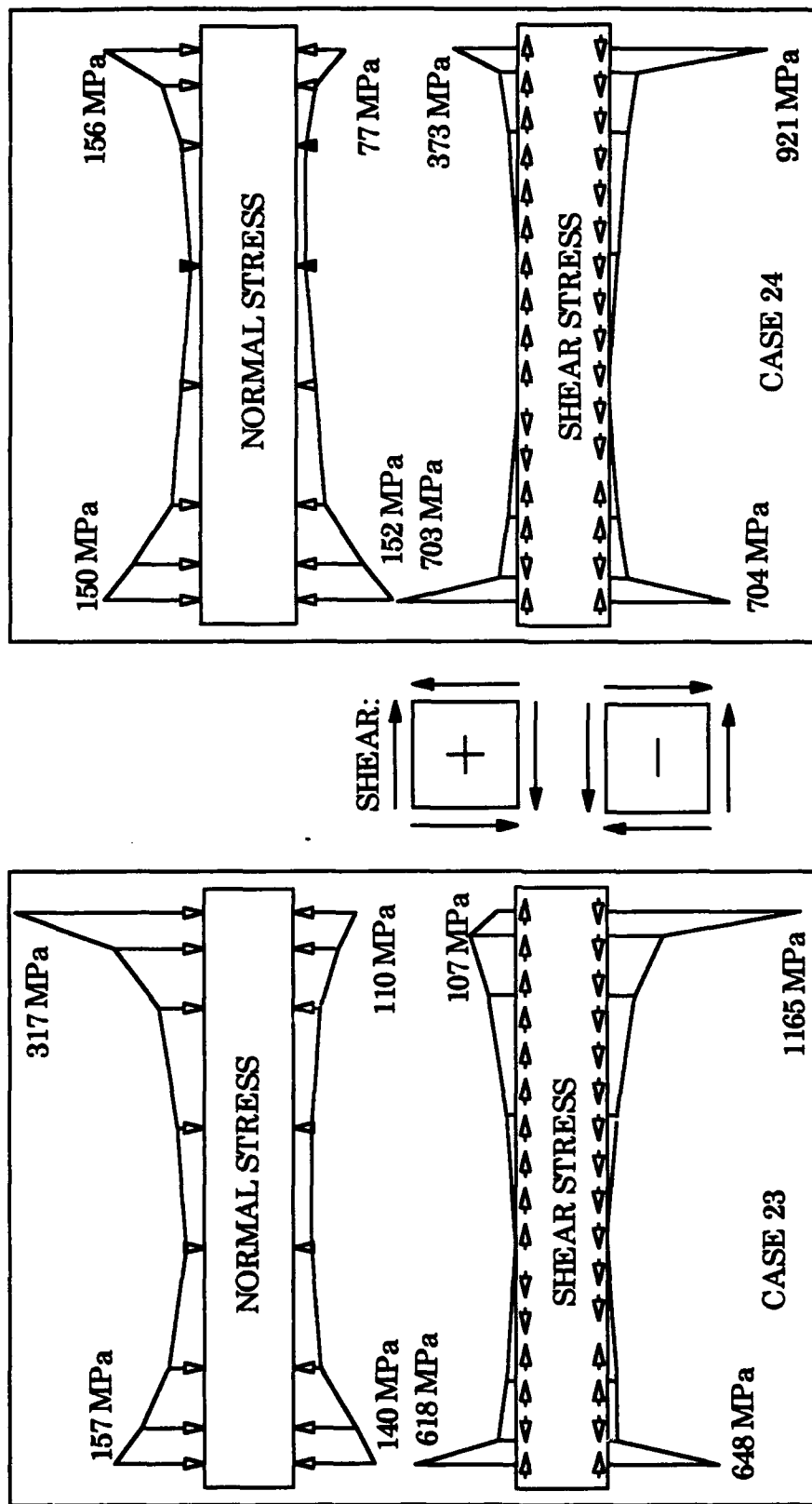
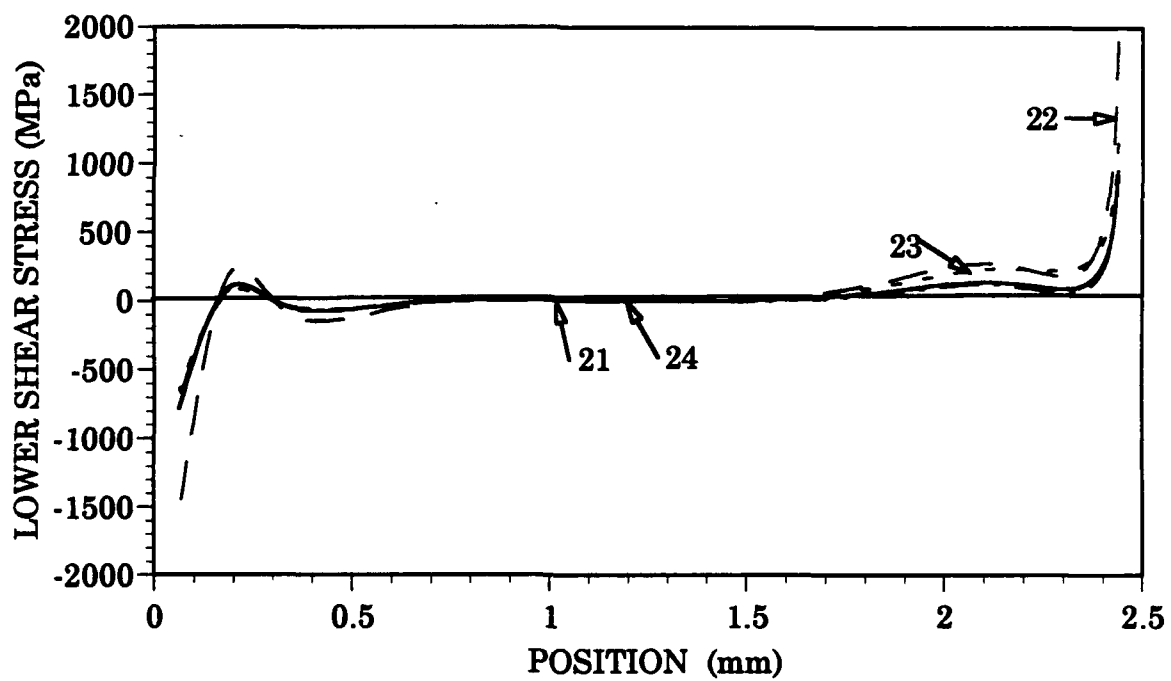
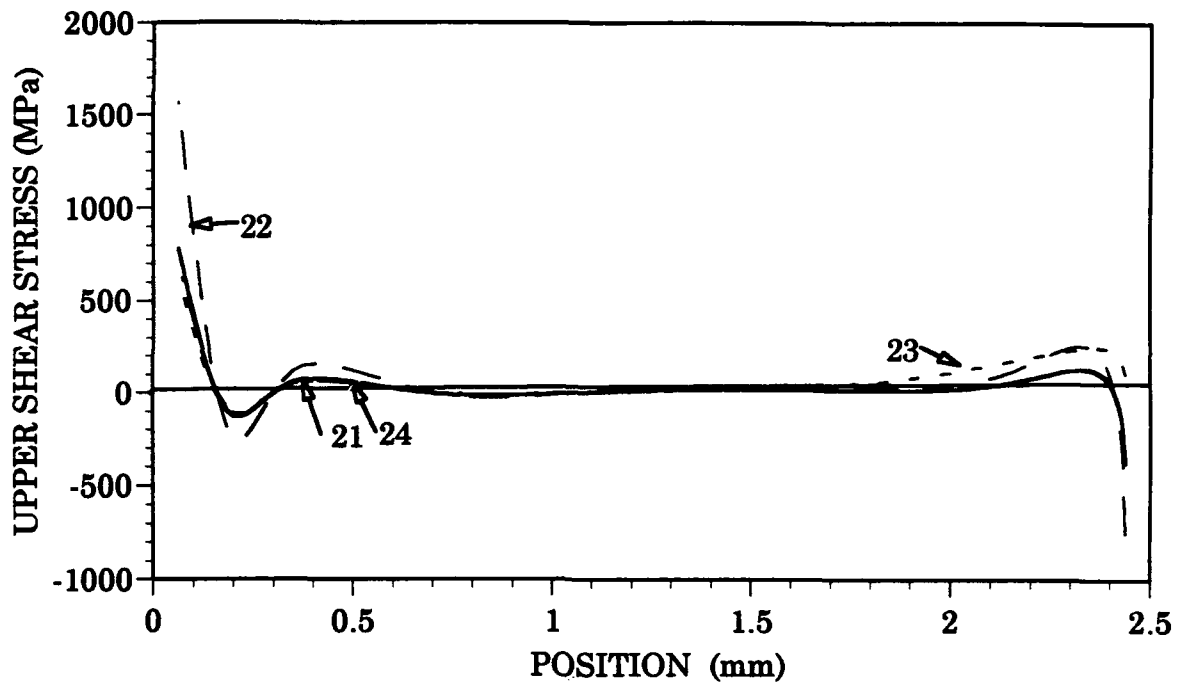


Figure 6.4 Shear And Normal Stresses On The Midlayer For Cases 21 And 22



	CASE 21	CASE 22	CASE 23	CASE 24
ΔT_A (°C)	100	200	200	Linear
ΔT_B (°C)	100	200	100	100
ΔT_C (°C)	100	200	100	100

Figure 6.5 Shear And Normal Stresses On The Midlayer For Cases 23 And 24



	CASE 21	CASE 22	CASE 23	CASE 24
ΔT_A (°C)	100	200	200	Linear
ΔT_B (°C)	100	200	100	100
ΔT_C (°C)	100	200	100	100

Figure 6.6 Shear Stresses At The Interfaces For Cases 21, 22, 23, And 24

were similar for all four cases. The maximum shear stresses occurred at the extreme right and left ends of the interfaces. Along the majority of the length of span the shear stresses fluctuated around zero. This fluctuation may have been due to a breakdown in the finite element program in dealing with the very small numerical values present.

As with the normal stresses, a comparison of case 21 ($\Delta T_A = \Delta T_B = \Delta T_C = 100^\circ\text{C}$) with case 23 ($\Delta T_A = \Delta T_B = \Delta T_C = 200^\circ\text{C}$) shows that the shear stresses at every point for the higher temperature increase were twice the value of those stresses for the lower temperature rise. This also displayed the direct relationship between system temperature increase and the resulting increase in shear stresses.

Case 23 ($\Delta T_A = 200^\circ\text{C}$, $\Delta T_B = \Delta T_C = 100^\circ\text{C}$) and case 24 ($\Delta T_A = \text{linear}$, $\Delta T_B = \Delta T_C = 100^\circ\text{C}$) produced shear stress distribution values very close to case 21. This suggests that for the particular tri-material configuration chosen for the chapter, increasing the temperature rise for one material does not appreciably change the system's shear stress response.

Displays of the shear stress distributions acting on the upper and lower interfaces for the four cases are shown in Figures 6.4 and 6.5.

C. SUMMARY

A study of the effects of a nonuniform temperature field produced a number of interesting results. A doubling of the system temperature rise resulted in a doubling of the normal and shear stresses. Normal stresses

remained bearing in different uniform and nonuniform temperature fields. The normal and shear stress distributions maintained the same general shapes regardless of temperature distribution. Increasing the temperature rise in just one material resulted in minimal change in system response. Finally, a temperature rise which was allowed to linearly decrease through the thickness of one material resulted in the lowest normal stress distributions.

VII. SUMMARY AND CONCLUSIONS

The results of this investigation into the behavior of a tri-material medium subjected to a temperature field leads to several conclusions. These conclusions are broken down into the following topics: effect of material properties, effect of thickness of midlayer, effect of length of midlayer, and effect of nonuniform temperature field.

A. EFFECT OF MATERIAL PROPERTIES

When both the temperature rise and the coefficients of thermal expansion were kept uniform throughout the system and only Young's Modulus was allowed to vary, no normal or shear stresses were developed.

Changing the coefficient of thermal expansion produced several results. As the mismatch between the coefficients of thermal expansion of the materials became greater, the normal and shear stress magnitudes along the upper and lower interfaces became greater. The shear stresses developed along the interfaces were much greater than the normal stresses. Depending on the values of the coefficients of thermal expansion, the normal stresses were either bearing or peeling. Finally, along the upper and lower interfaces the normal and shear stresses were very local in nature. Only in the immediate area of the left and right corners of the interface were the stresses significant.

B. EFFECT OF MIDLAYER THICKNESS

For the particular tri-material configuration studied the normal stresses remained bearing as the midlayer became thinner. The maximum normal and shear stresses decreased with decreasing material B thickness. As the midlayer was made thinner, the normal and shear stress distributions became more and more local in nature. It is believed that as the midlayer becomes extremely thin, the only stresses of any consequence would exist at the extreme left and right corners of the interfaces. The shear stresses generated were two to three times greater than the normal stresses. As the thickness of material B was decreased, the location of the maximum shear stress along the lower interface moved from the inner edge to the outer edge. However, along the upper interface the maximum shear stress remained fixed at the inner edge. Lastly, the maximum normal stress stayed at the left edge for both the upper and lower interfaces.

C. EFFECT OF MIDLAYER LENGTH

With the tri-material configuration used the resulting shear stresses were much greater than the normal stresses. The normal stresses developed were always bearing. As midlayer length was decreased to 1mm, the normal and shear stresses increased. Further shortening of the length of the midlayer resulted in slight decrease of the shear and normal stresses. On both interfaces the maximum shear stress occurred at the left hand edge. The only exception was the shortest length, where the maximum shear stress appeared

at the right hand edge. The maximum normal stress was experienced at the right hand edge for both the upper and lower interfaces. Additionally, the upper maximum normal stress was approximately 10 to 30 percent larger than the lower maximum normal stress.

D. EFFECT OF NONUNIFORM TEMPERATURE DISTRIBUTION

When the temperature rise for all three materials of the system was doubled, the result was a doubling of the normal and shear stresses. The normal stresses remained bearing and the shear and normal stress distributions maintained the same general shapes regardless of the temperature distribution. Increasing the temperature rise in just the upper layer resulted in minimal change in system response. Finally, a linearly decreasing temperature rise gave the lowest magnitude normal stress distributions.

E. RECOMMENDATIONS FOR FURTHER RESEARCH

A number of different areas for further research in this topic exist. Validate the tri-material response to nonuniform temperature fields by using a larger number of system configurations. Alter the finite element code to allow study of the system response to transient temperature fields. Refine the tri-material configuration to more closely match electronic component packaging. Finally, investigate the effect of thermal cycling on fatigue.

APPENDIX A FEM PROGRAM

```

*****
*
*                               FEM PROGRAM FOR WELD PROBLEM
*
*****
*
*   COMPILE AND RUN THIS CODE WITH THE SINGLE EXEC COMMAND: WELD
*
*
*   NEL      THE NUMBER OF ELEMENTS
*   NODES    THE NUMBER OF SYSTEM NODES
*   NDOF     THE NUMBER OF SYSTEM DEGREES OF FREEDOM
*   NBC      THE NUMBER OF ESSENTIAL BOUNDARY CONDITIONS
*   IBC      THE SUPPRESSED DEGREES OF FREEDOM
*   NFC      THE NUMBER OF APPLIED FORCES
*   IFC      THE SYSTEM NODES WITH APPLIED LOADS
*   ICORR    THE CORRESPONDENCE BETWEEN LOCAL AND SYSTEM DOF
*   NMAT     NUMBER OF DIFFERENT MATERIALS
*   IMAT     A PARTICULAR MATERIAL
*   ITYPE    = 0 FOR B.C.'S AT LEFT END ONLY,
*            = 1 FOR B.C.'S AT BOTH LEFT AND RIGHT ENDS
*   E        YOUNGS MODULUS OF IMAT MATERIAL
*   G        SHEAR MODULUS OF IMAT MATERIAL
*   X        THE X COORDINATE OF A NODE
*   HITE     THE HEIGHT OF AN ELEMENT
*   ZLEN     THE LENGTH OF AN ELEMENT
*   EK       THE 6 BY 6 ELEMENT STIFFNESS MATRIX
*   SYSMAT   THE NDOF BY NDOF SYSTEM STIFFNESS MATRIX
*   FLOAD    THE MAGNITUDE OF AN APPLIED LOAD
*   FORCE     THE SYSTEM FORCE VECTOR
*   U        THE SYSTEM DISPLACEMENT VECTOR
*   DELTMP   THE TEMPERATURE CHANGE
*   ALPHA    THERMAL COEFFICIENT OF EXPANSION
*   NNSCOL   THE NUMBER OF NONSOLDERED COLUMNS
*   NSCOL    THE NUMBER OF SOLDERED COLUMNS
*   NIROW    THE NUMBER OF ROWS IN THE CHIP
*   NJROW    THE NUMBER OF ROWS IN THE SUBSTRATE
*   PLSTRS   THE PEELING STRESS AT THE NODE TO THE RIGHT OF THE
*            COLUMN NUMBER
*   N3STRT   ELEMENT NUMBER BEFORE START OF LOWER SOLDER
*
*   INCLUDE 'WELDCOMN'
*   CHARACTER*20 NAME
*   COMMON /WORKSP/RWKSP
*   REAL RWKSP(137047)
*   CALL IWKIN(137047)
*
*   READ *, NAME
*
*   NOTE; INPUT THE NAME OF THE FILE TO BE OPENED AS FOLLOWS:
*   ' /FN FT'
*   THE FILENAME MUST BE PRECEDED WITH A '/' AND THE FILETYPE MUST BE
*   FOLLOWED BY A '. THE ONLY SPACE IS BETWEEN FN AND FT.
*
*   OPEN(9, FILE= NAME )
*
*   INPUT THE FEM PARAMETERS
*
*   READ(9,*) NEL, NODES, NMAT, NDOF, NBC, NFC, ITYPE

```

```

      READ(9,*) (IBC(I), I = 1,NBC)
*
      DO 50 IB = 1,NBC
50 CONTINUE
*
      IF (NFC .NE. 0) THEN
        READ(9,*) (IFC(I), FLOAD(I), I = 1,NFC)
        DO 70 IF = 1,NFC
70 CONTINUE
        ELSE
          ENDIF
*
      DO 80 IM = 1,NMAT
        READ(9,81) E(IM), POISS(IM), ALPHA(IM), HITE(IM)
80 CONTINUE
81 FORMAT (4F10.7)
*
*
      READ(9,22) (X(IN), IN = 1,NODES)
      DO 999 ILL = 1, NEL
        READ(9,20) IL,IMAT(ILL),(ICORR(ILL,IN),IN = 1,6), INODE(ILL,1),
& INODE(ILL,2)
999 CONTINUE
20 FORMAT(10I4)
22 FORMAT(7F10.5)
      READ(9,*) DELTMP
      READ(9,*) (TEMP(I),I = 1,NMAT+1)
      WRITE(14,*) ' '
      WRITE(14,*) 'DELTMP = ', DELTMP
*
* CALCULATE THE SHEAR MODULII
*
      WRITE(14,*) ' '
      WRITE(14,*) 'IMAT#, E, G MODULII, ALFA, POISSON AND HEIGHT FOLLOW'
      WRITE(14,*) ' '
      DO 100 IM = 1, NMAT
        G(IM) = 5.*E(IM)/(12.*(1+POISS(IM)))
        WRITE(14,105) IM, E(IM), G(IM), ALPHA(IM), POISS(IM), HITE(IM)
100 CONTINUE
105 FORMAT(3X, I3,2X,5E12.5)
*
      WRITE(14,*) ' '
*
*
      DO 350 I = 1,NDOF
        FORCE(I) = 0.0
        DO 340 J = 1,NDOF
          SYSMAT(I,J) = 0.0
340 CONTINUE
350 CONTINUE
*
* THE ELEMENT DO LOOP TO 500 FORMS THE SYSTEM MATRIX AND VECTOR
*
      DO 500 IEL = 1,NEL
        IM = IMAT(IEL)
*
* FORM THE ELEMENT STIFFNESS MATRICES
*
        IL = INODE(IEL,1)
        IR = INODE(IEL,2)

```

```

      ZLEN(IEL) = X(IR) - X(IL)
      H = HITE(IM)
*
      EE = E(IM)
      GG = G(IM)
      A = GG*ZLEN(IEL)/(4.*H)
      B = GG*H/ZLEN(IEL)
      C = EE*H/(6.*ZLEN(IEL))
      D = 0.5*GG
      AP2C = A + 2.*C
      ZMAPC = - A + C
      AM2C = A - 2.*C
      ZMAMC = - A - C
*
      EK(1,1) = AP2C
      EK(1,2) = ZMAPC
      EK(1,3) = D
      EK(1,4) = AM2C
      EK(1,5) = ZMAMC
      EK(1,6) = -D
      EK(2,1) = ZMAPC
      EK(2,2) = AP2C
      EK(2,3) = -D
      EK(2,4) = ZMAMC
      EK(2,5) = AM2C
      EK(2,6) = D
      EK(3,1) = D
      EK(3,2) = -D
      EK(3,3) = B
      EK(3,4) = D
      EK(3,5) = -D
      EK(3,6) = -B
      EK(4,1) = AM2C
      EK(4,2) = ZMAMC
      EK(4,3) = D
      EK(4,4) = AP2C
      EK(4,5) = ZMAPC
      EK(4,6) = -D
      EK(5,1) = ZMAMC
      EK(5,2) = AM2C
      EK(5,3) = -D
      EK(5,4) = ZMAPC
      EK(5,5) = AP2C
      EK(5,6) = D
      EK(6,1) = -D
      EK(6,2) = D
      EK(6,3) = -B
      EK(6,4) = -D
      EK(6,5) = D
      EK(6,6) = B
*
* ASSEMBLE ELEMENT MATRICES INTO GLOBAL STIFFNES MATRIX
*
      DO 480 ID = 1,6
      IN = ICORR(IEL,ID)
      DO 480 JD = 1,6
      JN = ICORR(IEL,JD)
      SYSMAT(IN,JN) = SYSMAT(IN,JN) + EK(ID,JD)
480 CONTINUE
*

```



```

500 CONTINUE
*
*   CONSTRUCT THE FORCE VECTOR DUE TO TEMPERATURE CHANGE
*
  WRITE(14,*) ' '
  IF (DELTMP .NE. 0.0) THEN
    DO 550 IEL = 1, NEL
      IM = IMAT(IEL)
      CHI2 = E(IM)*ALPHA(IM)*(2.*TEMP(IM)+TEMP(IM+1))*HITE(IM)/6.
      CHI1 = E(IM)*ALPHA(IM)*(TEMP(IM)+2.*TEMP(IM+1))*HITE(IM)/6.
      I1= ICORR(IEL,1)
      I2= ICORR(IEL,2)
      I4= ICORR(IEL,4)
      I5= ICORR(IEL,5)
      FORCE(I1) = FORCE(I1) - CHI1
      FORCE(I2) = FORCE(I2) - CHI2
      FORCE(I4) = FORCE(I4) + CHI1
      FORCE(I5) = FORCE(I5) + CHI2
550    CONTINUE
    ELSE
      ENDIF
*
*   MODIFY STIFFNESS MATRIX AND FORCE VECTOR FOR BOUNDARY CONDITIONS
*
  DO 610 I = 1, NBC
    II = IBC(I)
    DO 600 J = 1, NDOF
      SYSMAT(II,J) = 0.0
600    CONTINUE
    SYSMAT(II,II) = 1.
    FORCE(II) = 0.0
610    CONTINUE
*
  IF (ITYPE .EQ. 1) THEN
    READ(9,*) ILASTTOP
    WRITE(14,*) ' '
    WRITE(14,*) 'B.C. S AT BOTH ENDS; ILASTTOP = ', ILASTTOP
    DO 620 IN = 1, NDOF
      SYSMAT(ILASTTOP,IN) = 0.0
620    CONTINUE
    SYSMAT(ILASTTOP,ILASTTOP) = 1.
    SYSMAT(ILASTTOP,NDOF) = -1.
    FORCE(ILASTTOP) = 0.0
  ELSE
    ENDIF
*
  IF (NFC .NE. 0) THEN
    DO 630 IF = 1, NFC
      II = IFC(IF)
      FORCE(II) = FORCE(II) + FLOAD(IF)
630    CONTINUE
  ELSE
    ENDIF
*
*   SOLVE THE SYSTEM OF EQUATIONS FOR THE DISPLACEMENTS
*
  CALL DLSARG(NDOF, SYSMAT, NPARAM, FORCE, 1, U)
*
*   PRINT THE FORCE AND DISPLACEMENT VECTORS
*

```

```

      WRITE(14,*) ' '
      WRITE(14,*) ' FORCE AND DISPLACEMENT VECTORS FOLLOW'
      WRITE(14,*) ' '
      DO 680 IDOF = 1,NDOF
      WRITE(14,641) IDOF, FORCE(IDOF), U(IDOF)
680 CONTINUE
641 FORMAT(2X, I4, 4X, E12.5, 10X, E12.5)
*
*   CALCULATE THE STRESSES
*
      DO 700 IEL = 1, NEL
      I1 = ICORR(IEL,1)
      I2 = ICORR(IEL,2)
      I3 = ICORR(IEL,3)
      I4 = ICORR(IEL,4)
      I5 = ICORR(IEL,5)
      I6 = ICORR(IEL,6)
      U1BOT = U(I1)
      U1TOP = U(I2)
      V1 = U(I3)
      U2BOT = U(I4)
      U2TOP = U(I5)
      V2 = U(I6)
      IM = IMAT(IEL)
      EE = E(IM)
      GG = G(IM)
      SIGMABOT(IEL) = EE*((U2BOT - U1BOT)/ZLEN(IEL) - ALPHA(IM)*
& TEMP(IM+1))
      SIGMATOP(IEL) = EE*((U2TOP - U1TOP)/ZLEN(IEL) - ALPHA(IM)*TEMP(IM))
      TAUELEM(IEL) = GG*((U1TOP - U1BOT) + (U2TOP - U2BOT) ) /
& (2.*HITE(IM)) + (V2 - V1)/ZLEN(IEL) )
700 CONTINUE
*
      WRITE(14,*) ' '
      WRITE(14,*) ' STRESSES FOLLOW'
      WRITE(14,*) ' '
      WRITE(14,*) '          SGMABOT          SIGMATOP          TAUELEM '
*
      PSI = E(1)*ALPHA(1)*DELTMP
      DO 800 IEL = 1,NEL
      IM = IMAT(IEL)
      SIGBTNDL = SIGMABOT(IEL)/PSI
      SIGTPNDL = SIGMATOP(IEL)/PSI
      TAUNDL = TAUELEM(IEL)/PSI
      WRITE(14,801) IEL, SIGMABOT(IEL), SIGMATOP(IEL), TAUELEM(IEL)
*
800 CONTINUE
801 FORMAT((2X,I4,6(4X,G12.5)))
*
      WRITE(14,*) ' '
*
      READ(9,*) NNSCOL, NSCOL, N1ROW, N3ROW
*
      NCOL = NNSCOL + NSCOL
*
      DO 1300 IEL = 6, 70
      IM = IMAT(IEL)
      PLPCE(IEL) = TAUELEM(IEL)*HITE(IM)
1300 CONTINUE
      II = 6

```

```

      DO 1500 ICOL = 1,8
      IELF = 6 + (ICOL - 1)
      IELL = IELF + 64
      PLF = 0.0
      DO 1400 IEL = IELF, IELL, 14
      PLF = PLF + PLFCE(IEL+1) - PLFCE(IEL)
1400 CONTINUE
      UPLSTR(ICOL) = 2.*PLF/(X(II+2) - X(II))
      WRITE(14,31) ICOL, UPLSTR(ICOL)
      II = II + 1
1500 CONTINUE
31  FORMAT(1X,I2,' UPPER PEEL STRESS = ',G12.5)
*
      WRITE(14,*) ' '
      DO 1600 IEL = 121, 197
      IM = IMAT(IEL)
      PLFCE(IEL) = TAUELEM(IEL)*HITE(IM)
1600 CONTINUE
      II = 6
      DO 1800 ICOL = 1,8
      IELF = 121 + (ICOL - 1)
      IELL = IELF + 76
      PLF = 0.0
      DO 1700 IEL = IELF, IELL, 17
      PLF = PLF + PLFCE(IEL+1) - PLFCE(IEL)
1700 CONTINUE
      BPLSTR(ICOL) = (2.*PLF/(X(II+2) - X(II)))*(-1.0)
      WRITE(14,32) ICOL, BPLSTR(ICOL)
      II = II + 1
1800 CONTINUE
32  FORMAT(1X,I2,' LOWER PEEL STRESS = ',G12.5)
*
*  COMPARE MOMENTS DUE TO BENDING AND PEEL STRESSES
*
      AVEFCE(1) = 0.5*(SIGMATOP(1) + SIGMABOT(1))*HITE(1)
      ZMOMARM(1) = .0562 - .014
      AVEFCE(2) = 0.5*(SIGMATOP(15) + SIGMABOT(15))*HITE(2)
      ZMOMARM(2) = .0562 - .028 - .007
      AVEFCE(3) = 0.5*(SIGMATOP(29) + SIGMABOT(29))*HITE(3)
      ZMOMARM(3) = .0562 - .028 - .014 - .0035
      AVEFCE(4) = 0.5*(SIGMATOP(43) + SIGMABOT(43))*HITE(4)
      ZMOMARM(4) = .0035 + .00175
      AVEFCE(5) = 0.5*(SIGMATOP(57) + SIGMABOT(57))*HITE(4)
      ZMOMARM(5) = .00175
      ZMOMBDG = 0.0
      DO 1900 I = 1,5
      ZMOMBDG = ZMOMBDG + ZMOMARM(I)*AVEFCE(I)
1900 CONTINUE
*
      ZMOMPEEL = 0.0
      DO 2000 I = 1,8
      II = 7 + I
      JJ = II - 2
      KK = II - 1
      W = 0.5*(X(II) - X(JJ))
      Y = 0.25*(X(JJ) + X(II) + 2.*X(KK))
      ZMOMPEEL = ZMOMPEEL + W*Y*UPLSTR(I)
2000 CONTINUE
C  WRITE(14,*) 'MOMPEEL = ', ZMOMPEEL
*
```

```

      ZMOMBDG = 0.0
      IM = 0
      Y2 = 0.056
      DO 3000 I = 1,57,14
      IM = IMAT(I)
      Y1 = Y2 - HITE(IM)
      AOV3 = (SIGMATOP(I)-SIGMABOT(I))/(3.*HITE(IM))
      BOV2 = 0.5*(SIGMATOP(I)-(Y2/HITE(IM))*(SIGMATOP(I)-SIGMABOT(I)))
      ZMOMBDG = ZMOMBDG + AOV3*(Y2**3-Y1**3)+BOV2*(Y2**2-Y1**2)
      Y2 = Y1
3000 CONTINUE
      SIGMAT = 1.052
      SIGMAB = 2.3012
      Y2 = .001
      Y1 = .0005
      B = SIGMAT - (Y2/.0005)*(SIGMAT-SIGMAB)
      A = (SIGMAT-SIGMAB)/(.0005)
      STOP
      END

```

APPENDIX B PROGRAM EXEC

FORTVS2 WELD (AD(DBL4) ICA)
FILEDEF 14 DISK WELD OUTPUT (RECFM FB LRECL 102 BLOCK 10200)
LOAD WELD (START

APPENDIX C INPUT FILE

```

200 18 15 261 14 0 0
1 2 3 4 5 6 7 146 164 165 166 167 168 169
100.E+09 .3 100.E-06 .500
100.E+09 .3 100.E-06 .250
100.E+09 .3 100.E-06 .125
100.E+09 .3 100.E-06 .0625
100.E+09 .3 100.E-06 .0625
100.E+09 .3 300.E-06 .010
100.E+09 .3 300.E-06 .020
100.E+09 .3 300.E-06 .040
100.E+09 .3 300.E-06 .020
100.E+09 .3 300.E-06 .010
100.E+09 .3 10.E-06 .0625
100.E+09 .3 10.E-06 .0625
100.E+09 .3 10.E-06 .125
100.E+09 .3 10.E-06 .250
100.E+09 .3 10.E-06 .500
0.0 1.33333 2.66667 4.0 4.66667 5.0 5.25
5.50 6.0 7.0 8.0 9.0 9.50 9.750 } 5
10. 10.000001 10.000002 10.000003
1 1 3 1 2 10 8 9 1 2
2 1 10 8 9 17 15 16 2 3
3 1 17 15 16 24 22 23 3 4
4 1 24 22 23 31 29 30 4 5
5 1 31 29 30 38 36 37 5 6
6 1 38 36 37 45 43 44 6 7
7 1 45 43 44 52 50 51 7 8
8 1 52 50 51 59 57 58 8 9
9 1 59 57 58 66 64 65 9 10
10 1 66 64 65 73 71 72 10 11
11 1 73 71 72 80 78 79 11 12
12 1 80 78 79 87 85 86 12 13
13 1 87 85 86 94 92 93 13 14
14 1 94 92 93 101 99 100 14 15
15 2 4 3 2 11 10 9 1 2
16 2 11 10 9 18 17 16 2 3
17 2 18 17 16 25 24 23 3 4
18 2 25 24 23 32 31 30 4 5
19 2 32 31 30 39 38 37 5 6
20 2 39 38 37 46 45 44 6 7
21 2 46 45 44 53 52 51 7 8
22 2 53 52 51 60 59 58 8 9
23 2 60 59 58 67 66 65 9 10
24 2 67 66 65 74 73 72 10 11
25 2 74 73 72 81 80 79 11 12
26 2 81 80 79 88 87 86 12 13
27 2 88 87 86 95 94 93 13 14
28 2 95 94 93 102 101 100 14 15
29 3 5 4 2 12 11 9 1 2
30 3 12 11 9 19 18 16 2 3
31 3 19 18 16 26 25 23 3 4
32 3 26 25 23 33 32 30 4 5
33 3 33 32 30 40 39 37 5 6
34 3 40 39 37 47 46 44 6 7
35 3 47 46 44 54 53 51 7 8
36 3 54 53 51 61 60 58 8 9
37 3 61 60 58 68 67 65 9 10
38 3 68 67 65 75 74 72 10 11
39 3 75 74 72 82 81 79 11 12
40 3 82 81 79 89 88 86 12 13

```

1. Young's Modulus
2. Poisson's Ratio
3. Coefficient of Thermal Expansion
4. Row Height
5. Column Width

41	3	89	88	86	96	95	93	13	14
42	3	96	95	93	103	102	100	14	15
43	4	6	5	2	13	12	9	1	2
44	4	13	12	9	20	19	16	2	3
45	4	20	19	16	27	26	23	3	4
46	4	27	26	23	34	33	30	4	5
47	4	34	33	30	41	40	37	5	6
48	4	41	40	37	48	47	44	6	7
49	4	48	47	44	55	54	51	7	8
50	4	55	54	51	62	61	58	8	9
51	4	62	61	58	69	68	65	9	10
52	4	69	68	65	76	75	72	10	11
53	4	76	75	72	83	82	79	11	12
54	4	83	82	79	90	89	86	12	13
55	4	90	89	86	97	96	93	13	14
56	4	97	96	93	104	103	100	14	15
57	5	7	6	2	14	13	9	1	2
58	5	14	13	9	21	20	16	2	3
59	5	21	20	16	28	27	23	3	4
60	5	28	27	23	35	34	30	4	5
61	5	35	34	30	42	41	37	5	6
62	5	42	41	37	49	48	44	6	7
63	5	49	48	44	56	55	51	7	8
64	5	56	55	51	63	62	58	8	9
65	5	63	62	58	70	69	65	9	10
66	5	70	69	65	77	76	72	10	11
67	5	77	76	72	84	83	79	11	12
68	5	84	83	79	91	90	86	12	13
69	5	91	90	86	98	97	93	13	14
70	5	98	97	93	105	104	100	14	15
71	6	106	42	37	107	49	44	6	7
72	6	107	49	44	108	56	51	7	8
73	6	108	56	51	109	63	58	8	9
74	6	109	63	58	110	70	65	9	10
75	6	110	70	65	111	77	72	10	11
76	6	111	77	72	112	84	79	11	12
77	6	112	84	79	113	91	86	12	13
78	6	113	91	86	114	98	93	13	14
79	6	114	98	93	115	105	100	14	15
80	7	116	106	37	117	107	44	6	7
81	7	117	107	44	118	108	51	7	8
82	7	118	108	51	119	109	58	8	9
83	7	119	109	58	120	110	65	9	10
84	7	120	110	65	121	111	72	10	11
85	7	121	111	72	122	112	79	11	12
86	7	122	112	79	123	113	86	12	13
87	7	123	113	86	124	114	93	13	14
88	7	124	114	93	125	115	100	14	15
89	8	126	116	37	127	117	44	6	7
90	8	127	117	44	128	118	51	7	8
91	8	128	118	51	129	119	58	8	9
92	8	129	119	58	130	120	65	9	10
93	8	130	120	65	131	121	72	10	11
94	8	131	121	72	132	122	79	11	12
95	8	132	122	79	133	123	86	12	13
96	8	133	123	86	134	124	93	13	14
97	8	134	124	93	135	125	100	14	15
98	9	136	126	37	137	127	44	6	7
99	9	137	127	44	138	128	51	7	8
100	9	138	128	51	139	129	58	8	9

101	9	139	129	58	140	130	65	9	10
102	9	140	130	65	141	131	72	10	11
103	9	141	131	72	142	132	79	11	12
104	9	142	132	79	143	133	86	12	13
105	9	143	133	86	144	134	93	13	14
106	9	144	134	93	145	135	100	14	15
107	10	151	136	37	152	137	44	6	7
108	10	152	137	44	153	138	51	7	8
109	10	153	138	51	154	139	58	8	9
110	10	154	139	58	155	140	65	9	10
111	10	155	140	65	156	141	72	10	11
112	10	156	141	72	157	142	79	11	12
113	10	157	142	79	158	143	86	12	13
114	10	158	143	86	159	144	93	13	14
115	10	159	144	93	160	145	100	14	15
116	11	165	146	164	171	147	170	1	2
117	11	171	147	170	177	148	176	2	3
118	11	177	148	176	183	149	182	3	4
119	11	183	149	182	189	150	188	4	5
120	11	189	150	188	194	151	37	5	6
121	11	194	151	37	199	152	44	6	7
122	11	199	152	44	204	153	51	7	8
123	11	204	153	51	209	154	58	8	9
124	11	209	154	58	214	155	65	9	10
125	11	214	155	65	219	156	72	10	11
126	11	219	156	72	224	157	79	11	12
127	11	224	157	79	229	158	86	12	13
128	11	229	158	86	234	159	93	13	14
129	11	234	159	93	239	160	100	14	15
130	11	239	160	100	245	161	244	15	16
131	11	245	161	244	251	162	250	16	17
132	11	251	162	250	257	163	256	17	18
133	12	166	165	164	172	171	170	1	2
134	12	172	171	170	178	177	176	2	3
135	12	178	177	176	184	183	182	3	4
136	12	184	183	182	190	189	188	4	5
137	12	190	189	188	195	194	37	5	6
138	12	195	194	37	200	199	44	6	7
139	12	200	199	44	205	204	51	7	8
140	12	205	204	51	210	209	58	8	9
141	12	210	209	58	215	214	65	9	10
142	12	215	214	65	220	219	72	10	11
143	12	220	219	72	225	224	79	11	12
144	12	225	224	79	230	229	86	12	13
145	12	230	229	86	235	234	93	13	14
146	12	235	234	93	240	239	100	14	15
147	12	240	239	100	246	245	244	15	16
148	12	246	245	244	252	251	250	16	17
149	12	252	251	250	258	257	256	17	18
150	13	167	166	164	173	172	170	1	2
151	13	173	172	170	179	178	176	2	3
152	13	179	178	176	185	184	182	3	4
153	13	185	184	182	191	190	188	4	5
154	13	191	190	188	196	195	37	5	6
155	13	196	195	37	201	200	44	6	7
156	13	201	200	44	206	205	51	7	8
157	13	206	205	51	211	210	58	8	9
158	13	211	210	58	216	215	65	9	10
159	13	216	215	65	221	220	72	10	11
160	13	221	220	72	226	225	79	11	12

200.

100. 100. 100. 100. 100. 100. 100. 100. 100. 100. 100. 100. 100. 100 }6

100. 100.

5 9 5 5

80

APPENDIX D OUTPUT FILE

DELTMP = 200.00000000000000

IMAT#, E, G MODULII, ALFA, POISSON AND HEIGHT FOLLOW

1	0.10000E+12	0.32051E+11	0.10000E-03	0.30000E+00	0.50000E+00
2	0.10000E+12	0.32051E+11	0.10000E-03	0.30000E+00	0.25000E+00
3	0.10000E+12	0.32051E+11	0.10000E-03	0.30000E+00	0.12500E+00
4	0.10000E+12	0.32051E+11	0.10000E-03	0.30000E+00	0.62500E-01
5	0.10000E+12	0.32051E+11	0.10000E-03	0.30000E+00	0.62500E-01
6	0.10000E+12	0.32051E+11	0.30000E-03	0.30000E+00	0.10000E-01
7	0.10000E+12	0.32051E+11	0.30000E-03	0.30000E+00	0.20000E-01
8	0.10000E+12	0.32051E+11	0.30000E-03	0.30000E+00	0.40000E-01
9	0.10000E+12	0.32051E+11	0.30000E-03	0.30000E+00	0.20000E-01
10	0.10000E+12	0.32051E+11	0.30000E-03	0.30000E+00	0.10000E-01
11	0.10000E+12	0.32051E+11	0.10000E-04	0.30000E+00	0.62500E-01
12	0.10000E+12	0.32051E+11	0.10000E-04	0.30000E+00	0.62500E-01
13	0.10000E+12	0.32051E+11	0.10000E-04	0.30000E+00	0.12500E+00
14	0.10000E+12	0.32051E+11	0.10000E-04	0.30000E+00	0.25000E+00
15	0.10000E+12	0.32051E+11	0.10000E-04	0.30000E+00	0.50000E+00

FORCE AND DISPLACEMENT VECTORS FOLLOW

1	0.00000E+00	0.00000E+00
2	0.00000E+00	0.00000E+00
3	0.00000E+00	0.00000E+00
4	0.00000E+00	0.00000E+00
5	0.00000E+00	0.00000E+00

6	0.00000E+00	0.00000E+00
7	0.00000E+00	0.00000E+00
8	0.00000E+00	0.16022E-01
9	0.00000E+00	-0.51672E-02
10	0.00000E+00	0.12042E-01
11	0.00000E+00	0.10033E-01
12	0.00000E+00	0.90521E-02
13	0.00000E+00	0.85658E-02
14	0.00000E+00	0.80331E-02
15	0.00000E+00	0.32451E-01
16	0.00000E+00	-0.21458E-01
17	0.00000E+00	0.24079E-01
18	0.00000E+00	0.19888E-01
19	0.00000E+00	0.17771E-01
20	0.00000E+00	0.16716E-01
21	0.00000E+00	0.15765E-01
22	0.00000E+00	0.49296E-01
23	0.00000E+00	-0.50058E-01
24	0.00000E+00	0.36110E-01
25	0.00000E+00	0.29507E-01
26	0.00000E+00	0.26255E-01
27	0.00000E+00	0.24626E-01
28	0.00000E+00	0.22845E-01
29	0.00000E+00	0.57798E-01
30	0.00000E+00	-0.69213E-01
31	0.00000E+00	0.42198E-01
32	0.00000E+00	0.34279E-01
33	0.00000E+00	0.30238E-01
34	0.00000E+00	0.28255E-01
35	0.00000E+00	0.26546E-01

36	0.00000E+00	0.61934E-01
37	0.00000E+00	-0.80181E-01
38	0.00000E+00	0.45342E-01
39	0.00000E+00	0.36811E-01
40	0.00000E+00	0.32342E-01
41	0.00000E+00	0.29943E-01
42	-0.15000E+08	0.27144E-01
43	0.00000E+00	0.65005E-01
44	0.00000E+00	-0.88399E-01
45	0.00000E+00	0.47763E-01
46	0.00000E+00	0.38867E-01
47	0.00000E+00	0.34269E-01
48	0.00000E+00	0.31904E-01
49	0.00000E+00	0.29455E-01
50	0.00000E+00	0.68161E-01
51	0.00000E+00	-0.97019E-01
52	0.00000E+00	0.50215E-01
53	0.00000E+00	0.41041E-01
54	0.00000E+00	0.36432E-01
55	0.00000E+00	0.34170E-01
56	0.00000E+00	0.32225E-01
57	0.00000E+00	0.74620E-01
58	0.00000E+00	-0.11546E+00
59	0.00000E+00	0.55219E-01
60	0.00000E+00	0.45459E-01
61	0.00000E+00	0.40623E-01
62	0.00000E+00	0.38212E-01
63	0.00000E+00	0.35508E-01
64	0.00000E+00	0.87846E-01
65	0.00000E+00	-0.15715E+00

66	0.00000E+00	0.65382E-01
67	0.00000E+00	0.54158E-01
68	0.00000E+00	0.48522E-01
69	0.00000E+00	0.45704E-01
70	0.00000E+00	0.43179E-01
71	0.00000E+00	0.10123E+00
72	0.00000E+00	-0.20527E+00
73	0.00000E+00	0.75574E-01
74	0.00000E+00	0.62744E-01
75	0.00000E+00	0.56355E-01
76	0.00000E+00	0.53160E-01
77	0.00000E+00	0.49681E-01
78	0.00000E+00	0.11433E+00
79	0.00000E+00	-0.25976E+00
80	0.00000E+00	0.85778E-01
81	0.00000E+00	0.71538E-01
82	0.00000E+00	0.64345E-01
83	0.00000E+00	0.60737E-01
84	0.00000E+00	0.57389E-01
85	0.00000E+00	0.12051E+00
86	0.00000E+00	-0.28934E+00
87	0.00000E+00	0.90866E-01
88	0.00000E+00	0.76222E-01
89	0.00000E+00	0.68790E-01
90	0.00000E+00	0.64988E-01
91	0.00000E+00	0.60910E-01
92	0.00000E+00	0.12339E+00
93	0.00000E+00	-0.30467E+00
94	0.00000E+00	0.93387E-01
95	0.00000E+00	0.78682E-01

96	0.00000E+00	0.71308E-01
97	0.00000E+00	0.67581E-01
98	0.00000E+00	0.63741E-01
99	0.25000E+09	0.12604E+00
100	0.00000E+00	-0.32032E+00
101	0.37500E+09	0.95892E-01
102	0.18750E+09	0.81178E-01
103	0.93750E+08	0.73861E-01
104	0.62500E+08	0.70313E-01
105	0.46250E+08	0.67120E-01
106	-0.45000E+08	0.25831E-01
107	0.00000E+00	0.29799E-01
108	0.00000E+00	0.31288E-01
109	0.00000E+00	0.35675E-01
110	0.00000E+00	0.42187E-01
111	0.00000E+00	0.49705E-01
112	0.00000E+00	0.56277E-01
113	0.00000E+00	0.60826E-01
114	0.00000E+00	0.62514E-01
115	0.45000E+08	0.67226E-01
116	-0.90000E+08	0.24860E-01
117	0.00000E+00	0.29050E-01
118	0.00000E+00	0.30760E-01
119	0.00000E+00	0.34696E-01
120	0.00000E+00	0.41504E-01
121	0.00000E+00	0.48460E-01
122	0.00000E+00	0.55339E-01
123	0.00000E+00	0.59371E-01
124	0.00000E+00	0.61365E-01
125	0.90000E+08	0.65955E-01

126	-0.90000E+08	0.23563E-01
127	0.00000E+00	0.27710E-01
128	0.00000E+00	0.29341E-01
129	0.00000E+00	0.33167E-01
130	0.00000E+00	0.39696E-01
131	0.00000E+00	0.46422E-01
132	0.00000E+00	0.53003E-01
133	0.00000E+00	0.56897E-01
134	0.00000E+00	0.58707E-01
135	0.90000E+08	0.63070E-01
136	-0.45000E+08	0.23197E-01
137	0.00000E+00	0.27159E-01
138	0.00000E+00	0.28411E-01
139	0.00000E+00	0.32652E-01
140	0.00000E+00	0.38538E-01
141	0.00000E+00	0.45660E-01
142	0.00000E+00	0.51577E-01
143	0.00000E+00	0.55900E-01
144	0.00000E+00	0.57197E-01
145	0.45000E+08	0.61436E-01
146	0.00000E+00	0.00000E+00
147	0.00000E+00	0.71778E-02
148	0.00000E+00	0.14053E-01
149	0.00000E+00	0.20279E-01
150	0.00000E+00	0.23548E-01
151	-0.15000E+08	0.23941E-01
152	0.00000E+00	0.26069E-01
153	0.00000E+00	0.28720E-01
154	0.00000E+00	0.31633E-01
155	0.00000E+00	0.38716E-01

156	0.00000E+00	0.44524E-01
157	0.00000E+00	0.51618E-01
158	0.00000E+00	0.54641E-01
159	0.00000E+00	0.57231E-01
160	0.15000E+08	0.59728E-01
161	0.00000E+00	0.59728E-01
162	0.00000E+00	0.59728E-01
163	0.31250E+07	0.59728E-01
164	0.00000E+00	0.00000E+00
165	0.00000E+00	0.00000E+00
166	0.00000E+00	0.00000E+00
167	0.00000E+00	0.00000E+00
168	0.00000E+00	0.00000E+00
169	0.00000E+00	0.00000E+00
170	0.00000E+00	-0.62365E-02
171	0.00000E+00	0.66407E-02
172	0.00000E+00	0.60583E-02
173	0.00000E+00	0.49010E-02
174	0.00000E+00	0.26339E-02
175	0.00000E+00	-0.19392E-02
176	0.00000E+00	-0.24155E-01
177	0.00000E+00	0.12867E-01
178	0.00000E+00	0.11783E-01
179	0.00000E+00	0.96238E-02
180	0.00000E+00	0.52627E-02
181	0.00000E+00	-0.34704E-02
182	0.00000E+00	-0.52573E-01
183	0.00000E+00	0.18851E-01
184	0.00000E+00	0.17274E-01
185	0.00000E+00	0.14111E-01

156	0.00000E+00	0.44524E-01
157	0.00000E+00	0.51618E-01
158	0.00000E+00	0.54641E-01
159	0.00000E+00	0.57231E-01
160	0.15000E+08	0.59728E-01
161	0.00000E+00	0.59728E-01
162	0.00000E+00	0.59728E-01
163	0.31250E+07	0.59728E-01
164	0.00000E+00	0.00000E+00
165	0.00000E+00	0.00000E+00
166	0.00000E+00	0.00000E+00
167	0.00000E+00	0.00000E+00
168	0.00000E+00	0.00000E+00
169	0.00000E+00	0.00000E+00
170	0.00000E+00	-0.62365E-02
171	0.00000E+00	0.66407E-02
172	0.00000E+00	0.60583E-02
173	0.00000E+00	0.49010E-02
174	0.00000E+00	0.26339E-02
175	0.00000E+00	-0.19392E-02
176	0.00000E+00	-0.24155E-01
177	0.00000E+00	0.12867E-01
178	0.00000E+00	0.11783E-01
179	0.00000E+00	0.96238E-02
180	0.00000E+00	0.52627E-02
181	0.00000E+00	-0.34704E-02
182	0.00000E+00	-0.52573E-01
183	0.00000E+00	0.18851E-01
184	0.00000E+00	0.17274E-01
185	0.00000E+00	0.14111E-01

186	0.00000E+00	0.78855E-02
187	0.00000E+00	-0.45865E-02
188	0.00000E+00	-0.70479E-01
189	0.00000E+00	0.21520E-01
190	0.00000E+00	0.19760E-01
191	0.00000E+00	0.16317E-01
192	0.00000E+00	0.92685E-02
193	0.00000E+00	-0.50653E-02
194	0.00000E+00	0.22721E-01
195	0.00000E+00	0.21115E-01
196	0.00000E+00	0.17566E-01
197	0.00000E+00	0.10061E-01
198	0.00000E+00	-0.54197E-02
199	0.00000E+00	0.24327E-01
200	0.00000E+00	0.22481E-01
201	0.00000E+00	0.18660E-01
202	0.00000E+00	0.10718E-01
203	0.00000E+00	-0.57161E-02
204	0.00000E+00	0.26229E-01
205	0.00000E+00	0.24082E-01
206	0.00000E+00	0.19872E-01
207	0.00000E+00	0.11406E-01
208	0.00000E+00	-0.59275E-02
209	0.00000E+00	0.29553E-01
210	0.00000E+00	0.27155E-01
211	0.00000E+00	0.22365E-01
212	0.00000E+00	0.12883E-01
213	0.00000E+00	-0.62042E-02
214	0.00000E+00	0.35599E-01
215	0.00000E+00	0.32803E-01

216	0.00000E+00	0.27217E-01
217	0.00000E+00	0.15989E-01
218	0.00000E+00	-0.64446E-02
219	0.00000E+00	0.41621E-01
220	0.00000E+00	0.38408E-01
221	0.00000E+00	0.31968E-01
222	0.00000E+00	0.19138E-01
223	0.00000E+00	-0.65533E-02
224	0.00000E+00	0.47689E-01
225	0.00000E+00	0.44047E-01
226	0.00000E+00	0.36779E-01
227	0.00000E+00	0.22184E-01
228	0.00000E+00	-0.67637E-02
229	0.00000E+00	0.50965E-01
230	0.00000E+00	0.47029E-01
231	0.00000E+00	0.39072E-01
232	0.00000E+00	0.23484E-01
233	0.00000E+00	-0.68603E-02
234	0.00000E+00	0.52884E-01
235	0.00000E+00	0.48468E-01
236	0.00000E+00	0.39986E-01
237	0.00000E+00	0.23982E-01
238	0.00000E+00	-0.68389E-02
239	0.00000E+00	0.54036E-01
240	0.00000E+00	0.49242E-01
241	0.00000E+00	0.40488E-01
242	0.00000E+00	0.24321E-01
243	0.00000E+00	-0.66809E-02
244	0.00000E+00	-0.32032E+00
245	0.00000E+00	0.54036E-01

246	0.00000E+00	0.49242E-01
247	0.00000E+00	0.40488E-01
248	0.00000E+00	0.24321E-01
249	0.00000E+00	-0.66809E-02
250	0.00000E+00	-0.32032E+00
251	0.00000E+00	0.54036E-01
252	0.00000E+00	0.49242E-01
253	0.00000E+00	0.40488E-01
254	0.00000E+00	0.24321E-01
255	0.00000E+00	-0.66809E-02
256	0.00000E+00	-0.32032E+00
257	0.62500E+07	0.54036E-01
258	0.93750E+07	0.49242E-01
259	0.18750E+08	0.40488E-01
260	0.37500E+08	0.24321E-01
261	0.25000E+08	-0.66809E-02

STRESSES FOLLOW

	SGMABOT	SGMATOP	TAUELEM
1	-0.96832E+08	0.20163E+09	0.33346E+07
2	-0.97221E+08	0.23223E+09	0.42668E+07
3	-0.97662E+08	0.26336E+09	0.34617E+07
4	-0.86943E+08	0.27526E+09	0.17059E+07
5	-0.56664E+08	0.24077E+09	-0.22757E+08
6	-0.31570E+08	0.22852E+09	0.30736E+08
7	-0.19144E+08	0.26242E+09	0.22740E+08
8	0.80498E+06	0.29174E+09	0.14828E+08
9	0.16305E+08	0.32262E+09	0.54632E+07
10	0.19130E+08	0.33807E+09	0.15863E+06

11	0.20416E+08	0.30984E+09	-0.93561E+07
12	0.17685E+08	0.23665E+09	-0.30987E+08
13	0.85421E+07	0.15424E+09	-0.54002E+08
14	0.19906E+07	0.58011E+08	-0.78675E+08
15	-0.24752E+09	-0.96832E+08	0.45844E+07
16	-0.26088E+09	-0.97221E+08	0.58611E+07
17	-0.27857E+09	-0.97662E+08	0.44885E+07
18	-0.28418E+09	-0.86943E+08	0.99650E+07
19	-0.24033E+09	-0.56664E+08	-0.13647E+06
20	-0.17785E+09	-0.31570E+08	0.63424E+08
21	-0.13044E+09	-0.19144E+08	0.53303E+08
22	-0.11640E+09	0.80498E+06	0.31608E+08
23	-0.13006E+09	0.16305E+08	0.88319E+07
24	-0.14138E+09	0.19130E+08	-0.16488E+06
25	-0.12063E+09	0.20416E+08	-0.11367E+08
26	-0.63188E+08	0.17685E+08	-0.44518E+08
27	-0.16015E+08	0.85421E+07	-0.84443E+08
28	-0.17644E+07	0.19906E+07	-0.12074E+09
29	-0.32109E+09	-0.24752E+09	0.15406E+07
30	-0.34612E+09	-0.26088E+09	0.55932E+07
31	-0.36365E+09	-0.27857E+09	0.86522E+06
32	-0.40251E+09	-0.28418E+09	0.14019E+08
33	-0.36879E+09	-0.24033E+09	0.36426E+08
34	-0.22946E+09	-0.17785E+09	0.10874E+09
35	-0.13485E+09	-0.13044E+09	0.75305E+08
36	-0.16177E+09	-0.11640E+09	0.28705E+08
37	-0.21003E+09	-0.13006E+09	0.61505E+07
38	-0.21678E+09	-0.14138E+09	-0.35792E+06
39	-0.20095E+09	-0.12063E+09	-0.52206E+07
40	-0.11105E+09	-0.63188E+08	-0.21053E+08

41	0.70878E+07	-0.16015E+08	-0.67557E+08
42	0.21304E+08	-0.17644E+07	-0.12319E+09
43	-0.35756E+09	-0.32109E+09	0.48163E+06
44	-0.38872E+09	-0.34612E+09	0.34010E+07
45	-0.40678E+09	-0.36365E+09	0.57895E+06
46	-0.45566E+09	-0.40251E+09	0.54280E+07
47	-0.49365E+09	-0.36879E+09	0.69360E+08
48	-0.21563E+09	-0.22946E+09	0.16808E+09
49	-0.93571E+08	-0.13485E+09	0.81349E+08
50	-0.19161E+09	-0.16177E+09	0.16037E+08
51	-0.25080E+09	-0.21003E+09	0.46495E+07
52	-0.25433E+09	-0.21678E+09	-0.24469E+06
53	-0.24238E+09	-0.20095E+09	-0.22418E+07
54	-0.14975E+09	-0.11105E+09	0.41097E+07
55	0.37217E+08	0.70878E+07	-0.35371E+08
56	0.92679E+08	0.21304E+08	-0.14127E+09
57	-0.39752E+09	-0.35756E+09	0.12391E+08
58	-0.42008E+09	-0.38872E+09	-0.11199E+08
59	-0.46904E+09	-0.40678E+09	0.13011E+08
60	-0.44486E+09	-0.45566E+09	-0.26006E+08
61	-0.82061E+09	-0.49365E+09	0.10136E+09
62	-0.75409E+08	-0.21563E+09	0.29180E+09
63	0.10776E+09	-0.93571E+08	0.21460E+08
64	-0.34326E+09	-0.19161E+09	0.97283E+07
65	-0.23293E+09	-0.25080E+09	0.41638E+07
66	-0.34978E+09	-0.25433E+09	-0.26277E+07
67	-0.22926E+09	-0.24238E+09	0.39777E+07
68	-0.29578E+09	-0.14975E+09	0.80823E+07
69	0.13236E+09	0.37217E+08	0.64530E+08
70	0.35154E+09	0.92679E+08	-0.20324E+09

71	-0.14128E+10	-0.20754E+10	0.50013E+09
72	-0.24042E+10	-0.18922E+10	-0.15450E+09
73	-0.21226E+10	-0.23433E+10	0.51903E+08
74	-0.23488E+10	-0.22329E+10	-0.13578E+08
75	-0.22482E+10	-0.23498E+10	0.97283E+07
76	-0.23428E+10	-0.22293E+10	-0.26196E+07
77	-0.20902E+10	-0.22958E+10	0.20390E+08
78	-0.23248E+10	-0.18676E+10	0.13514E+09
79	-0.11151E+10	-0.16485E+10	-0.21072E+09
80	-0.13241E+10	-0.14128E+10	0.32412E+09
81	-0.23160E+10	-0.24042E+10	-0.81814E+08
82	-0.22127E+10	-0.21226E+10	0.25195E+08
83	-0.23192E+10	-0.23488E+10	-0.50890E+07
84	-0.23045E+10	-0.22482E+10	0.29591E+07
85	-0.23120E+10	-0.23428E+10	0.26092E+07
86	-0.21937E+10	-0.20902E+10	0.21170E+08
87	-0.22022E+10	-0.23248E+10	0.12030E+09
88	-0.11639E+10	-0.11151E+10	-0.68495E+08
89	-0.13412E+10	-0.13241E+10	0.30606E+07
90	-0.23475E+10	-0.23160E+10	0.42052E+06
91	-0.22348E+10	-0.22127E+10	-0.89273E+06
92	-0.23470E+10	-0.23192E+10	0.68946E+06
93	-0.23275E+10	-0.23045E+10	-0.12984E+07
94	-0.23418E+10	-0.23120E+10	0.57419E+07
95	-0.22213E+10	-0.21937E+10	0.30953E+08
96	-0.22758E+10	-0.22022E+10	0.90213E+08
97	-0.12551E+10	-0.11639E+10	0.21441E+09
98	-0.14152E+10	-0.13412E+10	-0.31989E+09
99	-0.24992E+10	-0.23475E+10	0.80553E+08
100	-0.21520E+10	-0.22348E+10	-0.24553E+08

101	-0.24114E+10	-0.23470E+10	0.48791E+07
102	-0.22878E+10	-0.23275E+10	-0.36850E+07
103	-0.24083E+10	-0.23418E+10	0.66497E+07
104	-0.21353E+10	-0.22213E+10	0.45573E+08
105	-0.24811E+10	-0.22758E+10	0.42590E+08
106	-0.13045E+10	-0.12551E+10	0.51209E+09
107	-0.21488E+10	-0.14152E+10	-0.49752E+09
108	-0.19394E+10	-0.24992E+10	0.14742E+09
109	-0.24174E+10	-0.21520E+10	-0.45783E+08
110	-0.22918E+10	-0.24114E+10	0.99768E+07
111	-0.24192E+10	-0.22878E+10	-0.66053E+07
112	-0.22906E+10	-0.24083E+10	0.74915E+07
113	-0.23955E+10	-0.21353E+10	0.55718E+08
114	-0.19640E+10	-0.24811E+10	-0.10628E+07
115	-0.20010E+10	-0.13045E+10	0.67659E+09
116	0.39805E+09	0.43834E+09	-0.12190E+08
117	0.36699E+09	0.41563E+09	0.10995E+08
118	0.34874E+09	0.36697E+09	-0.12801E+08
119	0.30036E+09	0.39032E+09	0.25549E+08
120	0.26053E+09	0.17822E+08	-0.10015E+09
121	0.54227E+09	0.75123E+09	-0.29445E+09
122	0.66086E+09	0.96063E+09	-0.19738E+08
123	0.56485E+09	0.48262E+09	-0.10095E+08
124	0.50460E+09	0.60825E+09	-0.39153E+07
125	0.50214E+09	0.48083E+09	0.14889E+07
126	0.50685E+09	0.60941E+09	0.53087E+07
127	0.55520E+09	0.50449E+09	0.53776E+08
128	0.66764E+09	0.93602E+09	0.91013E+08
129	0.36045E+09	0.89902E+09	0.56745E+09
130	59468.	-0.12464E+06	0.79085E+09

131	35680.	-74781.	0.79085E+09
132	11893.	-24927.	0.79085E+09
133	0.35437E+09	0.39805E+09	-0.57935E+06
134	0.32933E+09	0.36699E+09	-0.33031E+07
135	0.31182E+09	0.34874E+09	-0.67715E+06
136	0.27291E+09	0.30036E+09	-0.52327E+07
137	0.30660E+09	0.26053E+09	-0.69720E+08
138	0.44624E+09	0.54227E+09	-0.16835E+09
139	0.54043E+09	0.66086E+09	-0.81001E+08
140	0.51459E+09	0.56485E+09	-0.16459E+08
141	0.46481E+09	0.50460E+09	-0.41742E+07
142	0.46054E+09	0.50214E+09	-0.12006E+07
143	0.46389E+09	0.50685E+09	0.11140E+08
144	0.49645E+09	0.55520E+09	0.47156E+08
145	0.47539E+09	0.66764E+09	0.17594E+09
146	0.20980E+09	0.36045E+09	0.35491E+09
147	-2535.9	59468.	0.32965E+09
148	-1521.7	35680.	0.32965E+09
149	-507.45	11893.	0.32965E+09
150	0.26757E+09	0.35437E+09	-0.15447E+07
151	0.25421E+09	0.32933E+09	-0.55885E+07
152	0.23653E+09	0.31182E+09	-0.87117E+06
153	0.23091E+09	0.27291E+09	-0.14003E+08
154	0.27481E+09	0.30660E+09	-0.36549E+08
155	0.33732E+09	0.44624E+09	-0.10886E+09
156	0.38509E+09	0.54043E+09	-0.75559E+08
157	0.39860E+09	0.51459E+09	-0.28515E+08
158	0.38514E+09	0.46481E+09	-0.61843E+07
159	0.37509E+09	0.46054E+09	-0.19486E+06
160	0.38117E+09	0.46389E+09	0.10904E+08

161	0.35850E+09	0.49645E+09	0.55894E+08
162	0.26551E+09	0.47539E+09	0.14181E+09
163	0.10077E+09	0.20980E+09	0.20319E+09
164	3473.6	-2535.9	0.11629E+09
165	2084.3	-1521.7	0.11629E+09
166	694.89	-507.45	0.11629E+09
167	0.97544E+08	0.26757E+09	-0.45917E+07
168	0.97157E+08	0.25421E+09	-0.58539E+07
169	0.96713E+08	0.23653E+09	-0.44958E+07
170	0.10745E+09	0.23091E+09	-0.99519E+07
171	0.13776E+09	0.27481E+09	61981.
172	0.16289E+09	0.33732E+09	-0.63509E+08
173	0.17526E+09	0.38509E+09	-0.53328E+08
174	0.19540E+09	0.39860E+09	-0.31672E+08
175	0.21053E+09	0.38514E+09	-0.87828E+07
176	0.21496E+09	0.37509E+09	81373.
177	0.20458E+09	0.38117E+09	0.11422E+08
178	0.15989E+09	0.35850E+09	0.38791E+08
179	0.99276E+08	0.26551E+09	0.59307E+08
180	0.35805E+08	0.10077E+09	0.55522E+08
181	1175.8	3473.6	-0.55906E+08
182	705.45	2084.3	-0.55906E+08
183	235.10	694.89	-0.55906E+08
184	-0.24544E+09	0.97544E+08	-0.33428E+07
185	-0.21484E+09	0.97157E+08	-0.42584E+07
186	-0.18370E+09	0.96713E+08	-0.34705E+07
187	-0.17182E+09	0.10745E+09	-0.16839E+07
188	-0.20633E+09	0.13776E+09	0.22719E+08
189	-0.21854E+09	0.16289E+09	-0.30764E+08
190	-0.18458E+09	0.17526E+09	-0.22765E+08

191	-0.15534E+09	0.19540E+09	-0.14821E+08
192	-0.12404E+09	0.21053E+09	-0.55446E+07
193	-0.11087E+09	0.21496E+09	0.41476E+06
194	-0.12104E+09	0.20458E+09	0.47076E+07
195	-0.11932E+09	0.15989E+09	0.43322E+07
196	-0.91445E+08	0.99276E+08	-0.54208E+07
197	-0.36775E+08	0.35805E+08	-0.25159E+08
198	-2705.9	1175.8	-0.14118E+09
199	-1623.6	705.45	-0.14118E+09
200	-541.10	235.10	-0.14118E+09

1 UPPER PEEL STRESS = -0.13210E+09
 2 UPPER PEEL STRESS = -0.53388E+08
 3 UPPER PEEL STRESS = -0.19007E+08
 4 UPPER PEEL STRESS = -0.64454E+07
 5 UPPER PEEL STRESS = -0.78777E+07
 6 UPPER PEEL STRESS = -0.27239E+08
 7 UPPER PEEL STRESS = -0.69977E+08
 8 UPPER PEEL STRESS = -0.20688E+09

1 LOWER PEEL STRESS = -0.13335E+09
 2 LOWER PEEL STRESS = -0.53074E+08
 3 LOWER PEEL STRESS = -0.19075E+08
 4 LOWER PEEL STRESS = -0.64680E+07
 5 LOWER PEEL STRESS = -0.73789E+07
 6 LOWER PEEL STRESS = -0.23411E+08
 7 LOWER PEEL STRESS = -0.56982E+08
 8 LOWER PEEL STRESS = -0.15128E+09

LIST OF REFERENCES

1. Timoshenko, S.P., " Analysis of Bi-Metal Thermostats," *Journal of the Optical Society of America*, Vol 11, pp. 233-256, 1925.
2. Goland, M., and Reissner, E., " The Stresses in Cemented Joints," *Journal of Applied Mechanics, Transactions, ASME*, 11, pp. 17-27, March 1984.
3. Christensen, T.H., *A Finite Element Analysis of a Single Lap Shear Adhesive Joint With and Without an Edge Crack*, Master's Thesis, Massachusetts Institute of Technology, February 1976.
4. Burgreen, D., *Elements of Thermal Stress Analysis*, pp. 67-69 and 412-420, C.P. Press, 1971.
5. Lau, J.H., " Thermoelasticity for Electronic Packaging," *New Technology in Electronic Packaging*, pp. 111-119, ASM International, 1990.
6. Geschwind, G., and Clary, R., " The Technology of Multichip Modules," *New Technology in Electronic Packaging*, pp. 65-77, ASM International, 1990.
7. Tummala, R., and Rymaszewski, E., *Microelectronics Packaging Handbook*, Van Nostrand Reinhold, 1989.
8. Suhir, E., *Advances in Thermal Modeling of Electronic Components and Systems*, Vol 1, pp. 337-417, Hemisphere Publishing Co., 1989.
9. Royce, B., "Differential Thermal Expansion in Microelectronic Systems," *1988 Conference on Thermal Phenomena in Electronic Components*, IEEE, pp. 171-180, 1988.
10. Riches, S.T., " Assessment of Materials for Large Area Die Attach," *High Performance Electronic Packaging*, pp. 7-16, Abington Publishing, 1991.
11. Chung, K.K.T., and others," Low TG Epoxy Adhesives for Thermal Management," *High Performance Electronic Packaging*, pp. 24-34, Abington Publishing, 1991.

INITIAL DISTRIBUTION LIST

	No. of Copies
1. Library, Code 52 Naval Postgraduate School Monterey, California 93943-5002	2
2. Department Chairman, Code ME Department of Mechanical Engineering Naval Postgraduate School Monterey, California 93943-5000	1
3. Naval Engineering Curricular Office, Code 34 Naval Postgraduate School Monterey, California 93943-5000	1
4. Professor David Salinas, Code ME/Sa Department of Mechanical Engineering Naval Postgraduate School Monterey, California 93943-5000	4
5. Professor Young Kwon, Code ME/Kw Department of Mechanical Engineering Naval Postgraduate School Monterey, California 93943-5000	2
6. Defense Technical Information Center Cameron Station Alexandria, Virginia 22304-6145	2
7. LT Michael J. Neibert, USN Long Beach Naval Shipyard Long Beach, California 90822-5099	1